RETRIEVAL OF HANDWRITTEN HISTORICAL DOCUMENT IMAGES

A Dissertation Presented

by

TONI MAXIMILIAN RATH

Submitted to the Graduate School of the
University of Massachusetts Amherst in partial fulfillment
of the requirements for the degree of

DOCTOR OF PHILOSOPHY

September 2005

Computer Science

RETRIEVAL OF HANDWRITTEN HISTORICAL DOCUMENT IMAGES

A Dissertation Presented

by

TONI MAXIMILIAN RATH

Approved as to style and content by:

R. Manmatha, Chair

W. Bruce Croft, Member

Allen R. Hanson, Member

Paola Sebastiani, Member

W. Bruce Croft, Department Chair
Computer Science

To Mila

Ein Rauch verweht,

Ein Wasser verrinnt,

Eine Zeit vergeht,

Eine neue beginnt.

Joachim Ringelnatz

ACKNOWLEDGMENTS

I would like to thank my advisor R. Manmatha for his guidance, support and for always having an open door for discussion. With his encouragement and enthusiasm he has inspired me to tackle difficult problems. It was a pleasure to work in the friendly atmosphere he created. In addition, I would like to thank my committee members for their valuable input that helped improve this work.

I am also grateful to my colleagues at the Center for Intelligent Information Retrieval, particularly Jiwoon Jeon, Jamie Rothfeder, Shaolei Feng and Natasha Mohanty. Their company and collaboration has provided a very pleasant work environment. I will miss our weekly multimedia lunches. My collaboration with Victor Lavrenko has been particularly fruitful. I would like to thank him for our discussions about information retrieval problems, for sharing his code and for helping out with many small problems.

I am truly indebted to Máximo Carreras for his friendship and impeccable knowledge of probability theory, which he shared with me on many occasions. Many thanks go to my parents, who have inspired in me the desire to learn and explore. They have sparked my interest in science and languages. I owe my education to them. My brother Florian and sister Christine have always been there for me during the last few years, be it during visits home or through many telephone conversations. I would like to thank them for that. Special thanks go to my wife's family. They have provided me with a home away from home with countless cookouts and family gatherings. Without them, I would not know about the pleasures of grilled sardines and home-made wine. I am also lucky to have great friends both in Germany and the United States. Particularly, I would like to thank Andreas Lohr, Artur Ottlik,

Michael Arens, Stephan Wanke, Alexander Czornik, as well as Ibrahim (Slash) and Añira Dahlstrom-Hakki. Finally, I would like to thank my wife Maria for her love, patience and support during these years. I could not have done it without her.

This work was supported in part by the Center for Intelligent Information Retrieval and in part by grant #NSF IIS-9909073. Any opinions, findings and conclusions or recommendations expressed in this material are the author's and do not necessarily reflect those of the sponsors.

ABSTRACT

RETRIEVAL OF HANDWRITTEN HISTORICAL DOCUMENT IMAGES

SEPTEMBER 2005

TONI MAXIMILIAN RATH

Diplom, UNIVERSITÄT KARLSRUHE (TH), GERMANY

M.Sc., UNIVERSITY OF MASSACHUSETTS AMHERST

Ph.D., UNIVERSITY OF MASSACHUSETTS AMHERST

Directed by: Professor R. Manmatha

Historical library collections across the world hold huge numbers of handwritten documents. By digitizing these manuscripts, their content can be preserved and made available to a large community via the Internet or other electronic media. Such corpora can nowadays be shared relatively easily, but they are often large, unstructured, and only available in image formats, which makes them difficult to access. In particular, finding specific locations of interest in a handwritten image collection is generally very tedious without some sort of index or other access tool.

The current solution for this problem is to manually annotate a historical collection, which is very costly in terms of time and money. In this work we explore several automatic techniques that allow the retrieval of handwritten document images with text queries. These are (i) word spotting, an approach that clusters word images to identify and annotate content-bearing words in a collection, (ii) handwriting

recognition followed by text retrieval, and (iii) cross-modal retrieval models, which capture the joint occurrence of annotations and word image features in a probabilistic model. We compare the performance of these approaches empirically on several test collections.

The main contributions of this work are a detailed examination of retrieval approaches for historical manuscripts, and the development of the first image retrieval system for historical manuscripts that allows text queries. This system extends the field of digital libraries beyond machine printed text into historical handwritten documents. Building such a system involves challenges on numerous levels: the noisy historical manuscript domain requires adequate image filtering, normalization and representation techniques, as well as a robust and scalable retrieval framework. We describe the construction of a prototype system, which demonstrates the feasibility of the proposed techniques for a large collection of handwritten historical documents.

TABLE OF CONTENTS

LIST OF TABLES

Table **Page**

LIST OF FIGURES

Figure **Page**

CHAPTER 1

INTRODUCTION

Handwritten document retrieval holds great promise for providing access to historical manuscripts for a large audience. Given a user query, handwritten document retrieval would find images of manuscripts that are relevant ("answers") to the query, which saves the user the tedious work of browsing or reading through an entire collection when looking for a particular document. This work provides a thorough examination of several retrieval techniques for handwritten historical document images that allow queries to be entered as text. We also address image processing and feature representation techniques for degraded document images. The described approaches have been used in the creation of the first retrieval system for handwritten historical documents. It is particularly appealing that the queries are textual, a fact that makes this system very practical. Previous work assumes that users would provide examples of writing samples that they would like to retrieve, which severely complicates the formulation of queries.

The first part of this work is concerned with the description of image processing techniques that are necessary to extract information from handwritten historical documents. In particular, noise removal, word segmentation, word normalization and feature extraction will be described.

In the second part, different approaches to annotating (labeling) and retrieving handwritten historical documents are outlined. These are *word spotting*, *recognition and retrieval* and *cross-modal retrieval models*. Word spotting is a technique that builds clusters of unlabeled word images by performing pairwise comparisons between

them. Ideally, all word images with the same annotation/transcription are placed into one cluster. We show how clusters which make good indexing terms can be selected automatically. Such clusters may then be manually annotated, allowing us to build a partial index for a document collection, similar to the index in the back of a book. Previous work has focused on the development of pairwise similarity measures for word images. Here we extend this work by completing the word spotting process. We show how to use the similarity measures for word image clustering, and how to select clusters which make good candidates for indexing.

The recognition and retrieval approach follows the main line of research on analyzing handwritten documents. A recognizer is used to automatically create transcriptions of all manuscripts in a collection. Then standard information retrieval techniques may be used on the resulting electronic text, in order to find items that are relevant to a given query. The handwriting recognizer that is used in this work recognizes words holistically, i.e. without word segmentation, using a Hidden Markov Model (HMM). We evaluate the error rate of the recognizer on historical manuscripts and compare the retrieval performance with that of other models.

Cross-modal retrieval models capture the joint distribution of word image features and annotation terms, building on past work in cross-language information retrieval of text. This model may be used to either obtain content models from queries or to create probabilistic annotations which are used in retrieval. The content models are feature distributions, which may be used to retrieve matching image content. Probabilistic annotation distributions may be used to estimate term occurrence frequencies in documents from observed image features. This makes it possible to employ the widely used language modeling approach to document retrieval. We evaluate our cross-modal retrieval models, compare their performance with the recognition-and-retrieval approach and demonstrate their scalability on large datasets.

A prototype retrieval system has been built using the cross-modal retrieval model. Its components and a brief discussion of the user interface are documented in the appendix. We conclude this work with an outlook on future work and make recommendations on how the current demonstration system can mature into a commercial-grade product.

1.1 Motivation

Libraries contain extensive collections of handwritten historical documents. Typically, only a small group of people are allowed access to such collections, because the preservation of the material is of great concern. In recent years, libraries have begun to digitize historical document corpora that are of interest to a wide range of people, with the goal of preserving the content and making the documents available via electronic media. Examples of such collections are the letters of George Washington at the Library of Congress (see Figures 1.1 and 1.2 for examples) and Isaac Newton's manuscripts at the University of Cambridge.

Historical collections are of interest to a number of people, not just historians, students and scholars who need to study the historical originals. For example, biologists can use handwritten field notes [33] to compare the current state of an ecosystem with conditions in the past. Paleoclimatologists are also interested in historical handwritten notes, such as farmer's diaries, since they often contain references to weather, which are indicators of the climate in the past.

Unfortunately, digitization alone is not enough to render historical document collections useful for such purposes. Having the information available in an electronic image format makes it possible to share it with many people across large distances via the Internet, Digital Versatile Discs (DVDs) or other digital media. However, the size of a collection is often substantial and the content is generally unstructured, which makes it hard to quickly find particular documents of interest.

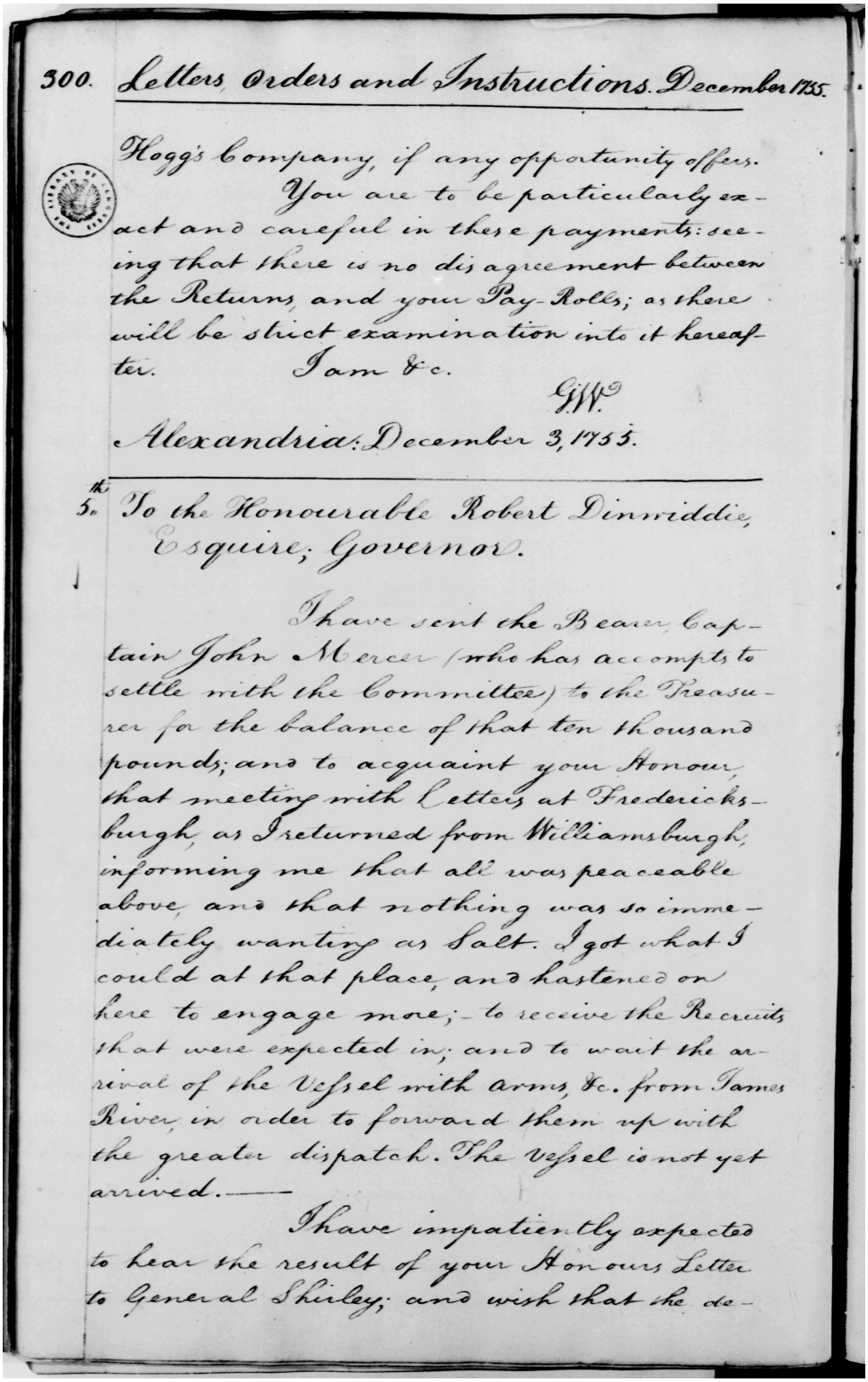

300. Letters Orders and Instructions. December 1755.

Hogg's company, if any opportunity offers.

You are to be particularly exact and careful in these payments: seeing that there is no disagreement between the Returns, and your Pay-Rolls; as there will be strict examination into it hereafter. I am &c.

G.W.

Alexandria: December 3, 1755.

5th To the Honourable Robert Dinwiddie, Esquire; Governor.

I have sent the Beaver, Captain John Mercer (who has accompts to settle with the Committee) to the Treasurer for the balance of that ten thousand pounds; and to acquaint your Honour, that meeting with Letters at Fredericksburgh, as I returned from Williamsburgh, informing me that all was peaceable above, and that nothing was so immediately wanting as Salt. I got what I could at that place, and hastened on here to engage more; - to receive the Recruits that were expected in; and to wait the arrival of the Vessel with arms, &c. from James River, in order to forward them up with the greater dispatch. The Vessel is not yet arrived. —

I have impatiently expected to hear the result of your Honours Letter to General Shirley; and wish that the de-

Figure 1.1. A scanned document from the George Washington collection.

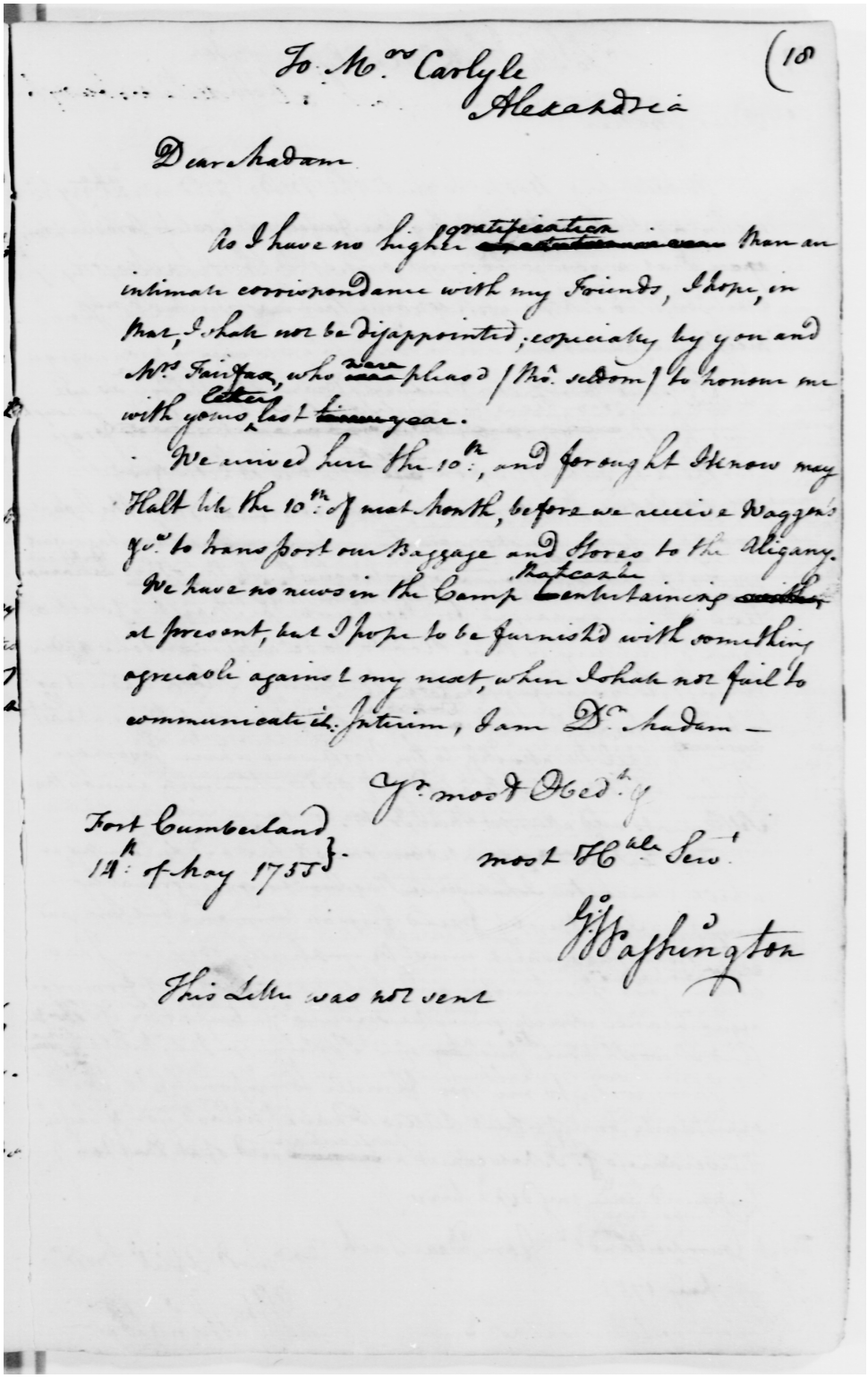

To Mrs Carlyle
Alexandria

(18

Dear Madam

As I have no higher gratification than an intimate correspondance with my Friends, I hope, in that, I shall not be disappointed; especially by you and Mrs Fairfax, who have pleas'd (tho' seldom) to honour me with yours, last year.

We arrived here the 10th, and for ought I know may Halt till the 10th of next Month, before we receive Waggons &c. to transport our Baggage and Stores to the Aligany. We have no news in the Camp but what is entertaining at present, but I hope to be furnish'd with something agreeable against my next, when I shall not fail to communicate it. Interim, I am Dr Madam —

Yr. most Obed.t &
most Hble Servt

Fort Cumberland
14th of May 1755

G.o Washington

This Letter was not sent

Various solutions for this problem that rely entirely on human labor are possible: a simple way of structuring a collection of historical documents is by ordering them chronologically. Electronic annotations of volumes or individual pages with the main subjects of discourse provide access at even finer granularity. A very high level of detail in content annotation may be achieved with transcription. It allows full-text search using a traditional text search engine. Because the cost for the electronic annotation of content increases substantially with the desired level of detail and the size of the annotated collection, usually a trade-off between detail and cost is chosen. In the case of the George Washington manuscripts, the Library of Congress decided to organize the approximately 152,000 page images in 9 *series*, each with a particular topic and ordered chronologically. Selected documents were transcribed to allow full-text search over portions of the corpus [110].

Automatic approaches to content annotation and retrieval are clearly desirable in order to reduce the often enormous cost of human transcription. Automatic recognition of handwritten historical documents may seem like an obvious choice, but handwriting recognition has only reached high levels of accuracy in two domains: these are *online* recognition, where a writer's pen strokes are recorded in real-time, and *offline* applications with small or highly constrained vocabularies, such as check processing or automatic mail sorting. Historical documents provide a host of challenges, including large vocabularies, inconsistent spelling, noisy document images. Such factors make it difficult to achieve good recognition results, and they require extra attention during the automatic processing of document images.

This work describes the techniques we have developed for the first automatic handwritten historical document retrieval system. We examine image processing and feature extraction techniques, three retrieval approaches and the construction of the first handwriting retrieval system that uses text queries. This system encompasses all levels of processing from an unordered collection of digitized images to a user interface

for the entire collection. The particular challenges that exist in various processing stages are addressed with appropriate solutions.

One of the biggest challenges for document image analysis systems is the great variability of handwriting. Many historical collections are the work of one author, which limits the amount of variation in the writing. Examples of such collections include the George Washington collection, Isaac Newton's handwritten documents and other collections that were authored by historical personalities. The techniques presented here assume that the analyzed document collection was produced by a single writer. This assumption is not strictly necessary. For example, G. Washington, whose papers are used extensively in this collection, employed multiple secretaries to write a substantial portion of his documents. Despite the variations in writing style, we were still able to apply the techniques presented here to his papers.

In the remainder of this chapter, we first define a number of terms which arise frequently in this work. Then we put our work in context by discussing related work, followed by a brief overview of the components of our retrieval system for handwritten documents.

1.2 Terminology

Various terms are used frequently in this dissertation. Some of the most common ones are defined here to establish a consistent terminology and in order to prevent confusion with similar related terms. The result may be seen as a mini-glossary, which the reader can refer to as terms occur.

This work is concerned with *handwritten historical documents*. In most places, we replace this somewhat bulky term by just *documents* or *manuscripts*[1]. In places where

[1]which, taken literally, means *written by hand*.

we discuss other types of documents, we use *printed documents* or *modern documents* to set them apart from handwritten or historical documents.

Our main objective is to look at document *retrieval*, using a query that is supplied by the user. The task of retrieval is to rank (order) the documents in the collection at hand according to their *relevance* to the query. This *ranked list* of documents is then presented to the user in that order, starting with the most relevant document. Retrieval is not limited to documents, but can often be easily extended to other *retrieval units*, such as paragraphs, lines and pages. In cases where this extensibility is straightforward we do not discuss it explicitly and just speak of retrieval units or documents, when discussing elements of ranked lists. As the title of this work indicates, we are retrieving *images* of text, so the user will always be presented with an image as the response to a query, be it of a line, a document, or of some other retrieval unit.

Retrieval systems usually establish an *index*, which organizes information about term occurrences in documents in such a way that it facilitates fast retrieval. Indexes can be as simple as the index in the back of a book, simply listing where certain important terms occur. Powerful text search engines often store more information, which may even allow the reconstruction of the original text content of the document collection the index was obtained from.

The question of what constitutes relevance to a particular query is difficult to answer and is often subject to debate. For our purposes, we consider a document relevant if it contains all of the query terms. This simple definition allows us to objectively assess the quality of various retrieval techniques. It has to be pointed out however, that most work in information retrieval typically uses a semantic notion of relevance. For example, in the widely used datasets of the TREC (Text Retrieval) conference [82], a topic is defined by a set of query words and a document is considered relevant to the query if it discusses the topic, even if none of the query words are used

in the document. This type of relevance definition requires a tremendous amount of human labor. Queries need to be selected and a large number of documents needs to be read in order to create relevance judgments. The cost of this approach would be prohibitive in our case. By using our simple definition of relevance, we are able to generate queries and relevance judgments automatically and we avoid controversy about whether a document is relevant or not.

When performing retrieval on documents in inflected languages, we might also consider documents relevant if they contain all of the query terms *in any morphological variation*. In that case, we would consider a document relevant to the query "walked", if the document contains the term "walking" because their *stem* is "walk". We can implement this definition of relevance by *stemming* both the query and the documents, and then using our earlier definition of relevance. Stemming reduces a morphological variant of a word to its root. For instance, in English the root form of a word is obtained by removing plural endings of nouns and using the infinitive in place of conjugated verbs. Inflections take many different forms depending on the language, requiring language-dependent stemmers.

Retrieval techniques are generally evaluated by running a set of queries. Intuitively, the higher a particular retrieval approach places relevant items in the ranked list, the better it performs. The two most common measures for judging the quality of a ranked result list are *recall* and *precision*. These measures are defined for a ranked list of a given length, starting with the highest (potentially most relevant) rank. Recall is the ratio of the number of relevant documents in the list and the total number of relevant documents. Precision is the proportion of the relevant documents in the ranked list. As more and more ranks are taken into account, recall increases monotonically, because more relevant documents will be found. At the same time precision typically decreases, because more non-relevant document will be appended to the list (usually relevant items tend to occur at the top of the ranked list). In

the information retrieval literature, it is customary to summarize a retrieval run by plotting interpolated precision at 11 recall levels (0 up to 1 in steps of 0.1; 0 recall is defined as the first returned relevant document), which are called *recall-precision* graphs. When multiple queries are used, the precision data points are averaged for the same recall level. Retrieval performance measures may be calculated with the `trec_eval` program [101], which can also test retrieval results for statistically significant differences.

In order to summarize a single ranked list with one measure, we will use *average precision*, which is the mean of all precision values at ranks where a relevant document occurs. When multiple ranked lists (resulting from multiple queries) are to be evaluated, we use *mean average precision*, which is the mean of the average precision values for each of the ranked lists.

This work is concerned with the retrieval of *images*. We refer to an image of a manuscript page, of a line of text, and of an individual word with the terms *page image* or *document image*, as well as *line image* and *word image*. By *page segmentation* we mean the process of breaking down a page into word images. *Word segmentation* refers to the segmentation of words into images of the contained characters.

Word images will be considered atomic units in this work, meaning they will not be broken down further into characters and analyzed in a bottom-up fashion as is customary in *analytical approaches*. We advocate a *holistic* approach to the analysis of word images. This allows us to avoid the difficult word segmentation problem and to solve the simpler page segmentation problem. A page segmenter turns page images into a collection of word images, which corresponds to the representation of electronic text documents, where the atomic units are also words.

1.3 Related Work

Previously published work related to this dissertation falls into the areas of handwriting recognition, content-based document retrieval approaches and recent developments in image annotation and retrieval. In the following sections, an overview of the relevant work in these fields is given.

1.3.1 Handwriting Recognition

Handwriting analysis research may generally be categorized into one of two areas [84]: *online* and *offline* handwriting. In both fields, Hidden Markov Models (HMM) are usually the tool of choice for recognition [86]. Originally used in speech recognition [40], they have later been applied to handwriting, because of the similarities to speech.[2] HMMs offer a way to infer the value of hidden/unobservable states (e.g. which words were written) using a sequence of observations (features extracted from the writing). Two particularly nice properties of HMMs are that they are computationally tractable using dynamic programming techniques (e.g. the Viterbi algorithm [25]) and can easily incorporate linguistic knowledge in the form of word or character bigrams. The latter can substantially improve recognition performance. HMMs have been applied at three levels in the recognition process: character recognition, word recognition and sentence recognition. Some of the most modern recognizers integrate all three in a hierarchical scheme (see for example [77]). Other techniques that have been used for handwriting classification include dynamic programming techniques and more recently Support Vector Machines (SVM).

In online handwriting recognition, a digital input device is used to record the x and y coordinates of the pen tip as a function of time and possibly other attributes such as pressure on the writing instrument, etc. The recognition rates that can be achieved

[2]The input to both speech and handwriting recognition is sequence data that is used to communicate text.

with such rich information are better than 80%, even for very large lexicons [84]. This success has prompted companies to deploy unconstrained handwriting recognition functionality in computers, such as TabletPCs and Personal Digital Assistants.

Offline handwriting recognition [84, 107, 115], on the other hand, is the task of recognition from a digitized image of the writing.[3] This branch of research has only yielded high recognition rates in domains that are highly constrained or have small vocabularies, such as mail sorting or automatic check processing [115]. Applications with small vocabularies tend to perform better, because there are fewer alternatives to select from, resulting in fewer recognition mistakes. If domain constraints are properly exploited, recognition rates may be improved. For example, a correctly recognized postal code of an address limits the choices for the city and street names.

Very high recognition rates are often achieved through rejection when the recognizer confidence is low. For example, the bank check reader described in [27] is claimed to have a recognition accuracy close to a human reader, but rejects about 30-40% of the checks. Current state-of-the-art offline recognizers achieve recognition rates of about 60% for vocabulary sizes ranging from 2703 to 7719 words [77] or 55.6% accuracy on a 1600 word lexicon [46]. Recently, recognition rates as high as 91% have been reported for a small single-writer test set of 117 lines [117]. As in most reported results, the datasets that were used in these experiments were obtained under controlled conditions to ensure straight writing, clean scans and other desirable properties. This is not the case with historical documents.

As a consequence, the recognition rates that can be expected on handwritten historical documents are lower: Tomai et al. [111] described an approach for mapping a perfect transcript to the corresponding historical document image, which used recognition. The lexicon of the recognizer was constrained to at most 11 words that were

[3]The present work is concerned with *offline* handwriting. Unless we indicate otherwise, our discussion here refers to the offline case.

obtained from the perfect transcript, but the alignment accuracy was still only 83% (some words that had poor image quality were not even considered in the evaluation). On a larger dataset, Lavrenko et al. [58] demonstrated that recognition of handwritten historical documents can be done holistically (without character segmentation) with an accuracy of 55% (65% if out-of-vocabulary words are not considered in the evaluation). These results were obtained with perfect word segmentation and good bigram statistics that were estimated using an external corpus.

Handwriting recognition approaches may further be classified into segmentation-based (or *analytical*) [77, 84, 107] and holistic analysis methods [64, 65]. Analytical recognition techniques segment word images into smaller units that can be recognized in isolation or when grouped. Characters are a natural unit and techniques for recognizing machine printed characters were developed by the optical character recognition (OCR) community. However, accurately determining the segmentation points cannot be done without first recognizing the characters. This is known as *Sayre's paradox* (segmentation requires recognition, which relies on segmentation) [103]. It has led researchers to consider multiple segmentation hypotheses by oversegmenting words into smaller units, such as strokes and image columns [107, 84]. In these approaches, the correct segmentation into characters typically arises *implicitly* from the recognition process, which attributes segments to recognized characters. Other approaches use *explicit* word segmentation. These attempt to segment a word into smaller units that are believed to be characters, which are then recognized [62].

Holistic word recognition techniques [65, 64, 58] view word images as a unit that will not be further segmented. They are often motivated by the *word superiority effect*, a phenomenon that was first observed by Cattell in 1886 [15] and later confirmed by Reicher in 1969 [96]. They found that humans have the ability to recognize characters faster than in isolation if they appear in valid (familiar) words. Other evidence that the global word shape plays an important role in the recognition of words was

found by Woodworth [120]. He noted that subjects could read lowercase text faster than uppercase text, which indicates that the changing word shape in lowercase text is used by humans when reading. Uppercase letters always have the same size, causing all-uppercase words to have approximately rectangular shape. In the domain of handwritten historical documents, other factors make a holistic approach attractive, such as the high level of noise and the writing variations, which can complicate the character segmentation.

The survey articles by Vinciarelli [115], Steinherz et al. [107] and Plamondon and Srihari [84] contain further reading on handwriting recognition.

1.3.1.1 Image Processing and Features

To a great extent, the accuracy of a handwriting recognizer depends on the preprocessing stage and the features which are used to represent the units to be recognized. Various processing steps need to be performed before the data is fed into a recognizer [115, 107]. Historical manuscripts often contain a substantial amount of noise that needs to be addressed, but modern documents also require preprocessing to normalize writing variations that may adversely affect recognition or retrieval performance.

Often times, scanned pages are slightly rotated (cf. Figure 1.1) or the binding is not removed from the originals, causing the scans to be warped. Such distortions may be reversed in the preprocessing stage. Hutchison and Barrett [36] present a technique for registering a set of documents containing information in a tabular format using the Fourier-Mellin transform to determine an affine warping transform. Cao et al. [14] reconstruct orthonormal projection images from pages that were scanned from an open book.

For historical data sets in particular, the removal of noise, such as border marks, paper discolorations and similar influences may be desired. Tan et al. [108] reported a technique for removing the effects of bleed-through (ink that travels through paper

from the other side of a page). Manmatha and Rothfeder [70] remove black margins and long lines that are used as layout elements before they apply their page segmentation algorithm.

The influence of noise and the lack of contrast in historical manuscripts due to faded ink may also require careful foreground/background separation. Leedham et al. compared several separation techniques in [59]. For historical Hebrew manuscripts, Bar Yosef et al. [123] described a multi-stage thresholding algorithm that works well for degraded and well-preserved documents.

Pages may contain non-text material, such as figures. In order to separate text from non-text regions, layout analysis and text detection techniques are necessary. Antonacopoulos et al. [1] described several algorithms that were submitted to the 2003 ICDAR page segmentation competition for printed documents. Breuel [11] presented an approach for finding maximal whitespace rectangles, which may be used for layout analysis. Once regions of text have been determined, they need to be broken down into lines and words. Relevant work in this area is discussed in more detail in the following section.

The appearance of word images typically varies in slant (tilt angle of writing) and skew (rotation angle). Such variations are typically removed, because they complicate classification tasks. Standard deskewing techniques are described in [10, 118], and deslanting techniques in [10, 44]. More details are given in chapter 2, where we describe the image techniques we used in our demonstration system.

The features that are used to represent recognizable image portions also play an important role. This work builds on features that were described in [89]. Other work on holistic features is by Madhvanath and Govindaraju [65, 64]. The literature describing features that are useful for the recognition of writing is large. A good overview of a variety of features for character recognition may be found in [113].

1.3.1.2 Page Segmentation

Page segmentation is an important part of any document analysis process. It turns a page image into a sequence of word images, which are the atomic units of our document retrieval system. Since it is one of the first steps in the analysis of documents, high accuracy is an important consideration. Page segmentation is usually performed by segmenting a page into lines, and then by further breaking up lines into words. When complex layout schemes or non-textual elements are used, e.g. when analyzing images of newspaper pages, a more elaborate process is necessary to extract blocks of text.

The difficulty of the problem depends largely on the spacing between adjacent lines or words. Not surprisingly, the segmentation of printed documents (e.g. [47]) is easier than the segmentation of manuscripts, because of the more consistent spacing.

Mahadevan and Nagabushnam [66] presented a gap metric approach for segmenting lines of handwritten text. All connected components are represented by their convex hull and a minimum spanning tree is used to connect the hulls from centroid to centroid. Segmenting a line now requires identifying connections between convex hulls, which are *inter-word* and not between characters within a word. The authors proposed a number of techniques to identify thresholds for cutting connections between convex hulls. Marti and Bunke [74, 76] also employed a gap metrics approach and proposed another way of picking a segmentation threshold. This algorithm was evaluated on a modern test collection of 541 text lines and yielded an error rate of 4.5%.

While earlier work has focused on documents of high contrast and neat writing, recent years have shown an increased interest in historical documents of unconstrained handwriting, which provide a greater challenge. Feldbach and Tönnies presented an approach for detecting and separating lines of handwritten text in historical church registers [23]. Their main problems were bending lines and the tight line spacing,

resulting in high overlap of the ascender- and descender-zones of adjacent lines. They estimated the location of the lower baseline by combining piecewise estimates to it; the upper baseline is then located in a search region that runs parallel to the lower baseline. On a collection of 246 lines, this algorithm was able to correctly identify and segment 90% of the lines.

The present work uses an approach by Manmatha and Srimal [71], which was later refined by Manmatha and Rothfeder [70]. The technique uses a scale-space approach [60] to segment word objects, which appear as connected "blobs" when the image is filtered with an anisotropic Laplacian of Gaussian kernel of a particular bandwidth (or *scale*). Manmatha and Rothfeder used a scale selection algorithm to choose the scale at which word images form connected blobs, but under- and over-segmentations are avoided.

Finally, we would like to mention that the page segmentation problem has also been investigated for online handwriting data (see for example [94] for line segmentation and [39] for a simple approach to word segmentation).

1.3.2 Document Retrieval

Document retrieval has been proposed for online handwriting data and offline documents (both printed and handwritten). Earlier approaches tend to require queries in the form of writing samples. Then the query can be compared with words in a collection using a matching function. Some later work supports text querying, which requires a way of turning textual queries into feature representations or vice versa. Retrieval may then be performed by matching in feature space or by using textual representations derived from images in the test collection.

1.3.2.1 Offline Documents

Tan et al. [109] described an approach to retrieving machine printed documents with a textual query (e.g. in ASCII notation). Their method describes both the query

and the words occurring in the document images with features, which may then be matched in order to identify query term occurrences. This paradigm of working in the content domain is not just applicable to retrieval, it may also be applied to other tasks. For example, Chen and Bloomberg [17] described an approach to generating document summaries from scanned images, which does not use OCR.

Early approaches to retrieving historical manuscript images made use of the *word spotting* idea, which was initially developed for speech data [42]. This technique can locate speech recordings that contain mentions of query words, by comparing a user-provided template to all candidate locations in a data base. When a 2-dimensional handwriting signal is transformed into a 1-dimensional signal, similar procedures can be applied to the handwriting domain.

The word spotting idea for handwritten documents was proposed by Manmatha et al. [69, 68, 67]. They suggested using a word image matching algorithm to cluster occurrences of the same word in a collection of handwritten documents. When clusters that contain interesting index terms are labeled, a partial index can be built for the document corpus, which can then be used for ASCII querying. Although a word image matching algorithm with high accuracy was presented and thoroughly evaluated by Rath and Manmatha [91], the experiments also showed that approaches based on matching words are computationally expensive and cannot yet be applied to very large collections. So far, all work on word spotting for document retrieval has focused on word matching techniques, which only allow retrieval using template queries, based on word image similarity. In this work, we complete the word spotting process by grouping word images into clusters, and automatically selecting candidate clusters for indexing.

Kołcz et al. [48] described an approach for retrieving handwritten documents using word image templates. Their word image comparison algorithm is based on matching the provided templates to segmented manuscript lines from the Archive of

the Indies collection. Kołcz et al.'s experiments only used a small number of queries and documents, and required multiple manually selected templates of the same word to yield good results. Since the query templates have to be provided in the image domain, the approach also does not allow textual queries.

More recently, Srihari et al. [106] have realized the importance of handwritten document retrieval and presented their own retrieval system that is mostly geared towards forensics applications such as writer identification. It combines word spotting, handwriting recognition and information retrieval techniques to allow textual and image queries for retrieval. The system only allows the retrieval of individual words or images thereof. Our work is more general, in that it allows the retrieval of units of text of arbitrary size, including documents, lines and individual words.

Vinciarelli [116] described retrieval experiments with a collection of 200 modern handwritten documents that were produced by a single author. He compared the retrieval performance on ground truth transcriptions and automatically recognized handwriting with a word error rate of 45%. When automatically generated transcriptions are used, the performance is worse with an acceptable decrease in precision.

Edwards et al. [21] described an approach to transcribing and retrieving medieval Latin manuscripts with generalized Hidden Markov Models. Their hidden states correspond to characters and the space between them. Only one training instance is used per character and character n-grams are used, yielding a transcription accuracy of 75%. The retrieval results seem strong, but the authors performed a non-standard retrieval evaluation without providing quantitative performance measures. Due to the choice of dataset, all characters exhibit little variation, so they appear almost as if they were printed. In terms of difficulty the problem appears to fall somewhere between isolated handwritten character recognition (often called ICR, Intelligent Character Recognition) and machine print recognition (i.e. OCR).

1.3.2.2 Online Documents

Lopresti and Tomkins [61] described an author-specific technique for searching online handwriting. They decomposed the query- and target-writing into strokes, which are then turned into sequences of quantized feature vectors (using feature clustering). A given query is compared to locations in the database using a dynamic programming approach, similar to the minimum edit distance algorithm. Recall at 22%/20% precision is 89%/81% for retrieval using roughly 6,000 query words from two writers.

In [39], Jain and Namboodiri presented an approach to retrieving online handwritten words from a given template, using dynamic time warping. Words are represented as one continuous stroke and three features are extracted at each sample point of the pen trajectory associated with a word. The authors reported a precision of 92% at 90% recall for individual word image retrieval, which outperforms Lopresti and Tomkins' approach above. However, the database is different, making a comparison difficult.

Kwok et al. [51] described a system for the retrieval of online documents with text queries. They used a recognizer to create "stacks" (vectors) of alternative recognition results per handwritten word. These stacks are then compared to a query stack using traditional retrieval models for document representations in vector space, such as Okapi [3] and cosine similarity. Their best results yielded about 80% precision at 80% recall.

Russell et al. [99] proposed a system for online handwritten document retrieval, which uses the concept of "N-best" recognition output (similar to Kwok et al.'s stacks [51]). A recognizer returns the N best recognition choices per word image, together with a probability as confidence score. These scores may be used in a probabilistic document retrieval framework. This and other retrieval techniques showed good performance on a large multi-writer dataset of 3342 documents, when using both textual

and template queries. The idea of using multiple words for annotating an image is also a theme that is common to the work in photograph annotation and retrieval, which is documented below.

1.3.3 Image Annotation and Retrieval

The cross-modal retrieval system described in this dissertation (chapter 6) is based on work in the image annotation and retrieval field. Most of the work in this area has been on general-purpose color photographs (e.g. from the *Corel* image collection), showing nature scenes, buildings, people, and other themes. These approaches annotate images with suitable text using recognition. Retrieval may then be performed using text queries with classical information retrieval models, instead of searching for matches in the image or feature domain (see e.g. [95]). The general approach is to model the statistical co-occurrence pattern of image annotations and image features. All of the approaches described below use annotated training collections to model the regularities of such patterns. More recently, some approaches have also targeted video keyframes (e.g. [24, 56]) and 2-D shapes [78].

Mori et al. [79] presented a system that can perform annotations of photographs. During the training phase, images are divided into regions using a regular grid, and similar regions are clustered based on color and image intensity gradient features. All annotation terms of the entire image are inherited by each region and used for learning an annotation distribution conditional on each cluster via maximum-likelihood estimation. When a new image is annotated, it is again divided into regions and an average annotation distribution is created from annotations of the closest region clusters.

Barnard et al. [6] extended Hofmann's hierarchical aspect model for text [34] to the domain of color images with annotations, in order to create a browsable hierarchy of images and to learn a mapping from image regions to annotation terms.

Observed images and their annotations are modeled as being composed of different aspects (semantic components) with an enforcement of a hierarchical structure, which implements the notion of a coarse-to-fine image composition. The Expectation-Maximization (EM) algorithm is used to train the model, which may then be used for browsing applications, image retrieval and annotation tasks.

An article by Duygulu et al. [5] showed an entirely new way to view the image annotation problem. The authors suggested treating object recognition as machine translation, an approach which they use for annotating general-purpose photographs. In their framework, images are segmented into regions, which are clustered to produce an image vocabulary of discrete tokens ("visterms", each token represents one cluster). Analogous to learning a lexicon from a parallel corpus in two languages, they train a translation model which can map image tokens to annotation words.

Jeon et al. [41] used the same representation but viewed the problem as cross-lingual retrieval and adapted Lavrenko et al.'s cross-lingual relevance model for text [53]. The resulting *cross-media* relevance models capture the joint occurrence pattern of words in two languages (one for annotation words and one for visterms). This information can then be used for image annotation and retrieval.

Recently, Lavrenko et al. [57] extended the relevance-based approach of Jeon et al. [41] by removing the need for discrete image representations. The resulting *Continuous-space Relevance Model (CRM)* operates on continuous representations of image regions in terms of multivariate feature vectors, and discrete image annotations in the form of words. This heterogeneous modeling captures the image representations in more detail, leading to significantly better performance than the previous relevance-based models, which operate strictly on discrete data.

Blei and Jordan [8] introduced three generative models for annotated data. The best-performing model, *correspondence LDA*, is an extension of Blei et al.'s *Latent Dirichlet Allocation (LDA)* [9]. The latter can explain discrete data, such as text, by

modeling it as being drawn at random from a mixture of probability distributions. Each mixture component is seen as a *topic*, which explains a particular aspect of the modeled distribution. Correspondence LDA models an image as consisting of multiple visual aspects, which themselves govern the annotations that are possible for the entire image. The authors present example results demonstrating good performance for image and region annotation, as well as text-based image retrieval.

Our cross-modal retrieval model (see chapter 6) builds on the discrete relevance model retrieval work by Jeon et al. [41] and its extension to continuous-space features [57].

1.4 System Components

Various processing stages are necessary to transform an unordered collection of manuscript images into an annotated corpus that supports retrieval with a user interface. Figure 1.3 shows an overview of our prototype system. The principal system components that this work is concerned with are image processing, feature extraction and content annotation. We also take a brief look at the retrieval system implementation with a suitable user interface. The term *content annotation* is used to refer to the part of the retrieval system that links manuscript images with text representations thereof. We have experimented with three approaches: word spotting, document recognition, and cross-modal models.

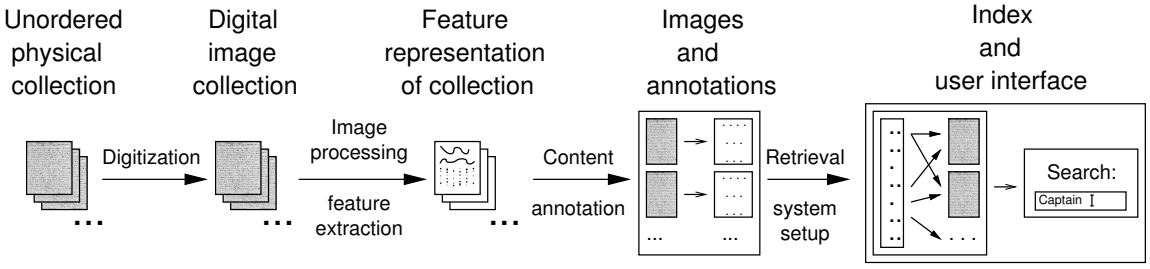

Figure 1.3. Main components and processing steps of the currently implemented prototype system.

In chapter 2 we describe the various image processing algorithms we use for page segmentation, noise removal and word image normalization. The features we use to represent word images are presented in chapter 3. The next three chapters (4 through 6) describe the three approaches for content annotation we have examined: word spotting in chapter 4, document recognition followed by text retrieval in chapter 5, and cross-media retrieval models in chapter 6. In appendix A we document the user interface of our prototype retrieval system, which was built using the cross-media retrieval model.

Before we describe the details of our retrieval system, we briefly explain the structure of our data and how it was collected in the following section.

1.5 Document Image Data

In this work, we present a number of retrieval approaches for handwritten historical documents. Assessing the relative performance of such techniques solely by looking at the procedures is very difficult. Convincing evidence of superior performance of an approach can only be obtained by testing the retrieval effectiveness on test data. In the following, we describe the structure and creation procedure of the datasets we used in our experiments.

1.5.1 Dataset Structure

Images of handwritten words are the atomic units that our retrieval approaches operate on. Hence, our datasets are sequences of word images, together with a label for each of the images. The label of a word image consists of the ASCII representation of all the characters and symbols that are visible in the word image (we ignore parts of characters from the line above or below the current word image). All word images result from applying a rectangular stencil (a *bounding box*) to the document image that contains them. Handwriting is commonly slanted (tilted) and can be tightly

spaced in the vertical direction. As a result, it is often impossible to separate an entire word image from a page image without also picking up parts from words to the left and right (or punctuation) and from the line above or below (see Figure 1.4 for an example).[4]

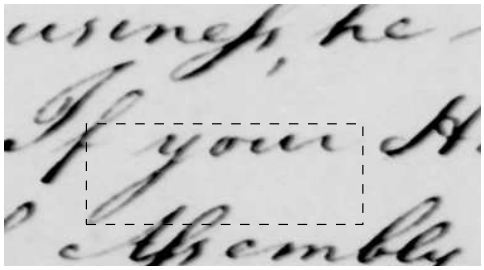

Figure 1.4. Unavoidable segmentation of parts from words other than the target word when using a rectangular stencil (target word inside dashed rectangle).

Each dataset consists of the original page images, the bounding box coordinate files (one per page image) and a file that assigns ASCII labels to each of the segmented word images. Organizing a dataset in this fashion is more flexible than just storing the sequence of word images that is produced by the page segmentation process: the current approach allows the use of different segmentation files together with the same page images and ensures that the entire page image is available for processing techniques that need to make use of it. The latter is particularly interesting for techniques that make use of spatial context when processing word images. The bounding box coordinates are stored in normalized notation, so they may be applied to page images at arbitrary resolutions.

1.5.2 Dataset Creation

A significant amount of time has been devoted to the creation of datasets for the evaluation of retrieval techniques. We used the following process:

[4]This could be remedied in some cases by preprocessing the page images before the word image segmentation. In particular, line deslanting (see section 2.3.3) and line separation would be useful. This is currently under investigation.

1. Selection of page images that will form the dataset. Depending on the intended use for the dataset, various aspects need to be taken into consideration. These include the quality of the documents (poor training data may impair retrieval performance), the handwriting style (when used as training data, should be a reasonable match for the test set), the topic (many words from different topics make a good training set) and others.

2. Obtain ASCII transcription data for the selected pages. Sometimes transcriptions can be obtained from an online archive (e.g. many transcriptions for the George Washington collection are available online [110]). If they are not available, they have to be entered manually by an annotator.

3. Tokenization of the transcriptions. The tokenization process splits transcriptions (which may be organized into lines, pages, ...) into a list of terms. Each entry in the tokenized list corresponds to a word image.

4. Automatic segmentation of page images. This step uses the algorithm proposed by Manmatha and Rothfeder [70] to turn a collection of page images into a sequence of word images.

5. Manually correct segmentation output. An annotator manually corrects the bounding box coordinates using the *BoxModify* tool [93]. The tool allows the manipulation of the segmentation output, and the displaying of word image labels (from the tokenization process) overlaid with each word location to quickly identify and correct alignment mistakes.

The above described procedure is intended for training data and test data with no segmentation mistakes, which may be used for evaluation under "ideal" conditions. In a more realistic setting, test data will be automatically segmented (no manual correction) and there may not be ground truth or it may only be available on a *per-*

page-image basis, not *per-word-image*. Section 6.3.2 discusses this problem in more detail.

In chapter 2, we now describe the challenges that historical manuscripts pose and we discuss how to reduce the influence of noise and handwriting variations with image processing techniques.

CHAPTER 2

NOISE, VARIABILITY AND IMAGE PROCESSING

Before scanned pages of historical manuscripts can be annotated or recognized, they have to undergo various processing stages. The reason for this is two-fold: first, the image data may be structured in a way that is unsuitable for downstream processes. For example, a downstream process might expect individual word images as input, but the available data is a sequence of page images. Second, the amount of noise and variability in the input data may complicate further processing. An example of this are ruler marks on a page which helped the author with the formatting. Such marks should be removed so that they are not mistaken for parts of words and misrecognized.

In this chapter, we describe all such processing steps that are performed on the image data. We begin by describing the noise and variability that is present in handwritten historical document images. Then we outline the segmentation of input page images into word images, followed by a description of noise suppression and image normalization strategies.

2.1 Noise and Variability

When working with historical documents, large amounts of image noise pose a challenge in addition to the typical writing variations that are present in handwritten documents. Most work on the analysis of handwritten documents focuses on modern documents, where the only concern is the variation in the writing (some exceptions are [23, 111, 21]). The documents used in such work are usually digitized

soon after their creation (e.g. see [77]), so that noise due to aging is not an issue. In this work, we focus on documents that have undergone an aging process, which has significant implications on their readability. The following sections describe where noise and variations occur that complicate the recognition or annotation of historical documents.

2.1.1 Handwriting Variations

Writing is a subconscious and highly individual process. Depending on the person, their physical condition, writing instrument and other factors, the appearance of the same text can vary when written at different times. Figure 2.1 shows several examples of the word *the* that were taken from the same page, so they were produced within a short time span. Even in this small sample there is a significant amount of variation that can be observed. The horizontal t stroke is not always present, varies in length when present, and sometimes takes on a second role as the stroke that connects the letters t and h.

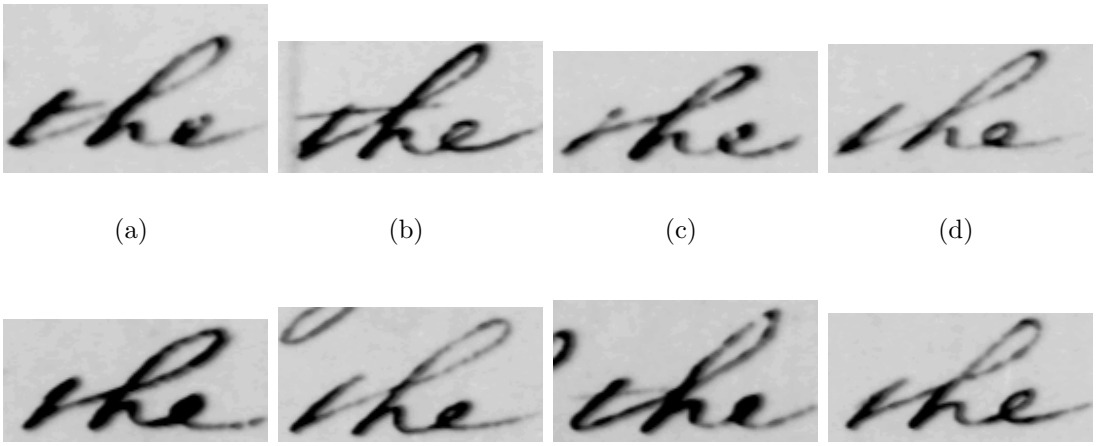

(a) (b) (c) (d)

(e) (f) (g) (h)

Figure 2.1. Examples of writing variations during a short period of time. All occurrences of the word *the* were taken from the same page. Notice variations in the horizontal t stroke, the connection between the t and h, as well as the presence of the opening/hole in the letter e and the size of the t compared to the e.

For the purpose of recognizing a word image, handwriting variations are similar to noise, since they add extraneous information which blurs the underlying structure that defines a word's identity. Such variations may have an artistic appeal for a human reader, but for a recognizer they are distracting details that should be filtered, just like digitization artifacts and smudges on a page.

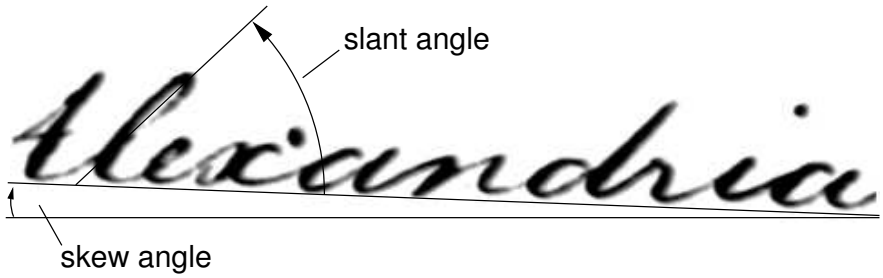

Figure 2.2. Slant and skew angle of a handwritten word.

When looking at the writing of a single person, the most common variations are differences in slant and skew (see Figure 2.2). The skew of a word is the rotation angle of the word with respect to the horizontal. Slant is the tilt angle of the writing. It is common practice in handwriting recognition [107, 115] to normalize the skew angle to 0 degrees and the slant angle to 90 degrees. Section 2.3.3 describes the slant and skew normalization techniques that are used in this work.

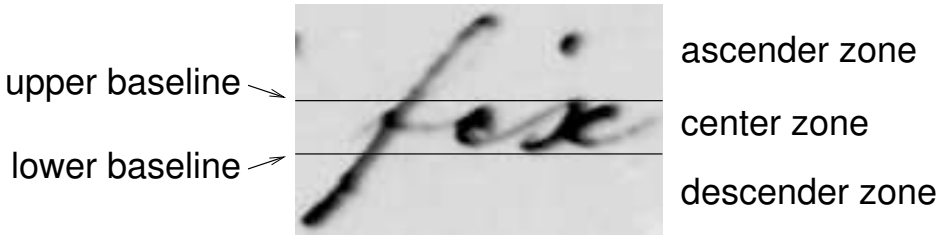

Figure 2.3. A word image with its three zones and the two baselines.

Another variation that is typical of handwriting is the size of the three word image zones. Figure 2.3 shows the three zones: the ascender-, center- and descender-zone,

which are defined by the upper and lower baselines. The two baselines determine the location of lower-case characters which have neither ascenders nor descenders (strokes which reach into the respective zones). The absolute and relative size of the three zones is often subject to variations. This is problematic if features are used which measure some location-dependent property in a word image. Feature values (and therefore positions) need to be comparable across different word images. This can be guaranteed by resizing the zones so that they occupy predefined fractions of a word image. Section 2.3.4 describes the word size normalization approach that was used in this work.

Finally, there are writing mistakes that have been crossed out, as well as variations and noise which were not intended by the author, such as ink spills and similar problems. In this work, we do not specifically address such noise. The page segmentation (section 2.2), however, ignores small ink spots and does not detect them as words.

2.1.2 Document Appearance Variations

Apart from the particular writing style, the author of a document makes various decisions about the appearance of the document. There are countless ways of arranging the same text on a page. This does not only affect where and how text is placed, but also what layout elements are used. For example, non-text elements such as boxes and rules may be added to the text. Even auxiliary components such as ruler marks may be mixed in with the actual writing. These are variations that occur as a choice of the author at the time of the document creation, and as such cannot be avoided. They require processing techniques that can extract text from documents in semantic blocks, which are then further analyzed.

Human readers have the ability to break down complex layout schemes into semantically coherent blocks and distinguish textual content from figures, layout elements or auxiliary components, such as ruler marks. The large amount of handwritten and

printed text that is used nowadays has resulted in an essentially unlimited number of layout schemes. Some documents follow strict rules (e.g. scientific publications), but quite often little or no layout rules exist (or they are ignored), and where they exist they may only loosely define the document structure.

This richness in structure explains the large body of work on text detection in images (e.g. [119, 121, 125]), on determining layout structure (e.g. [11]), and semantic blocks [30, 1]. The latter category is so challenging that it is even under investigation for documents that are available in an electronic format, which is used to define the layout (for example, for the semantic analysis of HTML pages see [80, 13]).

It is clear that a general solution to this problem does not yet exist. Therefore, in this dissertation we will focus on processing handwriting in documents once it has been located and separated from other document elements. In section 2.2 some techniques to discern writing from other objects are touched on.

2.1.3 Noise in Historical Documents

Depending on the age of a document, as well as the quality and timeliness of preservation efforts, historical manuscripts can exhibit a significant amount of noise. In addition, capturing an original manuscript as a digital image can also introduce further noise, depending on how much care is taken in the process. Here we describe the typical loss of quality that occurs (i) as an effect of time and (ii) during the digitization process.

2.1.3.1 Degradation Due to Age

Between their time of creation and digitization, historical documents are typically exposed to environments that adversely affect their quality. Common quality problems include tearing, water stains, mildew and others. Often times, the value of a collection is not known for a certain amount of time, so loss of quality occurs mostly before preservation efforts are made. However, if the preservation is not done

correctly, it can actually harm the quality of a collection. For example, the George Washington collection was initially administered by caretakers who tore signatures from pages in the belief this did not harm the value of the originals. They also dispersed parts of the collection, making it impossible to later collect the entire corpus in one place [110].

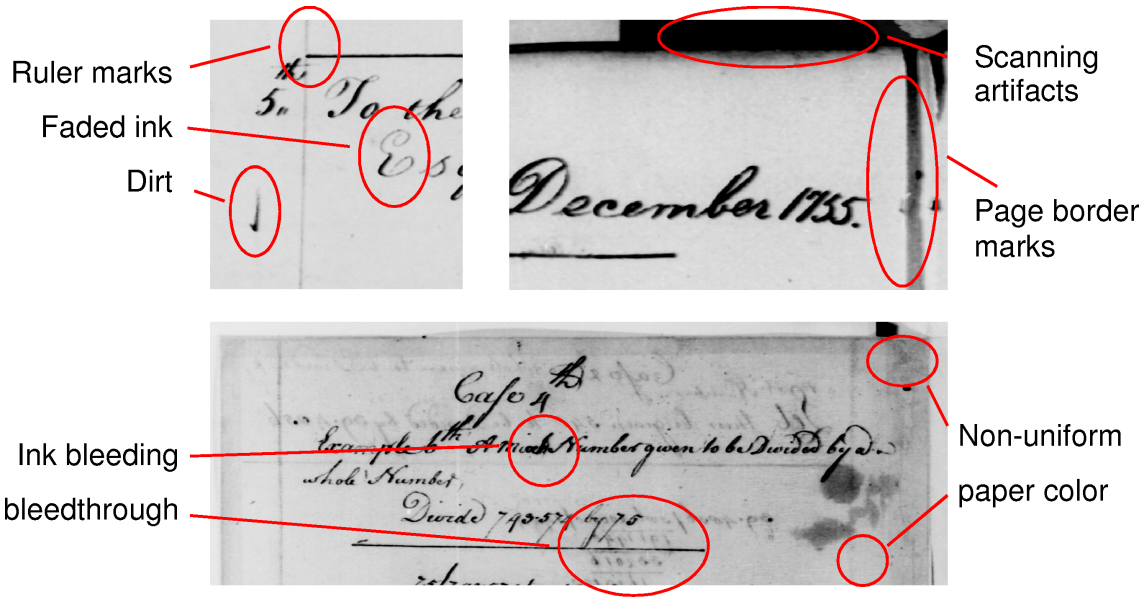

Figure 2.4. Examples of artifacts that typically occur in historical documents. All images are taken from the George Washington collection, which is used extensively in this work.

Figure 2.4 shows various types of document noise that can be observed throughout the Washington collection:

1. dirt marks,
2. non-uniform paper color: discoloration due to age,
3. stains and missing parts due to moisture, mildew and tearing,
4. faded ink, often not occurring uniformly across the page,
5. ink bleeding: ink that travels laterally in the paper,

6. bleedthrough: ink traveling through the paper from the other side of a page,

Once the damage has occurred to the originals, it is difficult to obtain high quality images from them. Sometimes scanning under special lighting conditions may reveal details that seemed lost to the naked eye. However, timely and professional preservation efforts are the key to high quality document images.

2.1.3.2 Noise from Digitization Procedure

The scanning procedure that is used to capture original documents in an electronic image format may also have a significant impact on the quality of the resulting images. Cost is often a major concern, which makes it difficult to use the best available equipment. Even though using the best possible procedures is desirable, it does not avoid all sources of noise. The following lists a number of noise sources that are typical of historical documents:

Digitization from reproductions: Some libraries already have copies of various documents on microfilm. This serves the dual purpose of making precious originals available to a greater audience, and to preserve a snapshot of an aging document collection. Handling original manuscripts is expensive and has to be performed by trained professionals, so scanning is often done from the microfilm, which does not require the same level of care and can be automated. This additional reproduction step adds noise and should therefore be avoided.

Document handling: When the scanning area is larger than the original document, the background behind the material is scanned. This usually results in borders of a particular color around a digitized manuscript. Since the originals may have holes and varying shapes due to disintegrating paper, the borders do not always have the same appearance.

Ideally, when the manuscripts to be scanned are bound, the binding is removed and the pages are laid out flat on a scanner. However, when pages of a bound

book are scanned, parts of the book may be visible in the digitized result. In addition, when the page is not flat, it may need to be rectified (see for example [14]). In the upper right corner of Figure 2.4 a part of a document binding is visible.

Sensor noise: Scanning sensors are subject to noise. For example, CCD sensor scans usually contain thermal noise components.

Sensor imperfection: A nonlinear scanner transfer function or hysteresis causes digitized images to have distorted pixel intensities.

Bilevel scanning: When bilevel scanning is used, the image intensity data is thresholded inside the capturing device. Usually there is no control over the threshold that is being used. This one-size-fits-all threshold may be appropriate for certain documents, but others can appear either overexposed or underexposed. While it may be possible to choose an optimal threshold for printed matter, historical documents usually should not be scanned in black and white. Grayscale or – even better – color scanning can help to capture fading ink and may also be used to distinguish the foreground (ink) from the background (paper, dirt, etc.).

Compression: Space is becoming less of a concern, but some digitization efforts have relied on lossy image compression formats, such as *JPEG*, to store scanned documents. Depending on the type of compression that is used, various artifacts may be introduced (see Figure 2.5 for an example).

Of course, this list is not complete and the particular types of noise that occur will always depend on the digitization procedure that is used. Humans are very good at discerning noise from structure. However, from our discussion here it should be clear that even if a document appears to be of reasonable quality, it probably contains a significant amount of noise.

(a) Edge image calculated from a lossless TIFF-compressed image.

(b) Edge image calculated from a lossy JPEG-compressed image.

Figure 2.5. Example of compression artifacts. Lossy JPEG compression introduces artifacts that can complicate image processing. The images show the influence of the artifacts on edge detection output.

2.1.4 The George Washington Collection

George Washington, the first president of the United States, was born on February 22, 1732 and died on December 14, 1799. All experiments in the present work were conducted on a portion of the approximately 152,000 pages of his papers that are held at the Library of Congress [110]. We will refer to this corpus as the *George Washington collection*, even though much of the writing is not Washington's but mostly of his secretaries. So the collection has been produced by a small number of writers, but only one author (George Washington).

All images exhibit quality problems that are typical for historical documents, such as faded ink, smudges, paper discolorations, ink bleeding and bleed-through. The images that were made available to us[1] were scanned from microfilm reproductions of the originals, which causes some loss of quality. All images are available in grayscale with 256 levels of intensity.

Many images have elevated counts of pixels with intensity level 193, an indication of a sensor imperfection. High-resolution TIFF images stored with lossless compression are available for most pages, but some are corrupted and only available in a lossy JPEG format at high compression. That format is inadequate for storing manuscripts,

[1]We would like to thank the Library of Congress for supplying the scanned manuscript images that were used in this work.

because of the artifacts it introduces around sharp edges (for example, strokes). Many of the manuscripts appear slightly rotated, which makes skew correction necessary.

In the following sections, we describe the processing stages that the manuscript images undergo, before they are handed to the feature extraction process.

2.2 Page Segmentation

After a collection of historical documents has been scanned, it consists of a series of page images. Our goal is to perform retrieval on the text contained in the pages, so we need to detect and extract the contained writing. To do this, each of the pages is passed to an automatic segmentation process, which produces a series of rectangle coordinates that can be used to extract word images from the input page. The detected word images are then passed to the subsequent processing steps in reading order. Figure 2.6 shows a portion of a page, with overlaid bounding boxes, as produced by the automatic segmentation process.

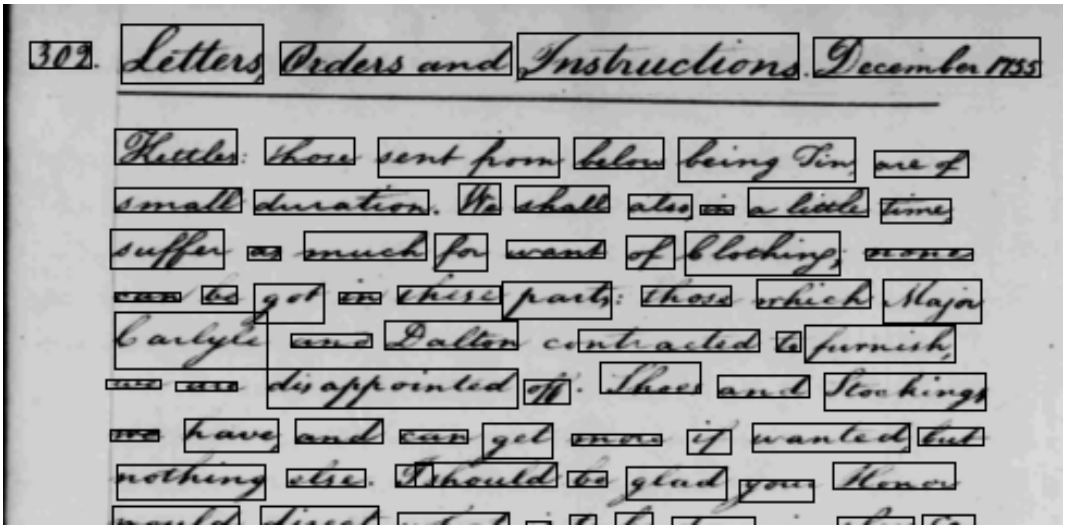

Figure 2.6. Portion of a historical document with detected word locations, as produced by the automatic segmentation process.

This problem may seem trivial at first glance, but the large amount of extraneous image content, the variations of ink and paper pixel intensities, and changing line-, word- and character-spacings make this a challenging problem. As shown above, historical documents often contain various defects and noise, such as border marks, dirt and faded ink, which can confuse automatic segmentation approaches. Therefore, simple segmentation techniques such as the gap-metric approach proposed by Marti and Bunke [76] cannot be applied to historical documents. They assume high-quality input documents, where the foreground and background can be easily separated and adjacent lines are spaced far apart. Bunke et al. developed their algorithm for segmentation of modern handwriting data that was carefully prepared to be clean of noise. Subjects that supplied writing samples were asked to write straight using ruler marks, to facilitate easy segmentation and processing [74].

In this work, we used the automatic page segmentation approach originally proposed by Manmatha and Srimal [71] and later refined by Manmatha and Rothfeder [70], which was developed specifically for historical manuscripts. It is based on scale-space theory [60], which can be used to segment objects of a particular scale in an image. The notion of scale is implemented by anisotropic Laplacian of Gaussian kernels, which are used to smooth the image in such a way that pixels forming an object will tend to appear as connected blobs.

Our objects of interest are handwritten words, so the goal is to choose a scale that allows the segmentation of words, but neither segments individual characters nor groups words together. Figure 2.7 shows an original image of a phrase and two scale-space versions of it. The chosen scale in figure 2.7(b) is not suitable for word segmentation, since blobs in the scale-space image correspond to units smaller than words (characters and word fragments) in the original. Figure 2.7(c) shows a scale-space image at the optimal scale for word segmentation. Here, each blob encompasses all characters in a word, without connecting across words. Manmatha et al.'s tech-

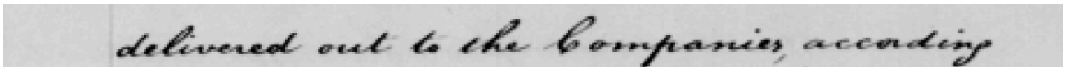

(a) Original phrase image.

(b) Non-optimal scale for word segmentation.

(c) Optimal scale for word segmentation.

Figure 2.7. Illustration of a phrase image in scale space at two different scales.

nique works best when the spacing between words and characters is consistent, and the space between characters is smaller than between words. Our experiments in section 6.3.1 show that segmentation mistakes have an adverse effect on the retrieval quality, but the performance decrease when compared to manual segmentation is acceptable.

Segmentation with this approach typically fails in the presence of layout elements, extraneous image content (e.g. stamps) and when the spacing is very narrow. In addition, since the words are segmented using rectangular bounding boxes, the slant of the words often causes the segmentation of parts from words to the left and right of the target word. When there is little space between adjacent lines, a word's bounding box may also contain parts of words from the line above or below. Section 2.3.2 describes an approach for removing such artifacts. The page segmentation algorithm removes borders around pages and some underlining by applying aspect ratio constraints to detected words. Additionally, detected regions are discarded if they contain very little intensity variation, which indicates a lack of text content. Therefore, we do not consider such cases in the further processing of word images.

2.3 Word Image Processing

In the current retrieval system, segmented word images undergo various processing stages that seek to remedy some of the most significant variations and noise that occur in historical document images. The following is a description of the processing techniques that we applied to filter noise and to normalize handwriting variations.

2.3.1 Contrast Enhancement

Fading and bleeding ink, as well as discolored paper may cause some word images to exhibit poor contrast. We enhance the contrast of all word images by scaling the image intensities linearly to span the maximum range of 0 to 255. This enhances the contrast of word images with faded ink, while altering images of high contrast only slightly.

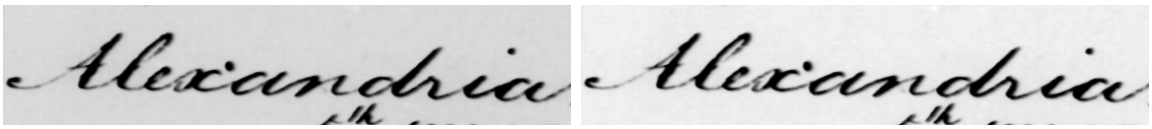

(a) Original image. (b) After contrast enhancement.

Figure 2.8. Example output of the contrast enhancement process.

We have conducted preliminary experiments with more advanced contrast enhancement techniques, that seek to fill in faded gaps by enhancing weak "bridges" of ink. This can be achieved by stronger enhancement of contrast in regions which have a high likelihood of containing faded ink, such as the area between the two baselines. So far, our efforts have not resulted in improved performance, but we believe that enhancements of weak ink strokes can result in more stable features and better recognition performance.

2.3.2 Artifact Removal

Artifact removal is the process that removes extraneous foreground content which is not part of the word in the given image. Parts from other words that reach into the bounding box of the target word image make up the bulk of such problems. This scenario happens most frequently when the line below or above the current line contains ascenders or descenders. Figure 2.9(a) shows a typical example of an image with ascenders from the line below reaching into the bounding box that is returned by the page segmenter.

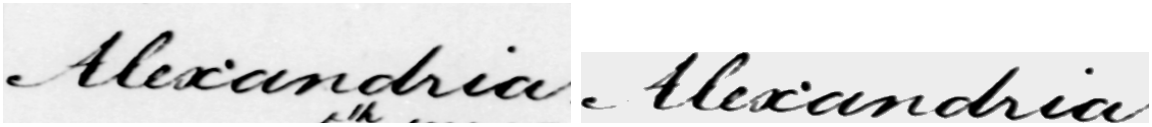

(a) Original image with artifacts. (b) Most artifacts removed.

Figure 2.9. Example output of the artifact removal process.

Previously used techniques [43] simply perform binarization of the image and connected component analysis. Components that do not exceed a certain size are then removed. While this preserves the main parts of the letters, it also discards important image components, such as i-dots and parts of the target word that may have become disconnected due to fading ink. In order to preserve smaller components, a different algorithm was developed. It fills in the space between the upper and lower baselines with black, and performs connected component analysis after binarization. All components that intersect with the upper and lower image boundary are removed. This is to make sure that only components are removed that *reach* into the box surrounding the word image, not components that are entirely contained within the image. Figure 2.9(b) shows the image in Figure 2.9(a) after artifact removal. It also reveals one weakness of the current approach: Along with small unconnected parts of words such as i-dots, dirt is also preserved (next to the letter x). We do believe,

however, that i-dots (or, more generally, diacritics in other languages) make very good features, similar to ascenders and consequently should not be discarded.

2.3.3 Deslanting and Deskewing

Skew and slant, i.e. the rotation and cursive tilt angle of a word are commonly normalized during the preprocessing stage, since they often have a strong effect on the feature representations of word images. Skew correction [10, 118] is generally performed by fitting a line to the local minima of the lower word contour near the lower baseline, ignoring minima that result from descenders. This is also the approach we use in this work.

(a) Skewed and slanted word image. (b) After deskewing. (c) After deslanting.

Figure 2.10. Example outputs of the deskewing and deslanting processes.

Various methods exist for determining the slant angle [10, 44]. One is to deslant a word at various angles and to use the slant angle that yields the largest distance between maxima and minima of the upper word contour (or some other measure of "deslantedness"). Another uses the orientation histogram of the word contour in order to estimate the slant angle.

In the currently implemented prototype system, both slant and skew are normalized to the same angle (90° and 0° respectively) before word features are extracted. Figure 2.10 shows a typical result of the deskewing and deslanting stage.

2.3.4 Word Size Normalization

Some of our features describe locations in a word image, such as the distance of the first ink pixel from the top of the image. Such features should be comparable

across images, even if they are of different sizes. A simple normalization could map the horizontal and vertical range of the image to the unit interval. However, this leads to problems with images that do not have descenders or ascenders, such as *arm* and *Alexandria*. With tight bounding boxes around the word images, the bottom of the word *Alexandria* corresponds to the location of the lower baseline, whereas the bottom of the word *Regiment* would correspond to the bottom of the descender-zone (because of the descender *g*). A similar problem occurs when a word does not have any ascenders.

(a) Input image.

(b) After padding to compensate for missing descender zone.

Figure 2.11. Example output of the word size normalization step.

We normalize the size of words by padding the images at the top and bottom as necessary to create an empty descender or ascender zone. Then the image parts above and below the lower baseline are scaled to move the lower baseline to a predefined location (2/3 of the height from the top).

After the completion of the processing steps described here, the images are passed to the feature extraction process, which is described in detail in the following chapter.

CHAPTER 3

IMAGE REPRESENTATION

Working on images in their original raw format, e.g. a pixel matrix produced by an upstream processing step, is often inefficient and difficult. Representing images in terms of *features* allows (among other things) a more compact and descriptive characterization of images with limited redundancy. The right feature representation makes classification easier, so it is an important choice [19, 73]. For example, word images are often highly redundant because neighboring pixels tend to have similar pixel intensities. Good feature representations of word images are usually of much smaller dimensionality, better suited for classification and more easily manageable. In this chapter, we lay out representation techniques we have chosen for word images in historical documents.

We advocate a holistic approach to word image analysis, that is, we annotate or recognize images of *entire words*, not characters or other units smaller than whole words. This is reflected by the features we choose for representing word images.

The various classification techniques we employ in this work constrain the features that can be used. Therefore, we do not present *one* feature representation that is used with all classifiers, but rather a variety. All of the representations have in common that they are derived from scalar features and profile features. Scalar features measure global image properties such as the image width, and profile features capture a word's shape in detail. Based on these features, we describe three word image representations: (i) raw features (scalars and profiles) that are extracted directly from

the images, (ii) feature vectors of constant length with continuous-valued entries, and (iii) representations that consist of entries from a discrete feature vocabulary.

3.1 Features

Many word images can be distinguished easily by looking at simple holistic features such as the width of the word in pixels. However, differing word images with the same coarse features require a more detailed description, in order to distinguish between them. Previous work [89, 91] has shown the value of profile-based features (e.g. projection profiles) for this task. Consequently, the feature set that is used for representing word images consists of a coarse-to-fine range of features.

Scalar features may be easily compared across different word images (height of one image vs. height of another), but the profile features we use vary in length based on the width of a word image and such profiles cannot be compared sample-by-sample, even when the length of the profiles is normalized.[1] A fixed-length description of profile features may be obtained by computing lower-order coefficients of a DFT (Discrete Fourier Transform) of each of the original profile-based features. Together, the scalar and profile-based features then form a vector of fixed length for word images of any size.

In the following sections, we first describe the scalar and profile features. We then show how these variable-length representations may be turned into feature vectors of constant length that may be compared component-by-component. Finally, we describe the generation of a discrete feature vocabulary that may be used to represent word images with tokens from the vocabulary. This allows us to represent word images as "documents" in the "image description language" which is generated by the feature vocabulary.

[1] This is, again, due to the variations in handwriting.

3.1.1 Scalar Features

Each of the features described here may be expressed using a single number. Some of them have been used previously (see e.g. [91]) to quickly determine coarse similarity between word images. The following information is collected from a given image with a tight bounding box (no extra space around the word):

1. the height h of the image in pixels,
2. the width w of the image,
3. the aspect ratio w/h,
4. the area $w \cdot h$,
5. an estimate of the number of descenders in the word, and
6. an estimate of the number of ascenders in the word.

While the aspect ratio and area features are redundant, their distributions differ from those of the height and width features.

3.1.2 Profile Features

These variable-length features capture a word's shape in much more detail than single-valued features can. Each feature results from recording a constant number of values per image column of the word, thus creating a profile or "time series" (x-axis=time) of the same length as the width of the image.[2] We will first look at 1-dimensional profiles (one extracted value per image column) and then turn to multidimensional profile features, which record two or more values per image column.

[2]Treating the feature profiles as time series allows us to apply techniques (e.g. the discrete Fourier transform) that have been developed for such series.

3.1.3 1-Dimensional Profiles

Figure 3.1 shows a set of 1-dimensional profile features and the image (shown twice in Figures 3.1(a) and 3.1(b) for easy comparison to the feature values) they were extracted from.

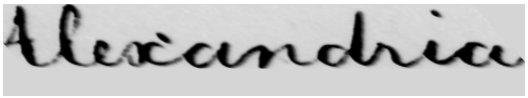

(a) Preprocessed image.

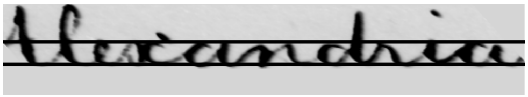

(b) With estimated baselines.

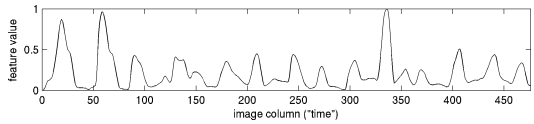

(c) Normalized (and inverted) projection profile feature.

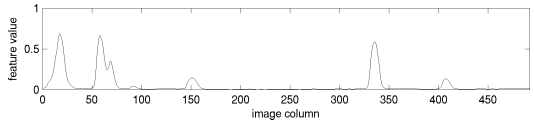

(d) Partial projection profile (pp) above both baselines ("upper projection profile").

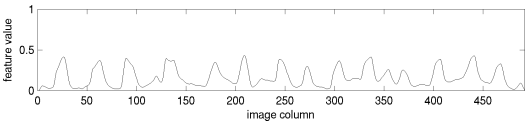

(e) Partial pp between baselines ("middle projection profile").

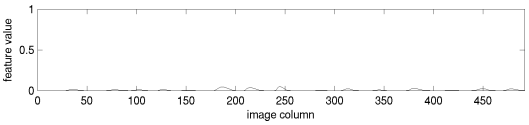

(f) Partial pp below baselines ("lower projection profile").

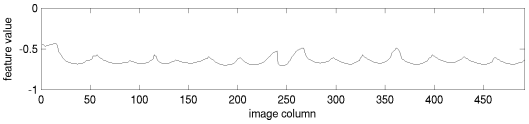

(g) Lower word profile.

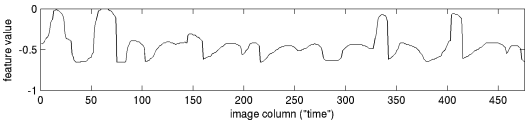

(h) Upper word profile.

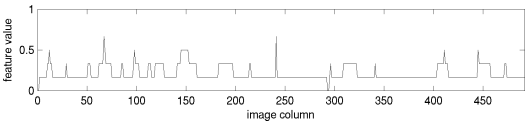

(i) Normalized number of background-to-ink transitions feature.

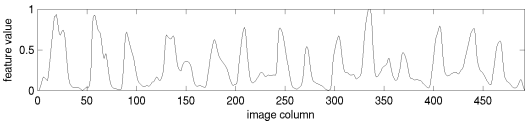

(j) Normalized variance of column pixel intensities feature.

Figure 3.1. Examples of profile features as extracted from the given preprocessed word images.

The profiles are:

Projection profile: Each value in the profile is calculated by summing over the pixel values in the corresponding image column. Figure 3.1(c) shows the plot of a typical projection profile. We invert the image before the calculation, causing concentrations of ink to create peaks, because we would like to measure the ink contained in each column. The descriptive power of the modified profile remains unchanged.

Partial projection profile: The three partial profiles in Figures 3.1(d), 3.1(e) and 3.1(f) result from calculating projection profiles for three horizontal strips in the original image: above, between and below both baselines. A single normalization factor is used for all of the three profiles, because the top and bottom strips can exhibit low variation of the feature values, when the word has no ascenders or descenders (e.g. see Figure 3.1(g)). If all profiles were normalized separately, slight errors in the baseline position estimation could seriously affect the result.

Upper/lower word profile: Upper (lower) word profile features are computed by recording – for each image column – the distance from the upper (lower) boundary of the word image to the closest "ink" pixel. Ink pixels are determined by a thresholding algorithm that classifies pixels into the categories *ink* and *paper*. If an image column does not contain ink, the feature value is computed by linear interpolation between the two closest defined values. Figures 3.1(g) and 3.1(h) shows two typical profiles (feature values are inverted).

Background to ink transitions: This feature (see Figure 3.1(i)) records, for every image column, the number of transitions from the background to an "ink" pixel.

Grayscale variance: The normalized variance of the grayvalue intensities in every image column is recorded for this feature (see Figure 3.1(j)).

The quality of the extracted features strongly depends on good normalization, as detailed in section 2.3.3. For example, slant can affect the visibility of parts of words in terms of the word profile features (e.g. the l leaning over the e in Figure 2.2).

3.1.4 Multidimensional Profile Features

The features we present here result from recording two or more feature values per column of a word image. Taken together, these values form one multidimensional profile with a length equal to the width of the image they were extracted from.

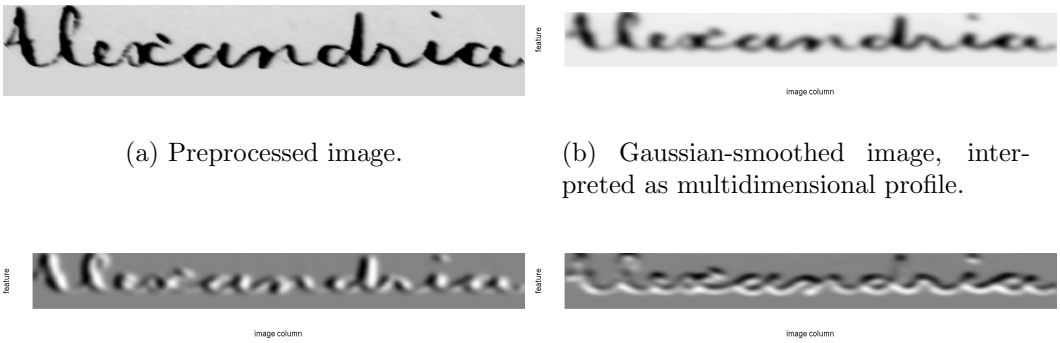

(a) Preprocessed image.

(b) Gaussian-smoothed image, interpreted as multidimensional profile.

(c) Horizontal partial derivative Gaussian kernel response.

(d) Vertical partial derivative Gaussian kernel response.

Figure 3.2. Multidimensional profile features (b)(c)(d) and the preprocessed image they were derived from (a). The multidimensional profiles are of dimension 15; feature values are visualized as grayscale intensities. The kernels' scale is $\sigma = 4$ pixels.

We investigated the following features:

Gaussian smoothing: The original image is smoothed with an isotropic Gaussian kernel and resized to a generic height (15). Each line of the resulting image is now interpreted as a separate feature profile. Figure 3.2(b) shows the feature set extracted from the original in Figure 3.2(a). All 15 profiles are shown together with the feature values displayed as grayscale intensities.

Gaussian derivatives: Similar to the feature set obtained from Gaussian-smoothing, these two sets are obtained from convolving the input image with a horizon-

tal/vertical partial derivative of a Gaussian kernel. These filters respond to horizontal and vertical edges in the original image, which are widely used as features in computer vision, because they can usually be reliably located. Figure 3.2 shows the resulting feature sets after convolution with horizontal/vertical derivative kernels and resizing to the generic height.

3.1.5 Feature Performance

The descriptive power of the above profile features was determined by evaluating their performance in a whole-word matching experiment [91]. 15 query images were selected from a dataset of 2381 word images [43] and each of the queries was used to rank the remaining images in the collection based on their similarity to the query. The ranking function is based on a *Dynamic Time Warping (DTW)* similarity measure defined on profile features (see section 4 for details). Unlikely matches were discarded beforehand by imposing a threshold on the scalar features that were extracted from both the query and the candidate image. Discarded images are not included in the ranked result list.

Test Run	**Description**	**Mean Avg. Prec.**
1-Dimensional Profiles	Projection Profile (∗)	50.29%
	Upper Projection Profile	49.91%
	Middle Projection Profile	30.83%
	Lower Projection Profile	24.85%
	Upper Word Profile (∗)	**64.29%**
	Lower Word Profile (∗)	42.99%
	Bg./Ink Transitions (∗)	42.46%
	Graylevel Variance	37.88%
Multidimensional Profiles	Gaussian Smoothing (∗∗)	**62.78%**
	Gauss. Horizontal Der. (∗∗)	59.63%
	Gauss. Vertical Der. (∗∗)	52.49%
Feature Combinations	(features marked with ∗)	**72.56%**
	(features marked with ∗∗)	67.31%

Table 3.1. Performance of various features and feature combinations, measured in terms of mean average precision.

We ran retrieval experiments using all of the 1-dimensional and multi-dimensional features separately, followed by combinations of the best-performing profile features in these two groups. Table 3.1 summarizes the obtained retrieval results using mean average precision.

Among the one-dimensional profile features, the upper word profile performs best with 64.29% mean average precision (MAP); among the multi-dimensional profile features, the Gaussian-smoothed feature performs best with 62.78% MAP. Since the features are designed to respond to different shape characteristics and should complement one another to some degree, we also analyzed combinations of the 4 best performing one-dimensional profiles and all three multidimensional profiles. The combination of the one-dimensional profiles outperforms the multi-dimensional profile combination with a MAP score of 72.56%.

These results are the motivation for using the combination of upper, lower, and projection profile together with the background-to-ink transitions profile in further experiments. However, we are not using the background-to-ink transitions profiles in the generation of length-normalized feature vectors, which we describe in the next section. The reason is that these profiles often contain a large number of strongly localized peaks (high-frequency components), which cannot be adequately captured by lower order Fourier coefficients (low frequency approximation).

3.2 Feature Vector Length Normalization

While the above profile features capture the shape of a word in great detail, they vary in length, and cannot be easily compared. One-to-one comparison of samples in two profiles obtained from different words is usually impossible, simply because the profiles are of different length. Even if one of the profiles were to be scaled to have the same number of samples as the other profile, a one-to-one comparison would not be adequate. The reason for this lies in writing variations, which cause the features to

be compressed and stretched in a non-linear fashion. As a consequence, linear scaling of one of the signals does not cause feature values which correspond intuitively to appear at the same sample points (see Figure 4.3 for an illustration of this effect).

Chapter 4 describes how two non-linearly scaled signals can be compared using *Dynamic Time Warping*. While this algorithm provides a good matching score that takes into account all details of the compared signals, it can be quite expensive and its indexability is limited as we will see. With a profile representation in terms of a vector with constant length, where the components can be compared in a one-to-one fashion, we could overcome these two shortcomings using fast distance measures (e.g. Euclidean distance) and spatial access methods [22].

3.2.1 Fourier Coefficient Representation

The Discrete Fourier Transform (DFT) [22] offers a nice way to obtain such a fixed-length feature vector from profiles of varying length. When the original signal is described by a number of lower-order DFT coefficients, an approximate reconstruction is possible. Most of the energy of the original signal is typically contained in the lower coefficients[3], yielding a good approximation of the global feature profile structure (see Figure 3.3), and hence the coarse word shape. Signal noise and fine-grained writing variations result in higher-order DFT coefficients that are not useful for classification. Such coefficients are discarded, because they can adversely affect classification performance. In the next section, we look at how the number of lower-order DFT coefficients to be used may be chosen empirically.

Figure 3.3 shows clearly that the effect of keeping lower-order coefficients and discarding the higher-order ones is that of a low-pass filter. Fine-grained detail and signal noise is ignored by smoothing the profile. The DFT representation also takes

[3]An exception are signals with many high-frequency components. For an example, see Figure 3.1(i).

into account that images may have different lengths, since one period of the lowest-order DFT basis function is equal to the number of sample points in the input signal (the DFT basis adapts to different input signal lengths).

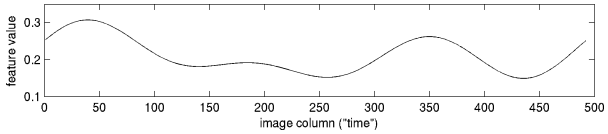

Figure 3.3. Projection profile time series from Figure 3.1(c), reconstructed using 4 lowest-order complex DFT coefficients (4 cosine components, 3 sine components).

The DFT is performed on the time series $\mathbf{f} = f_0, \ldots, f_{n-1}$ to obtain its frequency-space representation $\mathbf{F} = F_0, \ldots, F_{n-1}$:

$$F_k = \sum_{l=0}^{n-1} f_l \cdot \mathrm{e}^{-2\pi i l k/n}, \qquad 0 \leq k \leq n-1. \tag{3.1}$$

Then the first c real (cosine) components and $c-1$ imaginary (sine) components are extracted from the DFT representation for use as scalar features.[4] Together with the 6 scalar features, the first $2 \cdot c - 1$ components of $\mathbf{F}$ form feature vectors of constant length (dimensionality) $d = 6 + 3 \cdot (2 \cdot c - 1)$ (we use DFT coefficients from 3 profiles: projection profile, upper, and lower profile). Most of our experiments use $c = 4$, that is, a total of 27 features. We normalize the range of feature values along each dimension to lie in the range $[0, 1]$. Then all continuous-space feature vectors of constant length are members of the feature space $\mathcal{F} = [0, 1]^d$.

3.2.2 Length of DFT Representation

As we have pointed out in the previous section, the lower-order DFT coefficients capture the coarse word structure, while higher-order DFT coefficients either result from noise or writing variations which may have an adverse effect on the quality of

[4]For real-valued signals, the first imaginary (sine) coefficient of the DFT is always 0.

a classification process that uses the coefficients as features. This immediately raises the question of how many coefficients to use. When the number is chosen too small, relevant information about the structure of an image is discarded. On the other hand, using too many coefficients will introduce noise into the feature representation, which is likely to decrease classification performance.

In order to determine the ideal number of DFT coefficients, we recorded the word image recognition performance for various lengths of the frequency space representation. The experiment uses the 20-page dataset and 20-fold cross-validation setup described in [58]: 19 pages are used as the training set, while the word images in the remaining page are recognized. Classification is performed using 1-nearest-neighbor on a feature vector consisting solely of DFT coefficients from three profile features (projection profile, upper & lower profile; see section 3.1.2).

The coefficients in the frequency-space representation vary in very different ranges. Lower-order coefficients usually have a much higher magnitude than higher-order coefficients. We used both the raw coefficients ("No feature normalization") and a feature vector where all dimensions have been normalized to lie in the range $[0, 1]$ ("With feature normalization"). Figure 3.4 shows the *Word Error Rate (WER)* (1− classification rate) as a function of the number of DFT coefficients. One coefficient refers to both the real and imaginary part of a coefficient, so the feature vector for c coefficients from one profile has $2c-1$ components (we discard the first sine coefficient, because it is always zero).

The first thing to note about the graph is the location of the minimum word error rate. In the run with feature normalization, the minimum occurs at 6 coefficients (WER=47.9%); in the run without normalization it occurs at 8 coefficients (WER=53.2%). The run with feature normalization performed better, but also requires a more careful selection of the number of DFT coefficients: the error rate rises quickly with higher numbers of coefficients, whereas the run with non-normalized

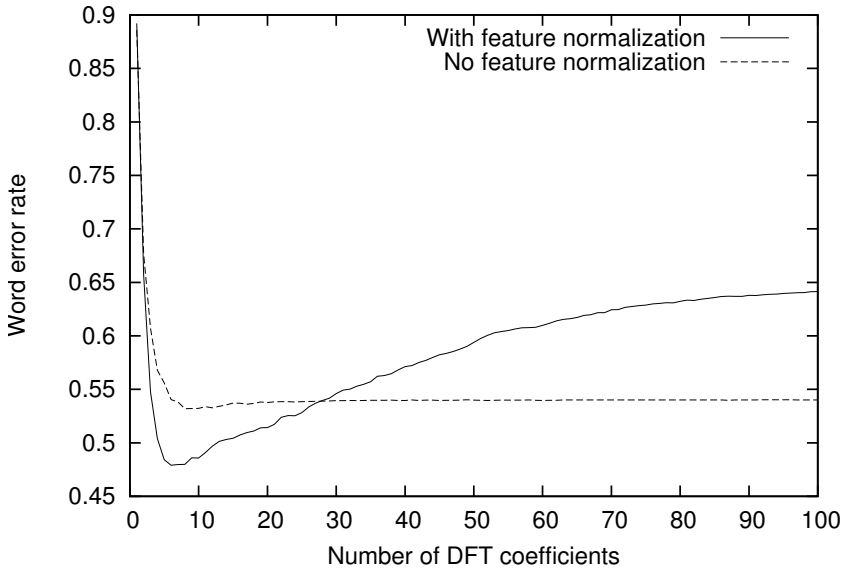

Figure 3.4. Word error rate as a function of the number of DFT coefficients. The two runs show the results with and without normalizing each feature vector dimension to the range $[0, 1]$.

feature vectors remains roughly at the same word error rate even for higher-order coefficients. The stable performance for a large range of mostly higher-order DFT coefficients can be attributed to the magnitude of the coefficients. The coefficient magnitudes decrease rapidly for increasing frequencies, causing higher-order coefficients to have a negligible impact on the distance we use for the nearest-neighbor classification.

The normalized run confirms our intuition about the descriptiveness of features: when too few coefficients are used, relevant information about a word's structure is discarded, leading to poor classification performance. When the right number of coefficients is used, the word error rate is minimal, but rises again for higher numbers, when noise and writing variations taint the word image representation.

We predict that the ideal number of DFT coefficients to use depends on the quality of the preprocessing. If the preprocessing is not effective at normalizing writing variations, the minimum error rate will be reached at a smaller number of coefficients, because higher-order coefficients will be too noisy to aid in classification of word

images. On the other hand, if the preprocessing removes most of the variations, even higher-order coefficients will contain information that can be used to compare the structure of a word image at a fine level of detail.

To allow a direct comparison of our performance figures with those in previously published work, most of our DFT coefficient representations in this work use $c = 4$ complex components (7 real coefficients) to represent a single profile feature. With the DFT coefficients from 3 profiles (projection, upper and lower profile) and 6 scalar features, this yields a total of 27 features. We note that while $c = 4$ did not yield the lowest word error rate in our experiment above (cf. Figure 3.4), it is very close to the optimal setting ($c = 6$) with a comparable word error rate.

3.3 Word Image Description Language

Two of the retrieval techniques that are described in this work were originally developed for cross-lingual information retrieval of *text* documents [53]. The cross-lingual framework allows a user to formulate a text query in a familiar language (e.g. English) and retrieve documents in a foreign language (e.g. French). We can extend this paradigm to images of words, which can be viewed as being the translation of their ASCII equivalent. In that sense, images of words are an equivalent representation of an ASCII word in an "image language". When we represent word images with (one or more) terms from a discrete *image description* dictionary, the cross-lingual retrieval approach can be applied to the domain of handwritten word images. The retrieval then spans two different media types and will thus be referred to as cross-*modal* retrieval.

In previous work [20, 41], continuous-space feature vectors have been turned into discrete feature tokens using k-means clustering. This spawns a vocabulary consisting of discrete items (henceforth *tokens*), which can be used to describe originally continuous-valued feature vectors with a discrete token. We believe that the clus-

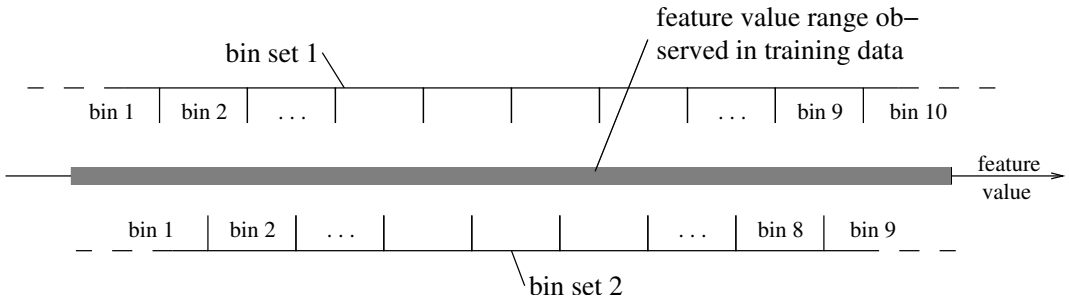

Figure 3.5. Illustration of the binning technique that is used to map continuous feature values to discrete feature tokens.

tering of entire feature vectors corresponds to a premature classification decision in feature space that may remove details which could aid in a subsequent classification.

We create a word image description vocabulary that preserves more detail by using a discretization strategy that proceeds in a dimension-by-dimension fashion. The observed range of training feature values in each dimension is divided into 10 quantization steps (or *bins*; see top portion of Figure 3.5) and another 9 steps of the same width, which overlap by half a bin size (bottom portion of Figure 3.5). Counting all dimensions of a d-dimensional feature vector, we get $19 \cdot d$ bins. Each of these bins is assigned a unique *feature token*. These $19 \cdot d$ feature tokens form the discrete feature *vocabulary* $\mathcal{F}$.

The reason for using the second set of nine bins is that feature values, which should be considered similar, might be mapped to different bins and will thus be assigned different tokens. Using the second set of bins guarantees that two similar feature values will always be assigned at least one common feature token.

In this chapter, we have described three feature representations for word images: (i) raw scalar and profile features as they are extracted from the word images, (ii) length-normalized feature vectors consisting of scalar features and DFT coefficients that are extracted from profiles, and (iii) feature tokens from a vocabulary of discretized feature values. In the following three chapters, we discuss approaches for retrieving handwritten documents, which are based on these representations.

CHAPTER 4

WORD SPOTTING

Word spotting is a technique for creating partial indexes for handwritten historical document collections, similar to indexes in the back of books. It was initially proposed by Manmatha et al. [69] and has prompted a number of publications that propose algorithms and features for the approach [71, 88, 91, 89, 98]. Word spotting takes an unlabeled collection of word images and clusters them using an image matching algorithm. Ideally, the clustering would create groups of images with the same label. Then "interesting" clusters may be labeled manually and an index for the clustered collection may be built, similar to indexes in the back of books. Here we present the word spotting idea, and the contributions of this work to the realization of the technique. These are *Dynamic Time Warping (DTW)* word image matching, which we compare to a number of other techniques, our extension of Keogh's DTW indexing approach for 1-dimensional time series [45] to multidimensional time series and word image clustering experiments which complete the word spotting process.

4.1 The Idea

The idea of word spotting (see Figure 4.1) is to use image matching for calculating pairwise "distances" between word images, which can be used to cluster all words occurring in a collection of handwritten documents. Ideally, each cluster would contain all the words with a particular annotation (without the annotations being known). Clusters that contain terms which are "interesting" for an index for the document collection are selected and labeled manually. By assigning the cluster labels to all

word images contained in a cluster, we get a partial transcription of the document collection. This in turn allows us to create a partial index for the collection, which permits the retrieval of text portions that contain only the manually assigned labels.

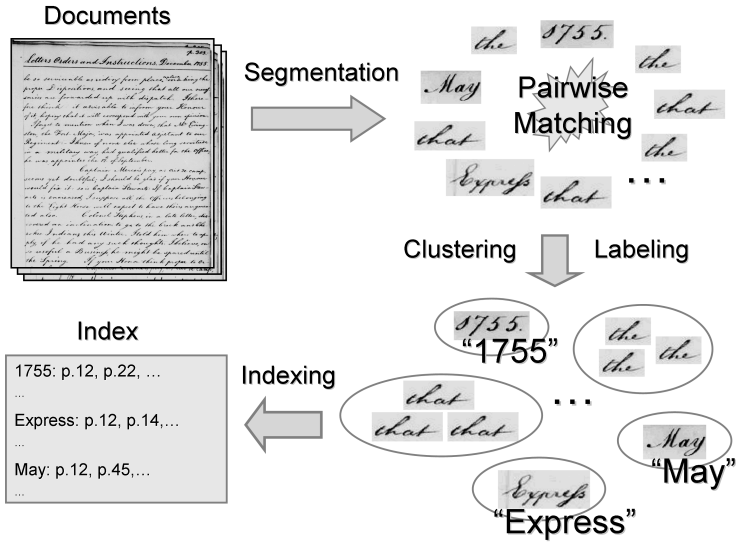

Figure 4.1. An illustration of the Word spotting process. Documents are segmented, and distances between word images are calculated. After clustering the word images, some clusters are manually labeled and can be used as index terms.

Early work in information retrieval by Luhn [63] gives some insight into what makes clusters "interesting". A plot of term frequencies, where terms are ordered by decreasing frequency of occurrence, exhibits a distribution that is known as *Zipf's law* [127].[1] That is, the frequency of the k-th most frequent term has a frequency that is f_0/k, where f_0 is the frequency of the most frequent term. Luhn argued that index terms should be taken from the middle of that distribution. Figure 4.2 shows an example of the actual distribution of term frequencies and the distribution predicted by Zipf. Note the large amount of mass that is concentrated in high-frequency terms and the long tail of the distribution to the right, which continues beyond the shown range. Of course, it would be desirable to index all terms that occur in a collection,

[1]The use of the word *law* is deceiving. Zipf's observation is of an empirical nature, but often provides a reasonable fit to the data.

as many modern information retrieval systems do. Luhn's contribution may be seen as identifying the best candidates for an index when only a fixed number of terms can be indexed.

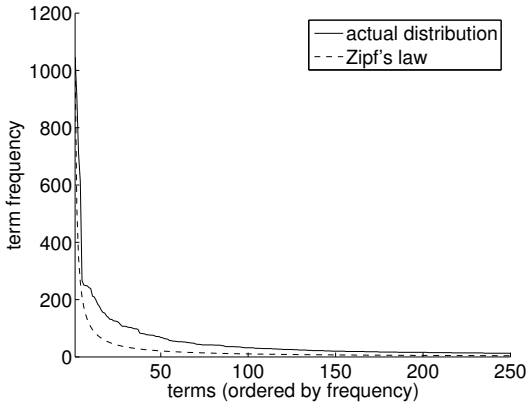

Figure 4.2. Zipf's law: The plots show the actual distribution of term frequencies and the prediction made with Zipf's law based on the actual frequency of the most frequent term. The collection size is 21324 words; only the left-hand portion of the graph is shown.

High-frequency terms (left side of the plot) are often *stop words*, such as *and/the/...*, which have no discriminating power, because they occur in virtually all documents. Terms with very low frequencies are often sporadic in the sense that their occurrence is not correlated to the topic of the text they occur in. Such terms are not descriptive of the content in the collection and may be omitted from the index. Terms that are descriptive of the content can often be found in the middle of the plot. Their repeated, but not excessive use suggests that they are essential to describing the content of the collection and should consequently be part of the index.

In the following sections we assume the output of a page segmentation algorithm and describe approaches to matching pairs of word images and clustering experiments.

4.2 Word Image Matching

One of the key parts of the word spotting approach is the image matching technique for comparing word images. Several techniques have been investigated [88, 91,

98], with the best performing being *Dynamic Time Warping* matching [91], which we explain here in detail.

For DTW matching, word images are represented by multidimensional profile features (see section 3.1). These profiles are then matched using DTW, a dynamic programming algorithm that is able to account for writing variations, which cause the profile features to be compressed and stretched nonlinearly with respect to one another.

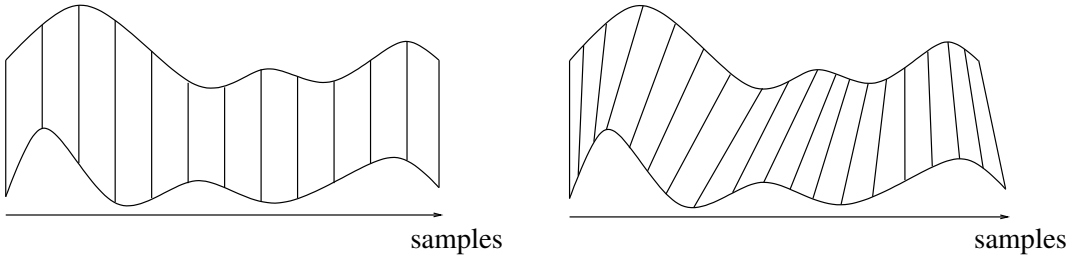

(a) Linear scaling alignment.

(b) Dynamic Time Warping alignment.

Figure 4.3. Two profiles, aligned using linear scaling and Dynamic Time Warping. DTW ensures that only corresponding locations will be compared.

DTW is described in detail in [102]. Its advantage over simple distance measures, such as linear scaling followed by a Euclidean distance calculation, is that it determines a common "time axis" (hence the term *time* warping) for the compared signals, on which corresponding profile locations appear at the same time. Due to the variations in handwriting, two profiles of the same word do not generally line up very well if they are just scaled linearly (see Figure 4.3).

4.2.1 Dynamic Time Warping

Dynamic Time Warping is a dynamic programming algorithm that finds corresponding locations in two signals and calculates a cumulative matching cost from all correspondences. Figure 4.4 illustrates this process: two signals (word images in this

case) are arranged as shown to form the two axes of a matrix. By aligning corresponding samples in the two signals (dashed lines in the figure), a *warping path* from the lower left to the upper right of the DTW matrix arises. The cost of matching the two signals is the cumulative cost of aligning all corresponding sample pairs along the path. A local distance measure determines the cost of matching two aligned samples. DTW recovers correspondences between sample locations by finding the warping path with the minimum accumulated sample alignment cost.

Typically, warping paths are constrained to remain close to the diagonal. This is called a *global path constraint* (shaded region in Figure 4.4). By constraining the warping path to lie within that region, pathological warpings, which map a small portion of one signal to a large portion in the other, are prevented.

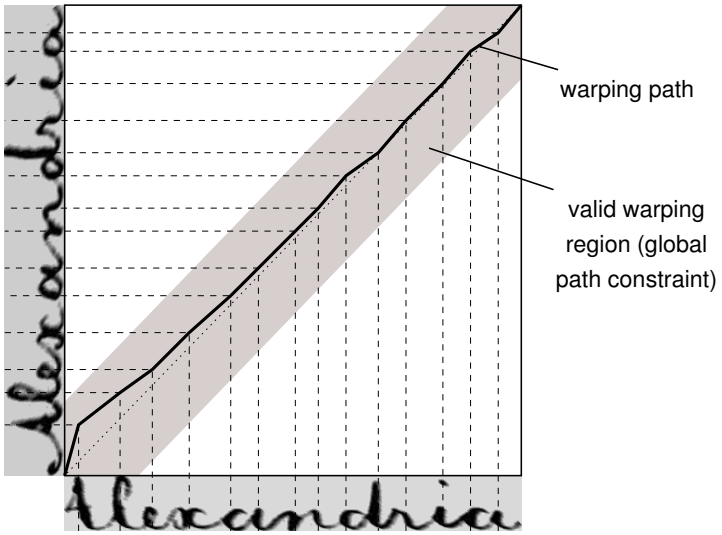

Figure 4.4. Dynamic time warping algorithm: two word images are compared by aligning corresponding locations. The result is a warping path through the DTW matrix.

Formally, when determining the DTW-distance[2] $dist(\mathbf{X}, \mathbf{Y})$ between two time series $\mathbf{X} = (x_1, \ldots, x_M)$ and $\mathbf{Y} = (y_1, \ldots, y_N)$, a matrix $D \in I\!R^{M \times N}$ is built, where

[2] $dist(\cdot, \cdot)$ does not satisfy all metric axioms.

each entry $D(i,j)$ $(1 \leq i \leq M, 1 \leq j \leq N)$ is the cost of aligning the subsequences $\mathbf{X}_{1:i}$ and $\mathbf{Y}_{1:j}$.

Each entry $D(i,j)$ is calculated recursively from some $D(i',j')$ plus an additional cost d, which is usually some distance (e.g. Euclidean) between the samples x_i and y_j. For instance, our implementation of the algorithm uses

$$D(i,j) = min \left\{ \begin{array}{l} D(i,j-1) \\ D(i-1,j) \\ D(i-1,j-1) \end{array} \right\} + d(x_i, y_j). \tag{4.1}$$

The recursive definition of $D(i,j)$ based on the three given values is a *local continuity constraint*. It determines which sample pairs (positions in the matrix) may be connected to form a warping path. The constraint in equation (4.1), which is also shown in graphical form in Figure 4.5(a)), ensures that no sample in any of the two input signals can be left out from the warping path. Other continuity constraints allow skipping of samples. For a more detailed discussion of continuity constraints and alternatives to the one used in this work, we refer the reader to [102].

Table 4.1 contains pseudo-code for the DTW algorithm (adapted from [112]) using the local continuity constraint from Figure 4.5(a). The algorithm determines a warping path composed of index pairs $((i_1,j_1),(i_2,j_2),\ldots,(i_K,j_K))$, which aligns corresponding samples in the input sequences $\mathbf{X}$ and $\mathbf{Y}$. Our implementation of DTW uses the *Sakoe-Chiba band* [100] global path constraint (see Figure 4.5(b); the warping path must lie in the shaded region), but the Itakura parallelogram [38] is also a popular choice. As a side effect, the constraint speeds up the computation of the DTW matrix, since it does not have to be entirely evaluated. We use $r = 15$ samples in our implementation of the word matching algorithm, which was chosen empirically to optimize matching performance on a small subset of word images. Recent work

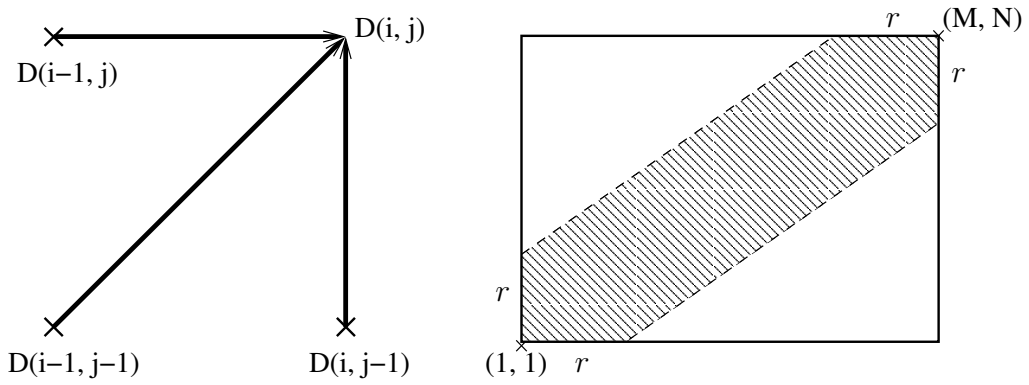

(a) Local continuity constraint, showing valid neighborhood relationships in a warping path.

(b) Global path constraint. The warping path must lie in the shaded region around the DTW matrix diagonal.

Figure 4.5. Constraints used in the current dynamic time warping implementation.

[87] shows that the shape of the global path constraint can be adapted, leading to faster DTW computations and better matching performance.

Input: $\mathbf{X} = (x_1, \ldots, x_M)$ and $\mathbf{Y} = (y_1, \ldots, y_N)$, distance function $d(\cdot, \cdot)$
Output: DTW matrix D
Algorithm:
1. $D(1,1) = d(x_1, y_1)$;
2. for $i = 1 : M$
3. $\quad D(i,1) = D(i-1,1) + d(x_i, y_1)$;
4. for $j = 1 : N$
5. $\quad D(1,j) = D(1,j-1) + d(x_1, y_j)$;
6. for $i = 2 : M$
7. $\quad$ for $j = 2 : N$
8. $$D(i,j) = min\begin{Bmatrix} D(i,j-1) \\ D(i-1,j) \\ D(i-1,j-1) \end{Bmatrix} + d(x_i, y_j);$$

Table 4.1. Pseudo code for the DTW algorithm (without backtracking).

Once all necessary values of D have been calculated, the warping path can be determined by backtracking the minimum cost path starting from (M, N). However, we are just interested in the accumulated cost along the warping path, which is stored

in $D(M, N)$. As it is, this matching cost is smaller for shorter sequences, so we offset this bias by dividing the total matching cost by the length K of the warping path, yielding

$$dist(\mathbf{X}, \mathbf{Y}) = D(M, N)/K. \tag{4.2}$$

4.2.2 Matching Word Images with DTW

We represent word images with single- or multi-dimensional profile features (see chapter 3). Single-dimensional profiles that were extracted from the same word have the same length, and may be "stacked" to create multidimensional profiles. Hence, when matching word images, the sequences $\mathbf{X}$ and $\mathbf{Y}$ consist of samples of dimensionality $d \geq 1$, i.e. $x_i, y_j \in \mathbb{R}^d$. This ensures that all profiles are warped in the same manner.[3]

In order to use DTW to match such profiles, we need to define a distance measure $d(\cdot, \cdot)$ that determines the (local) distance between two samples in a profile. Our implementation uses the square of the Euclidean distance

$$d(x_i, y_j) = \sum_{p=1}^{d} (x_{i,p} - y_{j,p})^2, \tag{4.3}$$

where the index p is used to refer to the p-th dimension of x_i and y_j. With this distance measure defined, we can now calculate the matching distance between two word images by comparing their profile features using DTW and equation (4.2). Then, our DTW matching algorithm in Table 4.1 computes

$$dist(\mathbf{X}, \mathbf{Y}) = \frac{1}{K} min \left\{ \sum_{k=1}^{K} d(x_{i_k}, y_{j_k}) \right\} = \frac{1}{K} min \left\{ \sum_{k=1}^{K} \sum_{p=1}^{d} (x_{i_k,p} - y_{j_k,p})^2 \right\},$$

i.e. the mean alignment cost along the path with the minimum total cost.

---

[3]Other work by Kołcz et al. [48] warped various profiles separately, potentially using different distortions, although all profiles were originally determined from the same word image.

4.2.3 Experimental Setup

The performance of the DTW word image matching algorithm was evaluated in a retrieval-by-example setup, where word images in a collection are ranked by decreasing similarity to a given template. Experiments were conducted on two test sets of different quality, both 10 pages in size (2381 and 3370 word images). The first set is of acceptable quality, see Figure 4.6(a)). The second set is very degraded (see Figure 4.6(b)) - even people have difficulties reading these documents. We used this data set to test how badly matching algorithms perform on manuscripts of such poor quality. Each page in the two test sets was segmented into words with an automatic page segmentation procedure [71]. While the quality of the segmentation algorithm has been improved in the meantime [70], we used the same segmentation results as in [43] for comparability.

We conducted four experiments on the test sets and compared the performance of various matching approaches. Each experiment involves selecting one of the above two data sets and identifying a subset that will be used for querying. Each of the queries is used to rank the images in the dataset according to their similarity to the query. The similarity scores are determined by a matching algorithm. Four experiments were conducted:

Experiment A: 15 images from test set 1 were selected as queries.

Experiment B: All images in test set 1 were used as queries. This yields a total of 2381 query images, 9 of which do not contain any letters.[4]

Experiment C: 32 images from test set 2 were selected as queries. 13 of these images contain words that occur only once in the collection.

[4]These images are the result of segmentation errors.

Experiment D: All images in test set 2 were used as queries. This yields a total of 3370 query images total, 108 of which do not contain any letters.[4]

Experiments A and C were initially proposed by Kane et al. [43]. We use their query sets to provide comparable performance figures. Due to the small size of these sets, they allow us to test algorithms which would otherwise take too long to run on the entire dataset. Experiments B and D are exhaustive query sets which do not suffer from potential bias that may have been introduced by the query selection for experiments A and C.

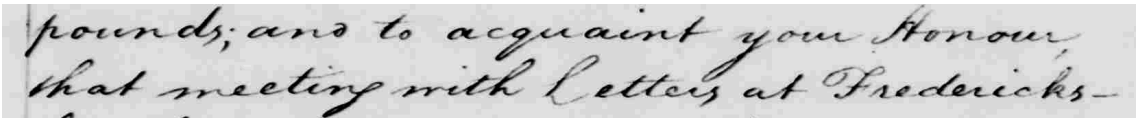

(a) Acceptable quality (set 1).

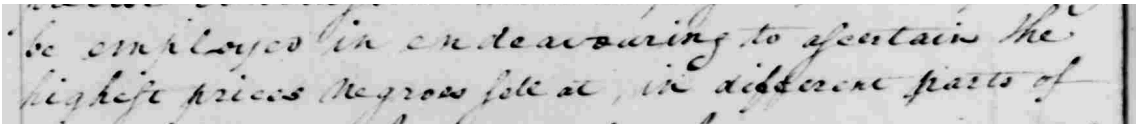

(b) Significantly degraded (set 2).

Figure 4.6. Document samples from the Dynamic Time Warping testbeds, showing the differing quality.

In order to reduce the number of pairwise comparisons that have to be made, we use a pruning strategy. It allows us to speed up the matching process and thus process larger data sets. A number of scalar features (image area, aspect ratio and number of descenders) are extracted from all images. The features are compared in pairs and a threshold τ is applied to determine whether the corresponding images are similar enough to be a positive match:

$$\frac{1}{\tau} \leq \frac{template\_feature}{candidate\_feature} \leq \tau \tag{4.4}$$

If the above condition is not met for any of the features that are used for pruning, the query and candidate images are considered to be a negative match. In that case, no DTW similarity score is calculated. For images that pass this conservative test of similarity, the dissimilarity measure is computed. The parameter τ, which varies depending on the feature, was chosen to provide a trade-off between pruning performance and pruning accuracy. More aggressive threshold settings cause more candidates to be pruned, but may also cause more true positive matches to be discarded. Table 4.2 shows the reduction of candidates through pruning, and how many true positives remain in the pruned candidate set.

Experiment	**Total #queries**	**Pruned candidates**	**Recall**
A	15	87.29%	90.72%
B	2372	86.43%	71.11%
C	32	86.99%	56.49%
D	3262	85.74%	55.05%

Table 4.2. Pruning statistics, showing the reduction in the total number of matches to be made and the percentage of remaining true positives (recall).

Ground truth was produced by labeling each word in the data sets with its ASCII equivalent. In case of segmentation errors, a label corresponding to all visible characters in the segmented word image was assigned. Based on this annotation, relevance judgments were produced for the data sets. Two word images were considered relevant if they have the same labels. For the evaluation, we used the `trec_eval` program to compute mean average precision scores.

4.2.4 Experimental Results

Table 4.3 shows mean average precision results for all data sets obtained with a range of different matching techniques:

XOR [43]: The images are aligned to compensate for shear and scale changes, binarized and then a difference (XOR) image is computed. The number of difference pixels is used as the matching cost.

SSD [43]: This approach translates the query and candidate images relative to one another to find the minimum cost based on the sum of squared differences. This cost is used as the matching cost.

SLH [43]: Scott and Longuet-Higgins algorithm [104]. This algorithm recovers an affine warping transform between sample points taken from the query and candidate images. The residual between query points and the warped candidate points is the matching cost.

SC [7]: Shape context matching. Sample points are taken from the outlines of the query and candidate image. Each point is assigned a *shape context histogram*, which is used to recover corresponding sample points in the query and the candidate image. The matching is done in an iterative process, which successively warps the candidate image. The matching cost is determined from the cost that is associated with the chosen correspondences.

EDM [43]: Euclidean distance mapping [18]. In the XOR image, difference pixels in larger regions are weighted more heavily, because they are likely to result from structural differences between the template and the candidate image, not from noise. The matching cost is the cumulative weight of the difference pixels in the XOR image.

CORR [98]: This technique recovers similarities between a small number of corner points in the query and candidate images. Points of interest are determined by a corner detector. The matching cost is calculated from the number of recovered

correspondences and the relative location of corresponding points in the two images.

DTW [91]: Dynamic Time Warping word image matching as described above.

The obtained mean average precision scores for experiments A and B had to be corrected, because of an evaluation problem in [43]. The reason is that Kane et al. ranked all the images in the dataset, including the query image. Queries with only one single relevant item (the query itself) produce average precision values of 1 (because the query image is retrieved at rank 1), which artificially inflates the retrieval scores. To solve this problem we have chosen to disregard 13 of the queries in set C and 960 queries in set D. Table 4.3 reflects the values after this correction.

Furthermore, we re-calculated the mean average precision scores for test runs that were available to us in ranked-list format, with the queries removed from the ranked lists. This gives the most accurate picture of the actual matching performance with respect to a standard ranked list evaluation. Table 4.3 shows the mean average precision scores of four runs, based on the corrected ranked lists.

Algorithm	**Exper. A**	**Exper. B**	**Exper. C**	**Exper. D**
XOR	.5414	n/a	n/a	n/a
SSD	.5266	n/a	n/a	n/a
SLH	.4243	n/a	n/a	n/a
SC	.4867	n/a	.4811	n/a
EDM	.7261	n/a	.1505	n/a
CORR	.7395	.6257	.5996	.5108
DTW	.7371	.6534	.5881	.5181

Table 4.3. Mean average precision scores for all experiments (XOR: matching using difference images, SSD: sum of squared differences technique, SLH: technique by Scott & Longuet-Higgins [104], SC: shape context matching [7], EDM: Euclidean distance mapping, CORR: corner-point correlation, DTW: dynamic time warping matching). Queries with no relevant word images were disregarded.

Algorithm	Exper. A	Exper. B	Exper. C	Exper. D
SC	.4058	n/a	.0946	n/a
EDM	.6767	n/a	n/a	n/a
CORR	.6969	.3623	.1484	.1549
DTW	.6792	.4098	.1304	.1650

Table 4.4. Mean average precision scores for selected experiments with the alternate evaluation technique (i.e. queries were discarded from the candidate set).

For experiment A, results are available with all matching algorithms. EDM, DTW and CORR clearly outperform any of the other techniques. SC was run with a number of sample points proportional to the width of the words being matched, with about 100 sample points for a word like *Alexandria*. More sample points would probably improve the effectiveness of the technique, but at the cost of further increasing the matching time (for 100 sample points it is already about 50 seconds per image pair, cf. Table 4.5).

The DTW and CORR algorithms were also used in experiment B (all images used as templates). The other algorithms were too slow to realistically run on this dataset. On query set B, the average precision scores for DTW and CORR are lower than on the smaller subset A. We attribute this effect mostly to the pruning method, which works much better on the smaller set A: while the pruning preserves about 91% of the relevant documents for data set A, it only produces 71% recall on data set B. The lower recall on set B (due to the pruning) then results in a lower average precision score after matching. While the performance of DTW was slightly worse than CORR's on the smaller query set A, DTW outperforms CORR on query set B, which is much larger and makes for a better comparison.

We compared the results of the SC, CORR, EDM and DTW techniques on data set C. While the performance of all approaches is generally low on data set C because it is significantly degraded, DTW's and CORR's performance is almost four times

better than that of EDM (.5881 and .5996 vs. .1505). DTW also performs similarly on the rest of the data set (.5181 average precision on data set D). This shows that the DTW and CORR matching techniques are more robust to document degradation than EDM, with DTW, again showing superior performance to CORR on the exhaustive query set. We would expect the results to be better if a more careful pruning was applied: after pruning, the recall percentages have already dropped to about 56% for sets C and D (see Table 4.2). This limits the maximum average precision achievable with the matching algorithms.

These results show that DTW performs best amongst the set of algorithms tried. However, a look at Table 4.4 shows that significant efforts need to be made in order to perform well on such challenging datasets as C and D. Whether this improvement will come from the preprocessing or from the matching algorithm itself remains to be seen.

Algorithm:	XOR	SSD	SLH	SC	EDM	CORR	DTW
Running time [s]:	13	72	121	∼50	14	∼1	∼2

Table 4.5. Average run times for the compared algorithms in *Matlab* on a 400MHz machine. The values include the time that is spent on normalization (e.g. relative scaling), feature extraction, and similar processing steps. Running times that are marked with '∼' are approximations, which are based on a smaller sample.

Comparing the running times of the investigated algorithms (see Table 4.5) shows CORR as the winner. CORR's superior execution time is a result of the very few corner points that are considered for establishing correspondences between the query and a candidate image. DTW is second in execution time, but we believe its performance can be improved substantially with optimization.

4.3 Performance Considerations

The increased matching accuracy comes at a considerable cost. Whereas the Euclidean distance metric has a complexity that is linear in the length of the profiles, DTW is linear in the product of the profile lengths. This is problematic because the clustering of a document collection of n words requires on the order of n^2 distance evaluations.

This problem was tackled by using simple word features, such as the width of a word image, to quickly eliminate unlikely matches. The matching process can be sped up tremendously using this approach, but still about 10% of the original candidate matches have to be processed, so the quadratic problem complexity has not actually changed.

An entirely different way to solve this problem has been reported in the database community: Keogh [45] proposed to use the technique of *lower-bounding* of dynamic time warping dissimilarities. The approach may be used to speed up searches for the k nearest neighbors (kNN) to a query and even to index time series using appropriate data structures (for example [28, 16]). Here we present our extension of Keogh's lower bound to multivariate time series and demonstrate its performance benefits for faster kNN searches on a test collection of 2381 word images (see [90] for a more detailed discussion).

4.3.1 Using Lower Bounds to Speed up Similarity Queries

Lower bounds have been used by the data base community to speed up similarity queries (e.g. see [22]): lb is a lower bound for a function f, if

$$\forall x : lb(x) \leq f(x) \tag{4.5}$$

For a 1-nearest-neighbor search, where a data base is searched for the entry that has the lowest distance $f(Q, \cdot)$ to a given query Q, [45] provides the search algorithm in Table 4.6 using the lower bound $lb(Q, \cdot)$ of f.

Compared to straightforward sequential scans with dissimilarity calculation, this algorithm can provide improved processing times under two conditions:

1. Calculating the lower bound lb must be cheaper than calculating the actual distance measure f.

2. The lower bound must be *tight*, that is, it should provide a good approximation to the actual distance f. Lower bounds that are not tight (e.g. $lb \equiv 0$ for positive distance measures) can cause the fast sequential scanning algorithm to be slower than a straightforward sequential scan. As a measure of tightness we use $tightness = lb(Q, C)/D(Q, C)$, which depends on the particular query Q and candidate C.

```
seq_scan(Q):
best_f = ∞;
% scan data base sequentially
for i = 1 to num_db_entries
   l = lb (Q, db_entry(i));
   if l ≥ best_f
      continue;                  % discarded using lower bound (1)
   d = f (Q, db_entry(i));
   if d ≥ best_f
      continue;            % discarded using distance measure (2)
   % db_entry(i) has lowest distance so far, remember it (3)
   best_f = d;
   best_idx = i;
end
% return entry with smallest distance to query
return best_idx;
```

Table 4.6. Fast sequential scanning algorithm for 1-nearest-neighbor search.

While the fast sequential scanning algorithm in table 4.6 is useful, it cannot be directly applied to the word spotting idea. The goal there is to find a *set* of k im-

ages that has the lowest distance to a given query. When k is chosen appropriately, the returned set will contain all images with the same annotation as the query. The dissimilarity measures that are associated with the images can then be used for clustering. To allow this functionality, we have extended the algorithm in Table 4.6 to a kNN algorithm, which may be found in the appendix (Table B.1).

4.3.1.1 Lower-Bounding for Univariate Dynamic Time Warping

The application of DTW to large databases may be infeasible, because of its high complexity. Consequently, several researchers have investigated lower-bounding techniques for DTW. While the initially proposed bounds were rather simple and not very tight [122], recent work by [45] has provided a convincing lower bound that can be tuned to provide high tightness to the actual DTW distance. It has to be pointed out that this lower bound can only be computed for the comparison of time series with the same length, a limitation that is later dropped. Additionally, Keogh's lower bound was only defined for *univariate* time series, that is, sequences consisting of scalars. Our contribution is the extension of his approach to multivariate time series. First we take a look at Keogh's lower bound for univariate time series and then our extension.

Keogh [45] exploits the fact that most implementations apply some sort of global path constraint, such as the Sakoe-Chiba band [100] or the Itakura parallelogram [38]. The path constraint can be seen as limiting the amount that the query sequence can be warped when aligning it with a candidate sequence. For example, the Sakoe-Chiba band with parameter r, which we use here, restricts the warping path as follows: for the index pair (i_k, j_k) at position k in the warping path, we get

$$i_k - r \leq j_k \leq i_k + r \qquad \text{and} \qquad j_k - r \leq i_k \leq j_k + r.$$

From now on, we drop the index k, when the dependency of i and j on k is clear. This constraint can be used to compute two time series $\mathbf{U} = u_1, \ldots, u_n$ and $\mathbf{L} = l_1, \ldots, l_n$ from the query series $\mathbf{Q} = q_1, \ldots, q_n$:

$$u_i = max(q_{i-r} : q_{i+r}) \qquad \text{and} \qquad l_i = min(q_{i-r} : q_{i+r}) \tag{4.6}$$

Here, u_i takes on the maximum value that $\mathbf{Q}$ can have under the maximum warping allowed by the constraint (l_i similarly for the minimum value under maximum warping of $\mathbf{Q}$). Figure 4.7 shows a projection profile time series with $\mathbf{U}$ and $\mathbf{L}$ for $r = 15$, the value used in our word spotting matching algorithm.

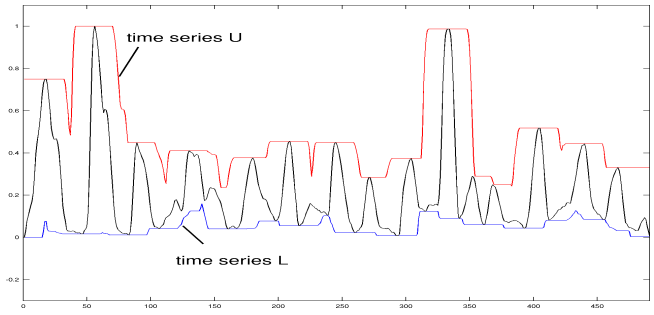

Figure 4.7. Projection profile feature with bracketing time series $\mathbf{U}$ and $\mathbf{L}$.

Using the time series $\mathbf{U}$ and $\mathbf{L}$, Keogh [45] defines his lower bound for comparing $\mathbf{Q}$ to a candidate time series $\mathbf{C} = c_1, \ldots, c_n$ as

$$LB\_Keogh(\mathbf{Q}, \mathbf{C}) = \sqrt{\sum_{i=1}^{n} \begin{cases} (c_i - u_i)^2 & \text{if } c_i > u_i \\ (c_i - l_i)^2 & \text{if } c_i < l_i \\ 0 & \text{otherwise} \end{cases}} . \tag{4.7}$$

Then he proves that LB_Keogh is a lower bound for his DTW dissimilarity formulation

$$DTW(\mathbf{Q},\mathbf{C}) = min\left\{\sqrt{\sum_{k=1}^{K} d(q_i, c_j)}\right\} = min\left\{\sqrt{\sum_{k=1}^{K}(q_i - c_j)^2}\right\}, \qquad (4.8)$$

where K is the length of the warping path. Note that the normalization technique (square root) differs from the one we use in equation (4.2) (normalization by the length K of the warping path).

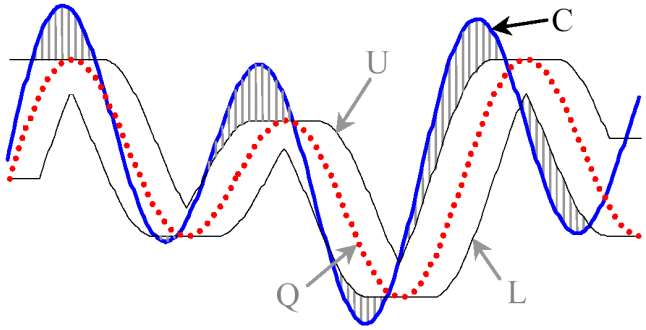

Figure 4.8. Illustration of the lower bound calculation: shaded areas yield positive contributions to the lower bound (figure courtesy E. Keogh).

Figure 4.8 provides an illustration of the lower bound calculation: if **C** takes on a value outside the envelope defined by **U** and **L**, the dynamic time warping algorithm would add at least the distance between **C** and the envelope to the total matching distance (cases 1 and 2 in equation (4.7)). The reason for this is that even if Q were warped maximally at the corresponding location, the remaining distance between **Q** and **C** would still be at least the distance contribution ($(c_i - u_i)^2$ or $(c_i - l_i)^2$, whichever is smaller). If **C** takes on a value within the envelope defined by **U** and **L**, it is generally possible that **Q** could be warped in such a way as to bring **Q** and **C** to an overlap at that position. Hence, the contribution to the lower-bound for such situations is assumed to be zero (case 3 in equation 4.7).

4.3.1.2 Lower-Bounding for Multivariate Time Series

The lower bound for DTW distances proposed in [45] is restricted to *univariate* time series, i.e. time series that are composed of scalars. However, the word image matching approach, which is used in the word spotting project, operates on *multivariate* time series, that is, sequences that are composed of vectors of a constant dimension d. We devised an extension of the univariate time series bound to multivariate time series, which is documented below. The proof that it is a valid lower bound can be found in the appendix (section B.2). Let

$$\mathbf{Q} = q_1, \ldots, q_n \qquad \text{and} \qquad \mathbf{C} = c_1, \ldots, c_n,$$

be multivariate query and candidate time series of length n with $q_i, c_j \in R^d$, where d is an integer constant ≥ 1. For $d = 1$ the lower bound presented here reduces to the univariate case.

Our lower bound requires that the distance between two aligned samples q_i and c_j is calculated as in equation (4.3):

$$d(q_i, c_j) = \sum_{p=1}^{d} (q_{i,p} - c_{j,p})^2,$$

where p is used to index the dimensions of q_i and c_j. Using the local distance measure, the DTW algorithm finds a warping path

$$W = (i_1, j_1), (i_2, j_2), \ldots, (i_K, j_K),$$

which aligns corresponding locations (i.e. indices i and j) in the two time series $\mathbf{C}$ and $\mathbf{Q}$. The path W that DTW recovers is the one with minimum accumulated cost:

$$DTW(\mathbf{Q}, \mathbf{C}) = min_W \left\{ \sqrt{\sum_{k=1}^{K} d(q_i, c_j)} \right\}, \tag{4.9}$$

where we have used the square root for normalization (we will later see that the choice of normalization does not have a substantial effect on performance).

Similarly to the univariate case, we define two time series **U** and **L**, such that they define an envelope that the time series **Q** must lie in, regardless of how much it is skewed under all possible warping paths that are allowed under the global path constraint (i.e. Sakoe-Chiba band [100]). **U** and **L** are defined as follows:

$$u_{i,p} = max(q_{i-r,p} : q_{i+r,p}) \qquad \text{and} \qquad l_{i,p} = min(q_{i-r,p} : q_{i+r,p}).$$

Using **L** and **U**, we define our multivariate lower-bounding measure as

$$LB\_MV(Q,C) = \sqrt{\sum_{i=1}^{n}\sum_{p=1}^{d} \begin{cases} (c_{i,p} - u_{i,p})^2 & \text{if } c_{i,p} > u_{i,p} \\ (c_{i,p} - l_{i,p})^2 & \text{if } c_{i,p} < l_{i,p} \\ 0 & \text{otherwise} \end{cases}} \tag{4.10}$$

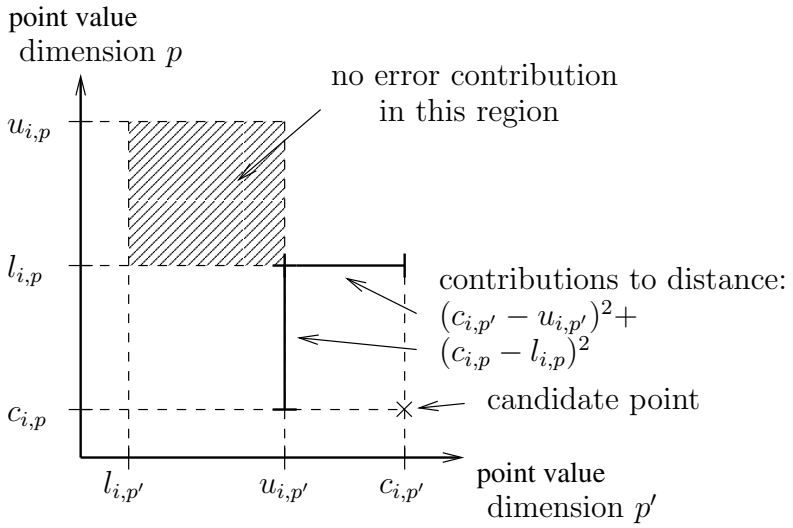

Figure 4.9. Contributions to the lower-bounding distance measure in the multivariate case (2 dimensions shown).

Figure 4.9 shows how distance contributions are counted in the lower-bounding measure. For a proof of the lower-bounding property of LB_MV, see appendix B.

4.3.1.3 Piecewise Constant Approximation

In [45], all time series are of the same length n. In order to reduce the dimensionality of the data, Keogh applied a *piecewise constant approximation* (PAA) scheme: in this technique, each time series (or the "envelope" time series $\mathbf{U}$ and $\mathbf{L}$) is approximated by two sequences $\hat{\mathbf{U}}$ and $\hat{\mathbf{L}}$, both consisting of Z samples ($Z < n$):

$$\hat{l}_i = min(l_{\frac{n}{Z}(i-1)+1} : l_{\frac{n}{Z}i}) \quad \text{and} \quad \hat{u}_i = max(u_{\frac{n}{Z}(i-1)+1} : u_{\frac{n}{Z}i}). \tag{4.11}$$

The two sequences $\hat{\mathbf{L}} = \hat{l}_1, \ldots, \hat{l}_Z$ and $\hat{\mathbf{U}} = \hat{u}_1, \ldots, \hat{u}_Z$ bracket the original time series (or envelope) from above and below (see figure 4.10). In this scheme, each value in the series $\hat{\mathbf{U}}$ and $\hat{\mathbf{L}}$ approximates n/Z samples.

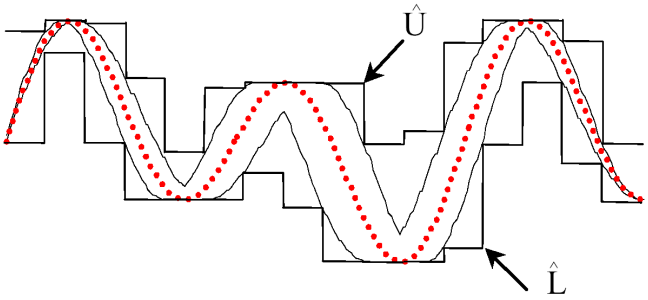

Figure 4.10. Piecewise constant approximation of the envelope around a time series. The global path constraint is the Itakura parallelogram (figure courtesy E. Keogh).

An approximate lower-bound to the actual DTW distance can still be computed in this lower-dimensional representation. Let $\hat{\mathbf{U}}$ and $\hat{\mathbf{L}}$ be the PAA of the "envelope" time series $\mathbf{U}$ and $\mathbf{L}$ extracted from a query sequence $\mathbf{Q}$. Then, for a candidate time series $\mathbf{C}$ with PAA $\hat{\mathbf{U}}^C$ and $\hat{\mathbf{L}}^C$, we get

$$LB\_PAA(\mathbf{Q}, \mathbf{C}) = \sqrt{\sum_{i=1}^{Z} \frac{n}{Z} \begin{cases} (\hat{l}_i^c - \hat{u}_i)^2 & \text{if } \hat{l}_i^c > \hat{u}_i \\ (\hat{l}_i - \hat{u}_i^c)^2 & \text{if } \hat{u}_i^c < \hat{l}_i \\ 0 & \text{otherwise} \end{cases}}. \tag{4.12}$$

This piecewise constant approximation scheme can not only reduce the dimensionality of the data, but also provide a means for normalizing time series of different lengths to a representation of constant length. This is an essential step, because the current lower-bounding technique does not allow lower bound calculations for the DTW distance between time series of different lengths. For our experiments with lower bounding, each time series is represented by a PAA and its original length. Then the following lower bound may be used for comparing time series $\mathbf{Q}$ and $\mathbf{C}$ with lengths n_Q and n_C, respectively:

$$LB\_DL(\mathbf{Q}, \mathbf{C}) = \sqrt{\frac{n_Q}{Z} \sum_{i=1}^{Z} \begin{cases} (\hat{l}_i^c - \hat{u}_i)^2 & \text{if } \hat{l}_i^c > \hat{u}_i \\ (\hat{l}_i - \hat{u}_i^c)^2 & \text{if } \hat{u}_i^c < \hat{l}_i \\ 0 & \text{otherwise} \end{cases}}, \tag{4.13}$$

where $\hat{\mathbf{U}}, \hat{\mathbf{L}}, \hat{\mathbf{U}}^c$ and $\hat{\mathbf{L}}^c$ are defined as before.

A very important point is that equation (4.13) is only guaranteed to form a lower bound, if $n_Q \leq n_C$. In fact, in cases where $n_Q > n_C$, distance contributions that are computed from the PAAs of $\mathbf{Q}$ and $\mathbf{C}$ are weighted too heavily and can result in *overestimation* of the actual DTW distance. For the purpose of word spotting, this constraint is not a great limitation, because words are only compared if they are of similar widths (pruning). This ensures that n_Q cannot get much larger than n_C, which limits overestimation. Furthermore, the mean tightness of our lower bound is about .42, which also decreases the chances for overestimation of the DTW distance.

The lower bound LB_DL has to be extended to *multivariate* time series, so that it can be used for matching sets of time series as is required by our matching algorithm. Given the lower bound formulation for multivariate time series, the necessary modifications are straightforward and yield

$$LB\_DL\_MV(\mathbf{Q},\mathbf{C}) = \sqrt{\frac{n_Q}{Z}\sum_{p=1}^{d}\sum_{i=1}^{Z}\begin{cases}(\hat{l}^c_{i,p}-\hat{u}_{i,p})^2 & \text{if } \hat{l}^c_{i,p} > \hat{u}_{i,p}\\ (\hat{l}_{i,p}-\hat{u}^c_{i,p})^2 & \text{if } \hat{u}^c_{i,p} < \hat{l}_{i,p}\\ 0 & \text{otherwise}\end{cases}} \quad . \tag{4.14}$$

Similarly to LB_DL, the measure LB_DL_MV is only a true lower bound if $n_Q \leq n_C$. Since overestimation of the actual DTW distance does not occur very often (see [90]), LB_DL_MV will still be referred to as a *lower bound* in the following.

With its complexity of $O(Z \cdot d)$, the lower bound is generally much more efficient than the original cost for comparing two time series $O(l \cdot n_Q \cdot n_C)$: Z and d are constants, whereas n_Q and n_C are the lengths of the input time series, which usually also satisfy $n_Q > Z$ and $n_C > Z$. However, turning the time series in a data base into a representation based on piecewise constant approximation comes at a cost that needs to be taken into consideration.

4.3.1.4 Experimental Results

We evaluate the lower bounding technique in a query-by-example fashion as we did in the evaluation of our DTW distance measure. A set of query time series (multivariate feature profiles) is selected and used to rank the time series in the data base of 2381 images (experiment A in section 4.2.3). Performance is measured with mean average precision. The lower bounding approach does not permit us to normalize the DTW dissimilarity by the length of the warping path. We used the square root instead, which did not have a substantial effect on retrieval performance (in fact, mean average precision increased slightly for a query set of 2381 time series).

We chose $Z = 50$ discretization steps, since it appeared to provide a good trade-off between tightness and compactness of the time series representation (see [90] for a more detailed discussion). This value was used in the fast sequential scanning experiments. Computing PAA representations for all 2381 time series in the data

set took 462 seconds on a 500MHz machine. The same machine was used in all lower-bounding experiments.

The mean tightness (calculated from 1100 multivariate time series comparisons) at $Z = 50$ is .4238. In order to get a tighter lower bound we investigated the possibility of scaling the lower bound values:

$$tighter\_lb(\mathbf{Q}, \mathbf{C}) = \frac{LB\_DL\_MV(\mathbf{Q}, \mathbf{C})}{scaling\_factor}, \tag{4.15}$$

where $0 < scaling\_factor < 1$. The scaling factor has to be chosen carefully, and can only be applied to lower bounds that tend to consistently underestimate the actual DTW distance. If the scaling factor is too low, the new lower bound will consistently overestimate and discard candidates that should be part of the nearest neighbors set.

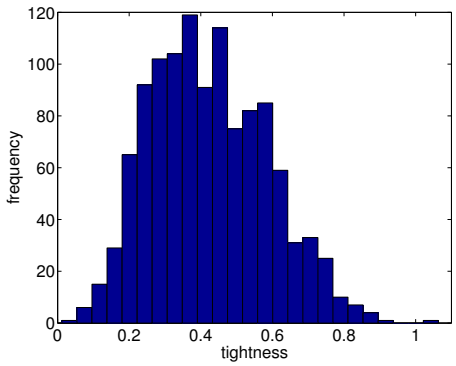

Figure 4.11. Histogram of 1100 tightness values at $Z = 50$.

A histogram of the 1100 tightness values looks roughly like a normal distribution (see Figure 4.11). In a normal distribution with parameters (μ, σ), roughly 66% of the probability mass is concentrated in the interval $[\mu - \sigma, \mu + \sigma]$, 95% in the interval $[\mu - 2\sigma, \mu + 2\sigma]$ and 99% in the interval $[\mu - 3\sigma, \mu + 3\sigma]$. This criterion may be applied to the distribution of tightness values at $Z = 50$ to select a scaling factor for the lower bound. For example, a scaling factor of $\mu + \sigma$ causes roughly $66/2 + 50 = 83$ percent

of the lower bounds to be scaled correctly. That is, the scaled lower bound is still a valid lower bound for those cases.

scaling factor	**disc(lb)**	**disc(dtw)**	**new kNN**	**m. avg. prec.**	**time[s]**
1	708	3131	665	.6388	2526
.9128 ($= \mu + 3\sigma$)	896	2943	665	.6386	2430
.7498 ($= \mu + 2\sigma$)	1338	2501	665	.6381	2189
.5868 ($= \mu + 1\sigma$)	2013	1836	655	.6285	1826
.4238 ($= \mu$)	2959	934	611	.6124	1203
baseline run: sequential scan, no lower bound				.6388	2905

Table 4.7. Test results displaying trade-off between speed and precision for different settings of the scaling factor in the kNN search with lower bound calculation (k=10). The timing results were obtained on a 500MHz machine (μ = mean tightness, σ = standard deviation of tightness, both at $Z = 50$). *disc(lb)*, *disc(dtw)* and *new kNN* refer to the number of times cases (1), (2) and (3) in Tables 4.6 and B.1 occurred.

Table 4.7 shows mean average precision scores and timing results obtained with different values of the lower bound scaling factor using the 15 queries from experiment A (cf. section 4.2.3). For comparison, the same results are reported for a baseline run that uses the straightforward sequential scanning algorithm. The number of images that were ruled out to be part of the kNN set are also reported as *disc(lb)* and *disc(dtw)* for ruling out based on the lower bound or the DTW distance (cases (1) and (2) in the algorithms in Tables 4.6 and B.1). *New kNN* is the number of times an image was added to the list of nearest neighbors (case (3) in Tables 4.6 and B.1).

The improvements in run time for conservative settings of the scaling factor are small, but grow larger with more aggressive settings of the scaling parameter. With shorter run times the scores drop because of the lower-bound scaling, which causes overestimations of the actual DTW distance. However, the decrease of the mean average precision scores is much slower than that of the run times. This suggests that many overestimation errors of the scaled lower bound do not hurt performance. Only in cases where the lower bound overestimates the DTW distance between a query and

a matching candidate, a loss in performance occurs because the candidate is falsely discarded. The small decrease in mean average precision scores for more aggressive settings of the scaling parameter indicates that most of the overestimation errors occur when non-matching candidates are compared to the query. When taking the preprocessing time into consideration, the fastest matching run is about twice as fast as the baseline run, with about 2.6% loss in mean average precision – an acceptable trade-off.

Keogh's bound and our multivariate extension of it have not been the last developments in this area. For example, Zhu & Shasha [126] have presented a lower bound that is tighter. So far, the speedup of nearest neighbor searches has been modest in the word image domain. Unfortunately, the analysis of large collections of handwritten documents with the word spotting approach must be deemed infeasible in the near future, considering the currently available processing power. With a matching time of roughly one second for a pair of word images, a collection of 2381 word images (10 page images), and a speedup-factor of 20, computing a sparse distance matrix takes about 3 days on a 500MHz machine. The discrete probabilistic annotation model (DPA) that is described in chapter 6 can process a collection of $\sim$250,000 word images (1000 pages) in roughly 10 days on the same machine, without any optimizations. The CPA annotation model, which is an extension of DPA to continuous-space feature vectors (and is also described in chapter 6), runs even faster.

4.4 Word Image Clustering Experiments

All of the previous work on word spotting has concentrated mostly on finding effective similarity measures for word image matching, but the clustering of word images has not been tackled. In this section, we perform word image clustering experiments, followed by simulated cluster annotations that are designed to imitate a human annotator.

Before we start clustering, we need to get a good estimate of the number of clusters that our data will form. *Heaps' law*, an empirical rule, provides the tool for the estimation, which is discussed in the following section. With an accurate cluster estimate we then move on to various clustering techniques that we apply to group word images.

4.4.1 Heaps' Law

Many clustering algorithms often require that the number of clusters to be created is known. In fact, all of the clustering algorithms that were used in our experiments require the target number of clusters as an input parameter. In the ideal case, each cluster contains all instances of a particular word, so there are as many clusters as there are distinct words in the collection at hand. In other words, the number of clusters is equivalent to the vocabulary size.

Early work in information retrieval by Heaps [32] provides an empirical estimate for the *vocabulary* size of a collection from the size of the collection in words. The rule, which is known to be quite effective [3], has become known as *Heaps' law*. It predicts that the vocabulary size of a collection of n words can be estimated to be

$$V(n) = K \cdot n^{\beta}, \tag{4.16}$$

where K and β are parameters that depend on the language of the collection.

We estimated K and β by fitting Heaps' law to the ground truth transcription of a collection of 100 pages (21324 word images) from George Washington's letters that does not include our test set on which we performed clustering experiments. In order to simulate a document of size n, we used the first n words from the transcription. We varied n from 1 to 21324 in steps of 1, determined the vocabulary size for each n, and then fitted Heaps' law to the resulting curve. Figure 4.12 shows a plot of the vocabulary size V as a function of n and the fitted curve.

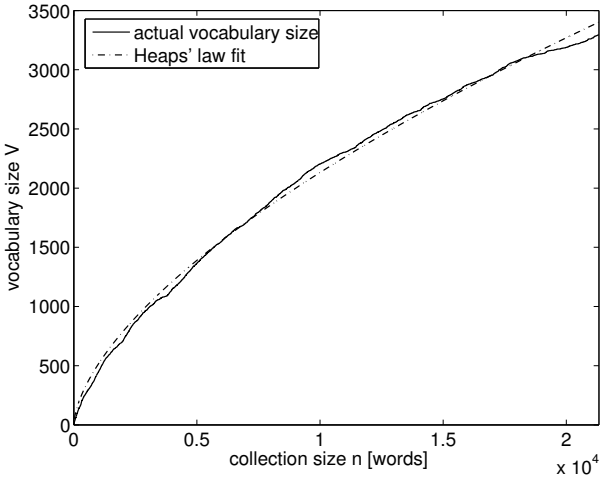

Figure 4.12. Actual vocabulary size as a function of the collection size and a fit of Heaps' law shown for collection sizes of up to 21324 words.

The fitting was performed with the "Nelder-Mead" optimization procedure [52], which minimizes the sum of squared differences between the actual vocabulary sizes and the ones predicted by Heaps' law. For the collection at hand, we estimated the optimal parameter settings to be $K = 7.2416$ and $\beta = .6172$, resulting in a tight fit.

#Images	Voc. size	Predicted Voc. size	Est. error
4856	1209	1365	13%

Table 4.8. Accuracy of the vocabulary size prediction (with Heaps' law).

We used these parameters to estimate the vocabulary size of a collection of 20 pages (4856 word images), our testbed for the clustering experiments. Table 4.8 shows the accuracy that Heaps' law achieves when predicting the vocabulary size of the testbed. Heaps' law overestimates by 13%, which appears acceptable considering the small size of the collection. It is also possible that a larger text source for the parameter estimation could yield better prediction results.

4.4.2 Clustering

With the desired number of clusters at hand we can now turn to grouping word images based on pairwise similarity and then determine the accuracy of the generated clusters. Our experiments were performed using three different data sets derived from the above testbed of 20 pages. The main difference between them lies in the features that are used for the representation:[5]

Dataset A: This set uses a representation consisting of 27 features. These are 21 DFT coefficients extracted from profiles, as well as 6 scalar features. This dataset is the same as was used in the recognition experiments described in [58]. We use it here to provide a basis for comparing word spotting with handwriting recognition.

Dataset B: This set uses a feature representation that solely consists of DFT coefficients extracted from profiles; no scalar features were used. 33 DFT coefficients were used to represent each word image, which is the optimal number that was determined for this dataset (see section 3.2.2)

Dataset C: This dataset does not consist of feature vectors, but rather of a 4860 $\times$ 4860 sparse matrix with pairwise distances. The distances were calculated using the Dynamic Time Warping word matching algorithm described in section 4.2.2 above. The matrix is sparse, because pairwise distances were only calculated if a word image pair was not ruled out by pruning. 76% of the matrix entries were not computed and were filled with the default distance value *infinity*. The calculation of the distance matrix required roughly one week on a multiprocessor machine with 4 500MHz CPUs.

[5]Due to a small number of annotation mistakes in dataset A, which were later corrected, datasets B and C are slightly larger (4860 word images) than dataset A (4856 word images).

We experimented with both the k-means clustering algorithm and various agglomerative clustering approaches on all data sets with one exception: since dataset C is not represented in feature space, but rather in terms of pairwise distances, k-means clustering cannot be applied. k-means keeps track of cluster centers, a notion that does not exist in pairwise distance space.

Numerous clustering techniques are described in the literature. The following is a brief overview of the clustering approaches that were used in our experiments. More detailed descriptions of clustering techniques can be found in the relevant literature, e.g. [31]. Except for k-means clustering, all others techniques are *agglomerative* bottom-up procedures, which build a hierarchical cluster tree by successively linking the most similar clusters. For such clustering techniques, we only list how inter-cluster dissimilarity is determined:

k-means: The algorithm is initialized with k randomly selected cluster centers. Then each feature vector is assigned to the nearest cluster, and the cluster centers are recalculated. This procedure is repeated until convergence.

Single linkage: The inter-cluster dissimilarity between two clusters is the distance between the closest items within the two clusters.

Complete linkage: The distance between the two furthest items in the clusters is used as the cluster dissimilarity.

Average linkage: Here the distance between two clusters is the average distance between all item pairs in the clusters.

Weighted linkage: A slight variation of the *Average Linkage* technique, which uses a weighted average for the cluster distance calculation.

Ward linkage: This linkage uses the sum of squares measure to assess the similarity between clusters. The sum of squares is the total squared distance of all items

in a cluster relative to the cluster centroid. The distance between two clusters is then taken to be the increase in the sum of squares measure, before and after joining the clusters.

Each of our experiments involves selecting a dataset and a clustering method. First, the desired number of clusters is estimated using Heaps' law. Then, we start the clustering of the data. In the case of k-means clustering, the feature vectors form the input for the clustering algorithm. All other clustering routines use a dendrogram as input, which may be constructed from pairwise distances between word images or their feature vectors. We used the Euclidean distance measure to calculate distances between feature vectors.[6] The output of the clustering is a vector of cluster labels, which assigns each word image to a single cluster.

The accuracy of a particular clustering output is evaluated by simulating the task of labeling clusters, which would be performed by a human annotator if we were to perform word spotting. For the purpose of the simulation, it is assumed that a human annotator would label a cluster with the vocabulary term that occurs most frequently in a cluster. This strategy is sound, because it minimizes the total number of wrong annotations, when cluster labels are spread over all word images within a cluster. Ground truth data is available for all word images, so this process may be easily simulated. Once all clusters have been annotated in this fashion, we assign each cluster label to all word images within the cluster, essentially transcribing the entire collection. Table 4.9 shows the word error rates of such transcriptions obtained from various clustering approaches.

Again, we can observe the importance of good features: the clustering tends to perform better on data sets B and C, although all sets were derived from the same 20 pages. Data set B yielded the best overall result, with *Ward* linkage clustering.

[6]Certain clustering algorithms (e.g. the Ward linkage) only produce meaningful output if the vector distances are Euclidean.

Clustering algorithm	A: WER	B: WER	C: WER
k-means	64.13%	41.58%	n/a
Single linkage	62.93%	65.10%	65.00%
Complete linkage	58.55%	37.24%	36.11%
Average linkage	58.44%	44.47%	34.12%
Weighted linkage	58.24%	41.03%	34.77%
Ward linkage	58.18%	**31.50%**	34.47%

Table 4.9. Performance of the clustering algorithms in terms of word error rate (WER), after simulated annotation of the entire collection.

Interestingly, the DTW dissimilarity data (set C) performs slightly worse than the best result (Ward linkage on set B), but otherwise consistently better than set B with word error rates between 34% and 36% (except for the single linkage algorithm). This suggests that the DTW distance measure captures different aspects of word image similarity than the features used in set B. The difference in performance between sets B and C can be attributed to the fact that the length of the feature vectors in set B (number of DFT coefficients) has been optimized for this exact dataset, yielding better performance. Furthermore, the matrix with DTW distances has not been entirely computed due to pruning, which probably has an adverse effect on performance (the pruning assigns *infinity* as the distance to some word image pairs). However, the magnitude of this effect is unknown.

Figure 4.13 shows histograms of the sizes of clusters that have been generated with the best performing methods on sets B and C (average linkage and Ward linkage respectively), as well as the output of a clustering technique with higher word error rate (k-means on set B). The clustering techniques with lower word error rate are a better match for the actual distribution of cluster sizes. This is also true of techniques for which no plots are provided. It is important for a good clustering approach to produce clusters of a variety of sizes. The output of the k-means clustering in Figure

4.13(d) shows that clusters which should have been large, were broken down into smaller pieces.

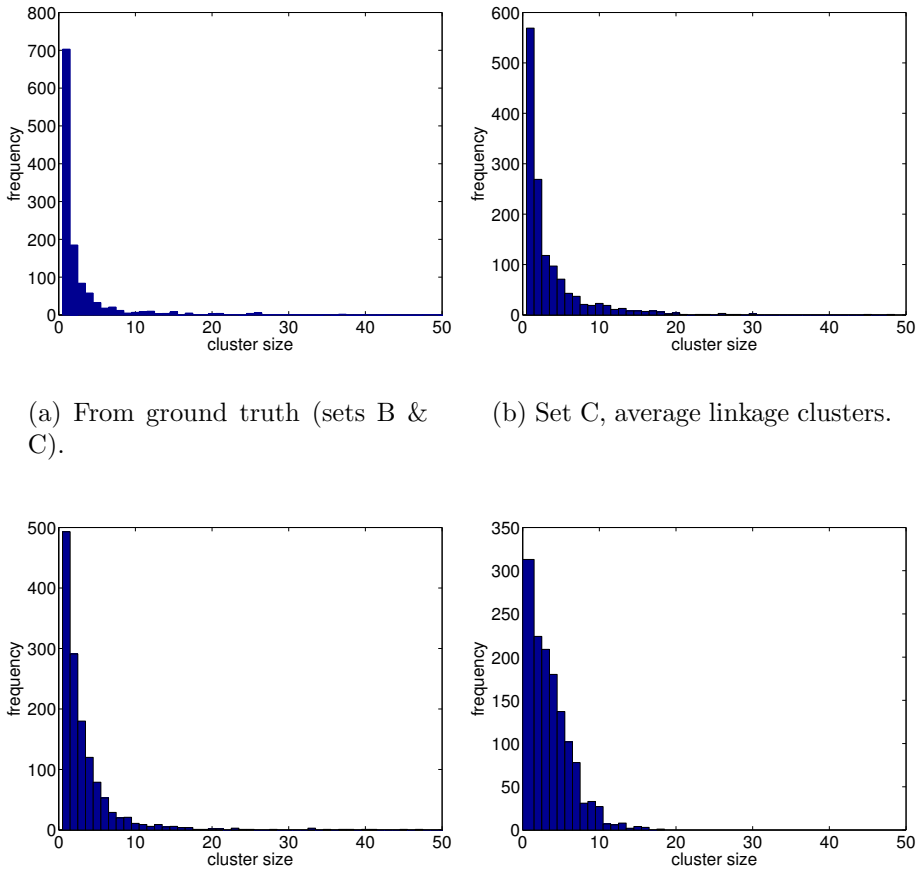

(a) From ground truth (sets B & C).

(b) Set C, average linkage clusters.

(c) Set B, Ward linkage clusters.

(d) Set B, k-means clusters.

Figure 4.13. Histograms of perfect and automatically determined cluster sizes. Some clustering algorithms achieve a good match to the actual cluster size distribution (b),(c), while others tend to produce clusters with a limited range of sizes (d). A small number of clusters with sizes greater than 50 has been omitted from (a) and (c) to allow the displaying of all histograms on the same x-scale.

Our goal is not to obtain labels for all word images in the collection. Following Luhn's line of thought, we can identify clusters that should make good candidates for an index. We constrained the simulated annotation to clusters with at least 3 members, but not more than 50, and calculated the word error rate for the simulated annotation that is restricted only to the selected clusters. Table 4.10 contains the

Clustering alg.	**A: WER/#Img**	**B: WER/#Img**	**C: WER/#Img**
k-means	70.03%/1832	50.80%/2941	n/a
Single linkage	33.80%/1148	3.83%/758	4.90%/715
Complete linkage	57.66%/1866	39.64%/2422	42.58%/2790
Average linkage	55.22%/1742	37.92%/2070	41.66%/2787
Weighted linkage	57.11%/1919	40.87%/2273	41.72%/2656
Ward linkage	58.95%/1956	38.12%/2867	41.88%/2827
Perfect clustering	0%/2586	0%/2567	0%/2567

Table 4.10. Performance of the clustering algorithms, computed for clusters with a moderate number of members. The word error rate was calculated for annotations from clusters with at least 3 members, but not more than 50. *#Img* refers to the total number of images that fall into such clusters. The last row of the table shows the correct value for *#Img*, according to the ground truth annotations.

Clustering alg.	**A: overl/stopw**	**B: overl/stopw**	**C: overl/stopw**
k-means	44.2%/25.7%	79.5%/43.9%	n/a
Single linkage	35.5%/10.0%	27.4%/**6.4%**	22.4%/12.1%
Complete linkage	50.1%/25.4%	72.7%/36.1%	77.8%/41.9%
Average linkage	48.1%/22.6%	62.2%/27.0%	80.1%/43.1%
Weighted linkage	51.9%/27.4%	68.1%/32.5%	75.7%/39.6%
Ward linkage	51.4%/27.8%	**83.8%**/46.7%	78.2%/40.6%
Perfect clustering	100%/51.3%	100%/51.0%	100%/51.0%

Table 4.11. Comparison of automatic and ideal Luhn clusters (cluster sizes between 3 and 50 members). For each clustering output, the overlap between elements in automatic and perfect clusters is shown (*overl*). The second value shows the fraction of all stop words in the collection that is contained in the Luhn clusters (*stopw*).

word error rates that were achieved for such clusters, and the number of word images in the collection that were assigned a label.

The results show increased word error rates (not including clusterings that underestimate #Img; see Table 4.10), indicating that the clustering performs slightly better on words that were excluded from the word error rate calculation. We also note that the clusterings based on data set A consistently underestimate the correct value of #Img. Only some clusterings of sets B and C come close to the desired number, with C having a slight advantage over B.

The cluster selection based on the single linkage clustering produces small word error rates, but this clustering approach performs poorly. The selected number of clusters is substantially lower than the target number, which is the cause of the low word error rates. The word error rates that can be expected from the word spotting approach should be taken from clusterings that produce better matches in terms of the desired number of clusters, e.g. the weighted linkage technique on data set C.

Table 4.11 shows the amount of overlap (*overl*) between the members contained in automatic and perfect (from ground truth) Luhn clusters. The overlap is high for clustering techniques that yielded low word error rates and a good match of *#Img* (cf. Table 4.10), e.g. the Ward linkage technique on data set B or the average linkage method on data set C. The second reported value (*stopw*) in Table 4.11 is the fraction of all stop words in the collection that is contained in Luhn clusters. Somewhat surprisingly, all automatic clusterings contain a smaller fraction of all stop words than the perfect clustering. This is expected for clusterings that substantially underestimate *#Img* (all clusterings of data set A and all single linkage clusterings). For the remaining clustering techniques, it seems that our Luhn cluster selection approach (selecting clusters with sizes between 3 and 50 members) works better for automatic clusterings than for the perfect clustering based on ground truth data. The large fractions of stop word content in the clusters also suggest that a more restrictive selection of Luhn clusters may be used.

Word spotting appears as an attractive alternative to the seemingly obvious *recognize-then-retrieve* approach to historical manuscript retrieval. With the capability to match word images quickly and accurately (e.g. using Euclidean distance between feature vectors), partial transcriptions of a collection can be obtained with reasonable accuracy and little human intervention. Because of the general complexity of the problem, however, which is $O(n^2)$ for datasets with n word images, very large datasets remain out of reach in the near future. Word spotting has the capability to

automatically identify indexing terms, making it possible to use costly human labor more sparingly than a full transcription would require. For example, using the Ward linkage clustering on data set B, it would be possible to obtain 2867 word image labels with a word error rate of 38.12%, by annotating just 291 clusters (cluster sizes between 3 and 50 members). That is, the word spotting procedure would have reduced 2867 annotations to about 10% of that. Even greater savings (in terms of percent) can be expected from larger collections, since vocabularies grow sublinearly in the size of the corresponding collections.

CHAPTER 5

RECOGNITION AND RETRIEVAL

Traditionally, information retrieval has been performed on electronic representations of text, e.g. document encodings in ASCII. The quality of retrieval systems for such documents has led to widespread use and commercial success. It is only natural to attempt to recognize the text in historical manuscript images, and then perform retrieval on the resulting automatic transcription. Here we describe our work on recognizing historical manuscripts, and take a look at the retrieval quality that can be achieved with the automatic recognition output.

5.1 Hidden Markov Document Model

In [58] a holistic recognition approach for handwritten historical documents was presented. It uses a Hidden Markov Model (HMM) [86] to describe the creation process of a document, which is represented as an ordered sequence of handwritten words (see Figure 5.1[1]). At each position i in the document, the author decides to write a particular word w_i, which is chosen based only on the word w_{i-1} at the previous position. Depending on the word choice w_i, a feature vector f_i is chosen. We assume that the feature vector entirely determines the visual appearance of the writing. This allows us to use the f_i as our observations in place of the actual word images, when we recognize a sequence of word images.

[1]We use upper-case characters to denote random variables, lower-case characters denote observed values.

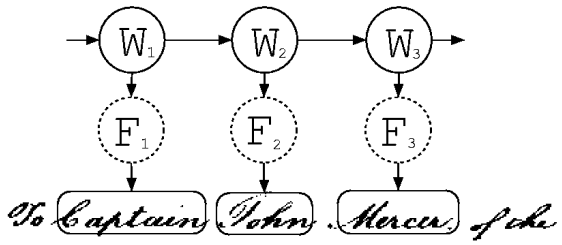

Figure 5.1. Hidden Markov Model of the document creation process. The document is modeled as a hidden sequence of handwritten words W_i, where each written word only depends on the word in the previous state. Based on the word choice W_i at position i, a feature vector F_i is randomly sampled from a word-conditional distribution $P(F_i|W_i)$.

During recognition, a sequence of continuous-space feature vectors f_i (as described in section 3.1) is given, and the task is to infer the values of the hidden state variables W_i from the features. Each random state variable W_i takes on values from a vocabulary $\mathcal{V}$ (e.g. all English words), so the output of the recognition process is a sequence of words.

The main distributions that are needed to specify an HMM are the conditional feature distributions $P(F_i|W_i)$ and a transition probability distribution $P(W_i|W_{i-1})$. We assume all of them to be stationary, so we omit the index i where possible. In the following sections, we describe the models for the feature generation and how the transition probabilities were obtained.

5.1.1 Observation Model

We assume a multivariate normal density for the conditional feature distributions and use annotated training data $\mathcal{T}$ to estimate the parameters. For a given word $w \in \mathcal{V}$, the likelihood of observing the d-dimensional feature vector f as its feature vector is taken to be

$$p(F = \mathbf{f}|W = w) = \frac{\exp\left\{-\frac{1}{2}(\mathbf{f} - \boldsymbol{\mu}_w)^\top \boldsymbol{\Sigma}^{-1}(\mathbf{f} - \boldsymbol{\mu}_w)\right\}}{\sqrt{2^d \pi^d |\boldsymbol{\Sigma}|}}, \tag{5.1}$$

where $\boldsymbol{\mu}_w$ is estimated from the training instances $\mathcal{T}_w$ for w and $\boldsymbol{\Sigma}$ from the entire training data:

$$\begin{aligned}
\boldsymbol{\mu}_w &= \frac{1}{|\mathcal{T}_w|} \sum_{\mathbf{f} \in \mathcal{T}_w} \mathbf{f}, \\
\boldsymbol{\Sigma} &= \mathbf{I} \cdot \sigma^2 = \mathbf{I} \cdot \frac{1}{d} \sum_{p=1}^{d} \left(\frac{1}{|\mathcal{T}| - 1} \sum_{\mathbf{f} \in \mathcal{T}} (f_p - \mu_{\mathcal{T},p})^2 \right),
\end{aligned}$$

where p is used to index dimensions and

$$\begin{aligned}
\mathcal{T}_w &= \{f_i \in \mathcal{T} | w_i = w\}, \\
\boldsymbol{\mu}_\mathcal{T} &= \frac{1}{|\mathcal{T}|} \sum_{\mathbf{f} \in \mathcal{T}} \mathbf{f}.
\end{aligned}$$

We constrain our conditional feature distribution to take the form of an isotropic Gaussian density. The covariance matrix $\boldsymbol{\Sigma}$ is the same for all states $W = w$, because its parameters can be estimated more reliably. The small size of our training collection $\mathcal{T}$ would otherwise yield unreliable estimates for $\boldsymbol{\Sigma}$.

For consistency with prior publications (e.g. [58]), all of the word images in the experiments in this chapter were represented with 27-dimensional feature vectors consisting of 6 scalar features, such as the word image width, and 21 DFT coefficients that were extracted from profile features (see sections 3.1.1 and 3.2.1).

5.1.2 Transition Model

The transition probability distribution corresponds to a word bigram frequency distribution over the considered vocabulary $\mathcal{V}$ that is usually represented as a stochastic table. It can be estimated from the training data and additional text corpora. In

order to fully specify a Hidden Markov model, we also need to provide a prior probability distribution over words. It determines the unigram probabilities $P(W_1 = w)$ for all $w \in \mathcal{V}$. If we define a special vocabulary item s that always marks the beginning of the sequence, but never occurs anywhere else, we can fold the prior probability distribution into the transition probability table.

Given a text collection $\mathcal{C}$, we can estimate the prior probabilities and transition probabilities as

$$P_{\mathcal{C}}(w|s) = \frac{c(w, \mathcal{C})}{|\mathcal{C}|} \tag{5.2}$$

$$P_{\mathcal{C}}(w|w') = \frac{c(w'w, \mathcal{C})}{\sum_{v \in \mathcal{V}} c(w'v, \mathcal{C})} \tag{5.3}$$

where $c(\cdot, \mathcal{C})$ is used to count how often the given string occurs in $\mathcal{C}$. Our annotated training collections ($\mathcal{T}$), which consist of word images with ASCII annotations, are rather small, so the accuracy of the above probability estimates must be expected to be low. For this reason, and to avoid zero probabilities, we use other text sources ($\mathcal{O}$) and a uniform backoff distribution to improve the estimates via smoothing:

$$\hat{P}(w|s) = \frac{1}{3}\left(P_{\mathcal{T}}(w|s) + P_{\mathcal{O}}(w|s) + \frac{1}{|\mathcal{V}|}\right), \tag{5.4}$$

$$\hat{P}(w|w') = \frac{1}{3}\left(P_{\mathcal{T}}(w|w') + P_{\mathcal{O}}(w|w') + \hat{P}(w|s)\right). \tag{5.5}$$

The following text sources were used in the estimation of the transition and prior probabilities. Due to their time of creation and the discourse, they provide a good match for our test collection of George Washington's writing:

Training collection ($\mathcal{T}$): An annotated collection, consisting of word images (represented by feature vectors) and the corresponding annotations/transcription. We use 2 training collections consisting of 20 and 100 page images (4856 and 24696 words respectively) in our experiments.

Jefferson collection ($\mathcal{O}_1$): These transcriptions (200,000 words) are part of the Jefferson corpus at the Library of Congress.

Washington collection ($\mathcal{O}_2$): A large corpus (4.5 million words) consisting of transcriptions that were obtained from the Library of Congress [110]. We excluded portions from this corpus that were used for testing.

Based on these collections, we calculate various unigram and bigram distributions to test the effect of increasingly accurate probability estimates on the recognition error rate. We describe these distributions and the results in the experiments section.

5.1.3 Recognition with Hidden Markov Models

Recognition may be loosely described as finding the state sequence $w_1 \dots w_N$ that best explains the observation sequence $f_1 \dots f_N$. Several solutions are possible, each optimizing a different quantity. For example, we could seek to optimize the likelihood of each state *individually* given the observations, which would maximize the expected number of correct states [86]. However, this may lead to state sequences that are impossible according to the state transition model (e.g. the word pair *the the* might be considered an invalid state sequence).

Since the goal of recognition is often to create a readable transcription of a document, we will recover the state sequence that *jointly* maximizes the likelihood of the observation sequence. This sequence may be determined with the *Viterbi* algorithm [25, 86], a dynamic programming technique. The algorithm recursively calculates

$$\delta_i(w) = \max_{w_1 \dots w_{i-1}} P(W_1 \dots W_i = w, f_1 \dots f_i)$$

using the recursion

$$\delta_{i+1}(w) = \left(\max_{w'} \delta_i(w') \cdot P(W_{i+1} = w | W_i = w') \right) \cdot P(F_i = f_i | W_i = w) \quad (5.6)$$

and the initial condition

$$\delta_1(w) = P(W_1 = w) \cdot P(F_1 = f_1 | W_1 = w).$$

When $\delta_i(w)$ has been computed for all pairs of i and w, the algorithm tracks back the most likely state sequence, starting from the state $\hat{w}_N$ in the trellis defined by $\delta_i(w)$:

$$\hat{w}_N = \underset{w}{\operatorname{argmax}}\, \delta_N(w).$$

From there, backtracking determines all arguments w that yielded the maximum value in equation (5.6). The algorithm terminates when the backtracking has determined the most likely state at position 1 in the sequence.

5.1.4 Recognition Experiments

Our recognition and retrieval experiments were conducted on three datasets. All datasets were first segmented automatically, and then corrected by a human annotator, who also supplied annotations that we use as ground truth for the evaluation of the recognition and retrieval results:

Dataset A: A dataset consisting of 20 page images (4856 word images[2]) from the George Washington collection.

Dataset B: 100 page images (24696 word images) from the Washington collection. dataset A is entirely contained in this set.

Dataset C: 100 page images (21324 word images) from the Washington collection.

Due to their larger size, datasets B and C have not received the same level of human attention. This causes these datasets to be less accurate in the sense that word segmentation coordinates are not as accurate and some ground truth annotations are incorrect. On the other hand, we believe dataset A to be almost free of such mistakes.

[2]The number of word images may be slightly different from other published results, because of a small number of corrections that have been made to the dataset.

5.1.4.1 Influence of Transition Model

Our first recognition experiment was performed entirely on dataset A, using 20-fold cross validation: 19 annotated pages were used for training the bigram (transition) and observation probabilities, and the remaining page was recognized using the above HMM recognizer. Since the recognition is performed at word-level, only terms that occur in the training data can be recognized. Terms that occur in the test document, but not in the training documents are called *Out-Of-Vocabulary (OOV)* terms.

The supplemental Washington and Jefferson collections that were downloaded from the Library of Congress were used to estimate various unigram and bigram models, which are listed here. Whenever a text source ($\mathcal{T}$ and/or $\mathcal{O}$) is not used in the estimation, the mixing weights in equations (5.4,5.5) need to be adjusted:

Uniform: No text source is used, all state transitions are equally likely.

Unigram: Only uses $\mathcal{T}$ for the estimation of the unigram frequencies. The unigram frequencies are used in place of bigram estimates: $\hat{P}(w|w') = \hat{P}(w|s)$.

19 pages: Both bigrams and unigrams are estimated only from the pages that make up the training set. No other ($\mathcal{O}$) text sources are used.

19+Jeff: The estimation uses the training pages as $\mathcal{T}$ and the Jefferson pages as other text sources ($\mathcal{O} = \mathcal{O}_1$). The probability estimation is exactly as in equations (5.4,5.5).

19+J+W: Same as above, but $\mathcal{O}$ is made up of the union of the downloaded Jefferson and Washington transcriptions ($\mathcal{O} = \mathcal{O}_1 \cup \mathcal{O}_2$).

Target: The bigrams are estimated from the page to be recognized. This is a cheating experiment that can be used to compute an upper bound on the recognition performance.

Table 5.1 shows the achieved word error rates for each of the above unigram and bigram estimates. Each error rate in the table is the average over 20 cross-validation runs. The analysis was performed both with and without considering OOV terms, yielding lower error rates when OOV terms are excluded.

Bigram Model		**Word Error Rate**	
Source	**Size**	**Excluding OOV**	**Including OOV**
Uniform	0	53.1% ± 5%	60.3% ± 5%
Unigram	4.6K	44.8% ± 5%	53.3% ± 5%
19 pages	4.6K	41.4% ± 6%	50.3% ± 7%
19+Jeff	191K	38.8% ± 5%	48.1% ± 6%
19+J+W	4,533K	34.9% ± 6%	44.9% ± 7%
Target	243	4.5% ± 3%	6.3% ± 4%

Table 5.1. Word error rates for handwriting recognition with a word-level Hidden Markov Model, using bigram estimates from collections of varying sizes. The analysis was performed both excluding and including Out-Of-Vocabulary words in the error rate calculation.

The beneficial effect of using large text sources for the estimation of the transition models can be seen very clearly. The word error rates (WER) drop substantially from 53% to 35% without considering OOV terms, when moving from a transition model that considers no text source at all, to a model that uses a large collection of text from the same time period and about approximately the same topic as the recognized text. Still, the error rates are generally high, and would be unacceptable to a human reader. They are, however, comparable to other results reported in the literature, which range from about 40% to 63%. These numbers were obtained on modern documents of high quality with vocabulary sizes from 525 to 7719 [46, 83]. The vocabulary size of test set A is 1187.

Not surprisingly, the lowest word error rate was achieved with the bigram model estimated from the page that is to be recognized. The large difference in performance compared to that of the second-best bigram model suggests that much improvement could be expected from further improvement of the transition model. This would

require even more text sources that are relevant to the collection to be recognized. However, since our documents are historical, such data is not readily available in electronic text formats.

Comparing the recognition results with those obtained from simulated annotation results on clustered word images shows the competitiveness of the word spotting technique. With all clusters annotated, word spotting has a word error rate of 34.12% using the average linkage clustering method and the DTW distance measure. This would require only 1365 cluster annotations (for a total of 4856 annotated word images), compared to roughly 4600 training annotations in the above recognition experiments for a total of 240 automatic word image annotations on one recognized page. When the collection of clusters is further limited by only annotating "interesting" clusters (cluster sizes between 3 and 50 members), word spotting still outperforms the best HMM recognition results including OOV terms with 41.66% WER versus 44.9%. In this case, only 278 cluster annotations need to be provided. However, the computational demands of the word spotting approach make the HMM recognition approach more desirable for large datasets.

5.1.4.2 Recognition of Large Datasets

The above experiment was performed on a small dataset. Only one page image was recognized, which is very little data (there are about 240 words per page on average) for assessing retrieval performance. Here we describe our recognition results on dataset C (100 pages), which is much better suited for this task. For training, datasets A (20 pages) and B (100 pages) were used.

The test set was recognized using two methods:

HMM: The Hidden Markov Model recognition approach described above.

BDT: A classification technique for word images that uses boosting to build an ensemble classifier from individual decision tree classifiers that operate on multi-

resolution bitmap representations of word images. The approach was described in [35]; we use the recognition output here for comparison.

Since we are recognizing George Washington's handwritten letters, we only used the training data and the Jefferson transcriptions in the estimation of the transition model for the HMM approach. Using all of the transcriptions that are available for George Washington's letters would result in a very good bigram model, but it is unrealistic to assume that such closely matching text sources are available in an actual recognition situation. The BDT classifier does not use the bigram language model.

Evaluation technique	**A/HMM**	**A/BDT**	**B/HMM**
WER (including OOV terms)	66.60%	55.83%	69.86%
WER (excluding OOV terms)	54.83%	39.51%	64.47%
Recognition vocabulary size	3722	3738	5980

Table 5.2. Word error rates (WER) and vocabulary sizes used in the recognition. The vocabulary sizes of the A/HMM and A/BDT experiments vary slightly, because a small number of corrections have been made to dataset A over time (A/BDT uses the most recent version).

Table 5.2 shows the word error rates we obtained with the above recognizers using datasets A and B for training. A/BDT clearly outperforms both A/HMM and B/HMM in terms of word error rate by a wide margin of more than 10%. However, we will see shortly that the superior performance of A/BDT does not necessarily translate into better retrieval performance. Somewhat surprisingly the error rate of B/HMM, which uses a much larger training set, is worse than that of A/HMM. Normally, one would expect a larger training set to yield better results. In this case, however, increasing the training set size comes with a significantly increased vocabulary (3722 to 5980). This makes classification harder, because of the increased number of categories that the recognizer is presented with. Large-vocabulary documents are the real challenge when performing handwritten document recognition. The cross-modal retrieval approach based on continuous features we present in chapter 6 does

not immediately suffer from this drawback. We show that its performance increases when a larger training set is used. The reason lies in its approach to classification, which avoids making hard decisions (as recognizers do).

5.2 Retrieval

We now use the recognition output and perform retrieval on it. To do this, the automatically generated transcription of a page image is treated as an electronic document, just as a manually generated transcription would be. We can then select a retrieval model and run experiments to test the retrieval performance.

5.2.1 Language Model Retrieval

A retrieval model specifies how documents are ranked in response to a query. For our experiments, we chose the language model retrieval approach [85], because it is well adapted to situations with probabilistic document representations. This fact makes language model retrieval particularly attractive for the probabilistic retrieval approaches in chapter 6. We use the same retrieval model here for comparability.

In language model retrieval, each document is represented by a probabilistic model that captures occurrence frequencies of terms in the document. Such *document models* can be used to calculate the probability of observing a particular combination of words when selecting terms from a document at random. Ponte and Croft [85] used the probability of observing a given query as a random sample from a document model M_D as the score for the document D. We will call this scoring function the *query-likelihood* approach in the following.

The original proposed language model retrieval advocated Bernoulli document models, but multinomial models [105] are now a more popular choice. With this model, the probability of sampling the query $Q = w_1 \dots w_k$ from the document model M_D may be calculated as

$$P(Q|M_D) = \prod_{i=1}^{k} P(w_i|M_D), \tag{5.7}$$

where $P(w_i|M_D) = \frac{c(w_i,D)}{|D|}$ is the maximum-likelihood estimate of the term frequency in the document D. In practice, the term frequency estimates are often smoothed with the collection frequencies, to avoid situations where a single query term with 0-frequency would cause a document to be assigned a score of 0 (see section 6.2.1 for smoothing with the Jelinek-Mercer approach).

5.2.2 Retrieval Experiments

Dataset C was used as the test collection for all retrieval experiments. Its size allows us to use it both for line retrieval (3336 lines) and document retrieval (100 pages/documents).

Each retrieval experiment involves grouping the word annotation results of the recognizer into retrieval units (either pages or lines, referred to as "documents" in the following). The resulting units are then stemmed using the Krovetz stemmer [50] and placed into an index. We selected a total of 400 queries, ranging from 1 to 4 words in length (100 queries for each query group). The query terms were sampled at random from all lines in the test set, to ensure that at least one relevant item exists for each query (see Table 5.3 for the number of relevant items per query group). Stop words and terms that did not occur in the training set were excluded from the query selection. This query set is also used in the evaluation of other retrieval techniques (see chapter 6).

Query length	**1 word**	**2 words**	**3 words**	**4 words**
Page retrieval	1453	625	471	203
Line retrieval	2193	192	232	118

Table 5.3. Number of relevant items per query group.

During retrieval, each query was used to rank the documents in the collection with the query-likelihood method. The smoothing parameter that controls the interpolation between the foreground and background term probability estimate, was set to 0.8, i.e. giving more weight to foreground term probability estimates. The resulting ranked lists were evaluated using the trec_eval program. A retrieved item was judged relevant to a query, if it contains each of the query terms at least once. Table 5.4 shows the mean average precision (MAP) scores that were achieved for retrieval on dataset C, with training sets A and B, using the HMM and BDT recognition model. The best result in each row was compared to the other results using the sign test [26]. If there was a statistically significant difference (significance level $\alpha = .05$), the lower result was marked with an asterisk ($*$).

Exper.	**Query len.**	**A/HMM**	**A/BDT**	**B/HMM**
Page retrieval	1 word	**.1818**	.1676	.1623
	2 words	**.2451**	.2293	.1984$*$
	3 words	**.2777**	.2481	.2097$*$
	4 words	**.3874**	.3410$*$	.2200$*$
Line retrieval	1 word	.0933	**.1018**	.0826
	2 words	**.1655**	.1603	.1175
	3 words	**.2630**	.2466	.1312$*$
	4 words	.2903	**.3766**	.1394$*$

Table 5.4. Mean average precision scores for the retrieval experiments conducted on automatically recognized pages. Each column shows results obtained with a particular training set (A or B) and recognition approach (HMM or BDT). Results that are significantly different from the best result in each row are marked with an asterisk ($*$).

Surprisingly, despite its substantially better recognition performance (cf. Table 5.2), the BDT technique does not yield the best retrieval performance. The HMM recognizer on dataset A outperforms or matches BDT's results, except for line retrieval with queries of length 4. It seems that the lower word error rates achieved with BDT have to be attributed to terms that are not used in queries, for example stop words.

In fact, it turns out that the WER for words on a standard stop word list is 28.70% (using the BDT recognizer), while the WER of non-stopwords is 82.33%.

Another reason for the difference in performance could be the length of the returned ranked list. Our test collection is rather small when compared to corpora that are typically used in information retrieval of text (e.g. TREC collections). This can have effects on the evaluation of ranked result lists, which typically are not observed in large collections. The reason lies in the trec_eval program, which assigns a precision of 0 to relevant items that do not occur in a ranked result list. When working with large collections, typically the top 1000 documents are returned, and relevant documents that were not retrieved have a precision close to 0 (less than 10^{-3}). However, when the ranked result list is short, as is the case here with document retrieval and short queries (or smoothing turned off), assigning a precision of 0 can significantly underestimate the precision. In this situation, simply returning a longer ranked list can improve the average precision score of a retrieval run. Since we are using smoothing, queries with more terms return longer ranked lists, which result in higher average precision scores.

Exper.	**Query len.**	**A/HMM**	**A/BDT**	**B/HMM**
Page retrieval	1 word	**.2740**	.2643	.2629
	2 words	**.2574**	.2405	.2208
	3 words	**.2811**	.2505	.2163
	4 words	**.3880**	.3417∗	.2228∗
Line retrieval	1 word	.0979	**.1062**	.0878
	2 words	**.1662**	.1611	.1186
	3 words	**.2631**	.2466	.1314∗
	4 words	.2903	**.3766**	.1395∗

Table 5.5. Mean average precision scores for the same experiments as in Table 5.4, calculated for ranked lists that contain all documents in the collection. Results that are significantly different from the best result in each row are marked with an asterisk (∗).

In order to test if the above evaluation effect plays a role in the lower precision scores of the BDT run (because BDT might tend to retrieve shorter result lists), we repeated the evaluation in Table 5.4, with ranked lists that contain all documents in the collection. The results are shown in Table 5.5. Still, the picture of the comparison between A/HMM and A/BDT remains exactly the same: for the most part, A/HMM performs better than A/BDT.

We can observe however, that in Table 5.5 the pattern of strictly increasing MAP scores with longer queries (in Table 5.4) has been broken in the document retrieval scores. It is still present in the line retrieval scores though, so there seems to be a general tendency for higher scores when longer queries are used. We attribute this to the query selection process, which selects queries from lines in the test set. This causes a relevant line to be retrieved, even if the recognition output contains only one of the query terms. The likelihood that at least one query term is contained in the recognition output increases with longer queries, causing increased MAP scores for longer queries.

As we would expect from its lower recognition rate, the retrieval performance of B/HMM falls short of that of A/HMM and A/BDT. This shows – again – the challenges that recognition/annotation techniques face in the presence of large-vocabulary applications. It has to be pointed out, however, that the query selection was performed on the intersection of the vocabularies of sets A and C, to guarantee that the same queries can be used in all experiments. A search engine built with the output of B/HMM would allow a wider range of query terms, because its training vocabulary is a superset of the vocabulary of set A. This fact was not considered in our evaluation here.

Table 5.6 shows precision scores at the top 5 retrieved items for all retrieval runs. The picture is similar to the mean average precision results in Table 5.5, with A/HMM performing best in the page retrieval experiments. In the line retrieval experiments,

Exper.	Query len.	A/HMM	A/BDT	B/HMM
Page retrieval	1 word	**0.3060**	0.2680	0.2940
	2 words	**0.2120**	0.2080	0.1940
	3 words	**0.1900**	0.1760	0.1640
	4 words	**0.1620**	0.1560	0.1140∗
Line retrieval	1 word	0.1680	0.1680	**0.1740**
	2 words	**0.0660**	**0.0660**	0.0540
	3 words	0.0840	**0.0860**	0.0560∗
	4 words	0.0800	**0.1120**	0.0500∗

Table 5.6. Precision at the top 5 retrieved items for retrieval runs based on recognition output. All ranked lists were padded to contain all documents in the collection. Results that are significantly different from the best result in each row are marked with an asterisk (∗).

A/BDT seems to perform slightly better than the remaining techniques, although not significantly better than A/HMM. The generally low level of the precision scores may be explained by the small number of relevant items per query (cf. Table 5.3), which causes the maximum achievable precision-at-5 of many queries to be substantially less than 100%, especially for queries consisting of multiple words. Another contributing factor to lower precision numbers are recognition errors, which cause relevant items not to be retrieved.

Recognizers make *hard* classification decisions, that is, they return a single annotation term for each word image on a page. In our case, that decision is based on a probability estimate, which indicates that a particular choice is more likely to be the answer than any of the alternatives. If the decision is made, the information about alternatives is no longer available. This could cause a document not to be retrieved (or at a very low rank) if a term used in the query was wrongfully dismissed by the recognizer. In the following chapter, which uses cross-modal models for the annotation of word images, we show how the information about alternative word image annotations may be used to improve retrieval performance.

CHAPTER 6

CROSS-MODAL RETRIEVAL

In this chapter, we focus on retrieval with *cross-modal* models. These models describe the joint occurrence of annotation words and features. Cross-media models were reported for automatic color photograph annotation and retrieval [41, 57]. Here we adapt such models for the cross-modal application of retrieving historical manuscripts using text queries [92]. Our models can exploit the statistical regularities of language and we show how a bigram language model may be used to constrain annotations of adjacent word images, yielding substantially improved retrieval results. In addition, our cross-modal models allow the retrieval of units of arbitrary size (e.g. pages or lines), not just individual images as in previous work.

Cross-modal retrieval models are closely related to previous work in *cross-lingual* information retrieval of text, where joint models of words in two different languages are used to retrieve documents in a language that differs from the query language. By analogy, word images and their annotations may also be seen as representations of the same concept in two languages.

We present three cross-modal retrieval models for historical manuscripts, evaluate their performance and compare them against the retrieval performance that can be achieved on recognition output. Finally, we look at ideas on how to tackle the problem of out-of-vocabulary terms with synthetic training data. This allows the use of such terms in queries despite the lack of training data.

6.1 Joint Models for Annotation Words and Features

Cross-modal models describe the joint occurrence of annotation words and features. We will look at annotations and features of word images and then move to larger retrieval units. Our model describes the probability of observing a particular annotation word w together with a particular feature representation $\mathbf{f}$ of a word image:

$$P(w, \mathbf{f})$$

We assume that w is selected from a vocabulary $\mathcal{V}$ (e.g. all English words) and the feature representation $\mathbf{f}$ is an element of some feature space $\mathcal{F}$. This model allows us to do two things:

Probabilistic Annotation: For a given feature representation $\mathbf{f}$, we can calculate a distribution over potential annotation terms $w \in \mathcal{V}$ using

$$P(w|\mathbf{f}) = \frac{P(w, \mathbf{f})}{\sum_{v \in \mathcal{V}} P(v, \mathbf{f})}. \tag{6.1}$$

That is, each entry in the vocabulary $\mathcal{V}$ is assigned a probability that it is the correct annotation term for the given feature representation. The annotation probabilities that occur within a retrieval unit may be used to estimate a unigram model for it, which is an approximation of the model that would arise from the true term counts in the retrieval unit.

Content Modeling: For a given annotation word w, we can predict a model/distribution in the feature space $\mathcal{F}$ that describes image content which we would like to retrieve. That is, w can be seen as a query, which returns a distribution over feature representations $\mathbf{f}$:

$$P(\mathbf{f}|w) = \frac{P(w, \mathbf{f})}{\sum_{g \in \mathcal{F}} P(w, \mathbf{g})}, \tag{6.2}$$

where we assume that the feature space $\mathcal{F}$ is discrete. The feature distribution may then be used to score word images (their features) by their degree of agreement with the distribution.

In chapter 3, we discussed a discrete feature representation and continuous-space feature vectors. Depending on the feature space $\mathcal{F}$, our model of $P(w, \mathbf{f})$ varies. We use the discrete feature representation for probabilistic annotation and content modeling, and continuous-space features for probabilistic annotation, yielding a total of three cross-modal retrieval models. We will refer to them as *DPA*, *CPA* and *DCM* respectively. Before we move on to the estimation of $P(w, \mathbf{f})$, we take a look at the origin of cross-modal retrieval.

6.1.1 Cross-Lingual Text Retrieval

Cross-lingual information retrieval of text documents allows a query to be formulated in one language, and the retrieved documents to be in another language. The problem of retrieving handwritten content using English queries is analogous to cross-lingual retrieval, if the handwritten content is described with an *image description language*. In section 3.3, we presented a discretization technique which turns continuous-space feature vectors into feature tokens from a token vocabulary $\mathcal{F}$. This allows us to adapt cross-lingual ideas for text documents to our multimedia content.

Lavrenko et al. [53] presented an approach to cross-lingual information retrieval of text that is based on *relevance models*. They assume that relevant documents and the queries that would retrieve them are random samples from a relevance distribution. If the relevance model R_Q were known for a given query $Q = e_1, \ldots, e_k$ of English words, one could use the relevance model to extract a language model $P(w|R_Q)$ in the other language. This target language model may then be used to rank documents in the foreign language.

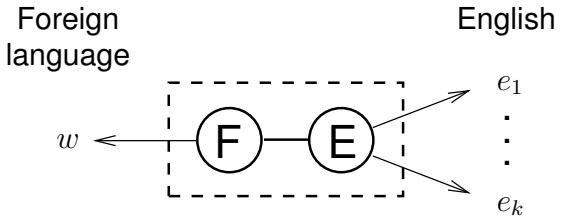

Figure 6.1. Graphical representation of a cross-lingual relevance model for text. The query is formulated in English and can be used to estimate a distribution over terms w in a foreign language from a parallel corpus of document pairs $\{F, E\}$.

However, R_Q is generally unknown, so Lavrenko and Croft [54] proposed to estimate $P(w|R_Q)$ directly from the query:

$$P(w|R_Q) \approx P(w|Q) = \frac{P(w, e_1, \ldots, e_k)}{\sum_{v \in \mathcal{V}} P(v, e_1, \ldots, e_k)} \tag{6.3}$$

The joint probability $P(w, e_1, \ldots, e_k)$ may be determined from a parallel corpus[1] $\mathcal{T}$ of document pairs $\{E, F\}$ in English and the foreign language, with the models $\{M_E, M_F\}$:

$$P(w, e_1, \ldots, e_k) = \sum_{\{M_E, M_F\} \in \mathcal{T}} P(\{M_E, M_F\}) P(w|M_F) \prod_{i=1}^{k} P(e_i|M_E), \tag{6.4}$$

which assumes conditional independence of the English and foreign words. $P(\cdot|M_F)$ and $P(\cdot|M_E)$ are modeled with multinomial distributions, whose parameters may be estimated using maximum likelihood estimation. Figure 6.1 shows a graphical representation of this model. We now look at how the same estimation strategy can be used to calculate the probability of jointly observing English annotation words w and feature representations $\mathbf{f}$.

[1]Parallel corpora contain documents in two languages. For each document, a translation is available in the other language.

6.1.2 Cross-Modal Model

We can readily extend the cross-lingual relevance modeling idea for the purpose of calculating $P(w, \mathbf{f})$. Instead of a parallel text corpus, we use a training collection $\mathcal{T}$ of word images and their English annotations. $\mathcal{T}$ consists of pairs $\{v, \mathbf{g}\} \in \mathcal{V} \times \mathcal{F}^k$ of annotations and feature representations, where the integer $k = 1$ if $\mathcal{F}$ is a continuous feature space (e.g. $\mathcal{F} = [0, 1]^d$) and $k > 0$ if $\mathcal{F}$ is a discrete feature vocabulary. $|\mathcal{T}|$ refers to the number of training instances, that is, the number of pairs $\{v, \mathbf{g}\} \in \mathcal{T}$.

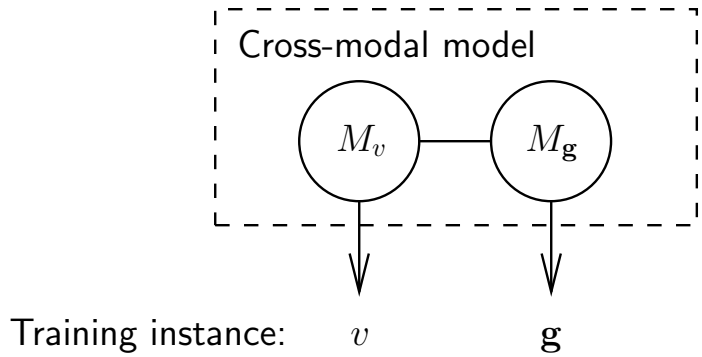

Figure 6.2. Illustration of the cross-modal model for a single training instance $\{v, \mathbf{g}\}$. The training annotation v and the feature vector $\mathbf{g}$ are assumed to be random samples from their respective distributions $P(\cdot|M_v)$ and $P(\cdot|M_{\mathbf{g}})$.

By analogy with the cross-lingual case, we get

$$P(w, \mathbf{f}) = \sum_{\{v,\mathbf{g}\}\in\mathcal{T}} P(\{M_v, M_{\mathbf{g}}\})P(w, \mathbf{f}|\{M_v, M_{\mathbf{g}}\}) \quad (6.5)$$

$$= \sum_{\{v,\mathbf{g}\}\in\mathcal{T}} \frac{1}{|\mathcal{T}|} P(w|\{M_v, M_{\mathbf{g}}\})P(\mathbf{f}|\{M_v, M_{\mathbf{g}}\}) \quad (6.6)$$

$$= \sum_{\{v,\mathbf{g}\}\in\mathcal{T}} \frac{1}{|\mathcal{T}|} P(w|M_v)P(\mathbf{f}|M_{\mathbf{g}}), \quad (6.7)$$

where we assume a uniform prior on the training instances. Together, M_v and $M_{\mathbf{g}}$ form the cross-modal relevance model that the training instance $\{v, \mathbf{g}\}$ was sampled from (see Figure 6.2). The above calculation of $P(w, \mathbf{f})$ may be interpreted as a mixture model of distributions $P(w, \mathbf{f}|\{M_v, M_{\mathbf{g}}\})$ that arise from the training instances. We

now show how to estimate M_v from v and $M_{\mathbf{g}}$ from $\mathbf{g}$, which permits us to calculate $P(w|M_v)$ and $P(\mathbf{f}|M_{\mathbf{g}})$.

$P(w|M_v)$ is the probability of sampling w from the annotation model M_v. Observing any annotation other than v should be impossible, since v is the only correct annotation for the training instance $\{v, \mathbf{g}\}$.[2] Therefore we set

$$P(w|M_v) = \begin{cases} 1 & \text{if } v = w \\ 0 & \text{otherwise} \end{cases} \tag{6.8}$$

We assume the training feature vector $\mathbf{g}$ is a random sample from the distribution $P(\cdot|M_{\mathbf{g}})$. If handwriting were a process that is executed with mechanical precision and would always yield the same result, we could use a similarly restricted probability calculation for $P(\mathbf{f}|M_{\mathbf{g}})$ as in equation (6.8). However, this is not the case and we would like to assign non-zero probabilities even when $\mathbf{f}$ is not exactly the same as $\mathbf{g}$. Depending on the type of feature representation, we can achieve this in two ways:

1. If $\mathcal{F}$ is a vocabulary of discrete feature tokens as described in section 3.3, we have $\mathbf{f} = (f_1, \ldots, f_k)$ and $\mathbf{g} = (g_1, \ldots, g_k)$. We treat $\mathbf{g}$ as a document and estimate the distribution $P(\cdot|M_{\mathbf{g}})$ that it was sampled from, assuming a multinomial distribution. We may then calculate $P(\mathbf{f}|M_{\mathbf{g}})$:

$$P(\mathbf{f}|M_{\mathbf{g}}) = \prod_{i=1}^{k} P(f_i|M_{\mathbf{g}}) \tag{6.9}$$

where

$$P(f_i|M_{\mathbf{g}}) = \lambda \frac{c(f_i, \mathbf{g})}{k} + (1 - \lambda) \frac{1}{|\mathcal{T}|} \sum_{\{u, \mathbf{h}\} \in \mathcal{T}} \frac{c(f_i, \mathbf{h})}{k}. \tag{6.10}$$

[2] In other domains this may not be the case. For example, photograph annotations are often ambiguous. If a training photograph has been annotated with v, other annotations could also be valid.

$c(a, \mathbf{b})$ counts the number of occurrences of a in $\mathbf{b}$. The smoothing parameter λ interpolates between the foreground probability estimate that is obtained from the current training instance, and the background probability from the entire training set $\mathcal{T}$. It may be determined empirically using the training set.

2. If $\mathcal{F}$ is continuous, e.g. $\mathcal{F} = [0, 1]^d$ for some integer $d > 0$, we can use a kernel density estimate with a Gaussian kernel [3] for $P(\cdot|M_{\mathbf{g}})$:

$$p(\mathbf{f}|M_{\mathbf{g}}) = \frac{1}{\sqrt{(2\pi)^d|\mathbf{\Sigma}|}} \exp\left(-\frac{1}{2}(\mathbf{f}-\mathbf{g})^T\mathbf{\Sigma}^{-1}(\mathbf{f}-\mathbf{g})\right) \tag{6.11}$$

We use $\mathbf{\Sigma} = \sigma^2\mathbf{I}$, where σ is determined empirically on the training set.

With these tools for the estimation of cross-modal models for individual word images, we now turn to how they can be applied for retrieval of arbitrary units.

6.2 Cross-Modal Retrieval

6.2.1 Probabilistic Annotation

The probabilistic annotation approach annotates each word image in the test collection with each word from the annotation vocabulary $\mathcal{V}$. That is, for the word image with feature representation $\mathbf{f}$, $P(w|\mathbf{f})$ is calculated for all $w \in \mathcal{V}$. The result is an annotation *distribution* $P(\cdot|\mathbf{f})$.

Typically, retrieval applications retrieve units of text U that are larger than individual words (e.g. pages or documents). In order to perform retrieval of larger text portions, the probabilistic annotation results need to be aggregated. This may be done by averaging the distributions of word images that fall into the same retrieval

[3] In that case, $p(\mathbf{f}|M_{\mathbf{g}})$ is a probability density function, which we indicate with a lower-case p.

unit U. The result is an approximation to the language model M_U that would result from maximum likelihood estimation from a ground truth transcription of U:

$$\hat{P}(w|M_U) = \frac{1}{|U|} \sum_{\mathbf{f} \in U} P(w|\mathbf{f}) \tag{6.12}$$

If the $P(w|\mathbf{f})$ were perfect predictors of the actual annotations, $\hat{P}(\cdot|M_U)$ would be equivalent to the maximum likelihood estimate of the language model. In the presence of imperfect annotation models, $\hat{P}(\cdot|M_U)$ may be seen as an approximation to the language model of U that would result from a perfect transcription. When constructing probabilistic document models using maximum-likelihood estimation (see section 5.2.1), each word image corresponds to one term count within U. Probabilistic annotation can then be seen as dividing up the one term count a word image represents, among various alternative terms from the vocabulary $\mathcal{V}$.

The retrieval units may then be ranked using the query likelihood approach (see section 5.2.1). In order to run retrieval, the following steps are executed:

1. The training and test sets are preprocessed and features (either discrete or continuous) are extracted from each word image.

2. All word images in the test set are automatically annotated with all $w \in \mathcal{V}$ using $P(w|\mathbf{f})$.

3. The per-word-image annotations are grouped to form language models of the desired retrieval units (pages, paragraphs, lines, ...). For practical reasons, the language models M_U are truncated to contain only the terms with the highest annotation probabilities. We discard terms with probabilities $\hat{P}(w|M_U) < 10^{-4}$.

4. The language models are placed into an inverted file for fast access during retrieval. An inverted file consists of inverted lists, one for each vocabulary

term. Each list contains the retrieval units in which the corresponding term (w) occurred, together with the probability $\hat{P}(w|M_U)$.

5. Retrieval proceeds by extracting the inverted lists for all terms that occur in the query. The score of a particular document is the product of its scores in the extracted lists, smoothed with the background term probability:

$$P(Q|M_U) = P(w_1, \ldots, w_k|M_U) = \prod_{i=1}^{k} \left(\mu \hat{P}(w_i|M_U) + (1-\mu) \frac{c(w_i, \mathcal{T})}{|\mathcal{T}|} \right),$$

where μ is a smoothing parameter[4] and $c(w_i, \mathcal{T})$ counts how many times w_i occurred in the training set $\mathcal{T}$. This is the query likelihood ranking approach that was used in chapter 5 for retrieval on automatically generated transcriptions.

The retrieval technique based on probabilistic annotation has 2 tuning parameters that affect system performance: i) Smoothing parameter λ, which controls the degree of smoothing on the feature distributions when using a discrete feature vocabulary. When using continuous features, the relevant tuning parameter is the kernel bandwidth σ. ii) Smoothing parameter μ to prevent zero probabilities during retrieval.

Figure 6.3 shows examples of word images after preprocessing and the top 5 annotation labels w with probabilities $P(w|\mathbf{f})$ that were assigned to them. The first two examples (*Orders* and *Instructions*) were generated with the continuous-space probabilistic annotation model CPA, the third example was generated with the discrete annotation model DPA. All annotation labels are stemmed (reduced to their morphological root), so *order* is the correct annotation for the image containing the word *Orders*. The *Instructions* example illustrates the effect of annotation mistakes in the training collection (the second label (*instuction*) is the result of a typo).

[4]Smoothing prevents a retrieval unit U from getting a probability score of 0 if one of the query terms in Q did not occur in U. This would be undesirable, because a single missing or misclassified term would cause U not to be retrieved, even if all remaining query terms are present in U.

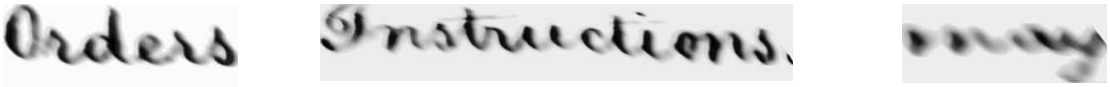

Annotation probability	Label
.975	order
.010	adam
.004	kill
.002	submit
.001	because
...	...

Annotation probability	Label
1.0	instruct
$< 10^{-3}$	instuction
$< 10^{-3}$	ammunition
$< 10^{-3}$	lieutenant
$< 10^{-3}$	cumberland
...	...

Annotation probability	Label
.458	any
.290	may
.099	neces–
.057	carry
.018	my
...	...

Figure 6.3. Examples of probabilistic annotation output. For each word image, the top 5 annotation labels w and corresponding probabilities $P(w|\mathbf{f})$ are shown. The *Orders* and *Instructions* examples were generated with the CPA model, the third example was generated with the DPA model.

6.2.2 Content Modeling

The content modeling approach takes as input a query term, which is used to predict a distribution over feature tokens that would be expected to co-occur with the given annotation. This target model of the desired content may then be used to score word images in the test set using their feature representations. This model uses a discrete feature representation $\mathcal{F}$.

In the first step, the single-word query w is used to calculate a distribution $P(\cdot|w)$ over the feature vocabulary $\mathcal{F}$:

$$\forall f \in \mathcal{F} \quad \text{calculate} \quad P(f|w) \tag{6.13}$$

This target distribution $P(\cdot|w)$ of the content (features) we are looking for can then be used to score empirical distributions $P(\cdot|M_{\mathbf{g}})$ that are derived from word images (represented by $\mathbf{g}$) in the test set. The empirical distribution of a test instance is obtained from its feature representation $\mathbf{g} = (g_1, \ldots, g_k)$ via smoothing:

$$P(f|M_{\mathbf{g}}) = \theta \frac{c(f,\mathbf{g})}{k} + (1-\theta)\frac{1}{|\mathcal{T}|}\sum_{\{v,\mathbf{h}\}\in\mathcal{T}} \frac{c(f,\mathbf{h})}{k}, \tag{6.14}$$

where we also assume that $P(\cdot|M_{\mathbf{g}})$ is multinomial. As before, $c(f,\mathbf{g})$ counts how many times f occurs in $\mathbf{g}$.[5] The degree of disagreement between the model $P(\cdot|w)$ and the empirical distribution $P(\cdot|M_{\mathbf{g}})$ derived from the test instance $\mathbf{g}$ may be determined using the *Kullback-Leibler divergence* (also *relative entropy*) [72, 55, 124]. It measures the additional amount of information that would be required to encode events from one distribution (our target) with a model of it (the empirical distribution):

$$D\left(P(\cdot|w)||P(\cdot|M_{\mathbf{g}})\right) = \sum_{f\in\mathcal{F}} P(f|w)\log\frac{P(f|w)}{P(f|M_{\mathbf{g}})} \tag{6.15}$$

This "distance" measure allows us to rank *word* images in the test set in response to a *1-word* query. What remains is the calculation of scores for larger retrieval units and support for queries consisting of multiple words. The following provides this functionality by pooling scores obtained for multiple query terms and for all word images in a retrieval unit.

The content modeling approach does not lend itself well to situations with multi-word queries and retrieval units greater than words. Calculating a feature distribution conditional on two or more annotation words – for example $P(\cdot|w,w')$ – is not advisable, because it would determine a feature distribution that is a mixture of the distributions obtained with the annotation words separately. $P(\cdot|w,w')$ models word image content that shares visual characteristics of the classes w and w'. Consequently, query terms have to be processed separately.

We cumulate the scores that a word image receives for all terms in a query Q:

[5] Because of the feature representation we have chosen, this can be at most 1. However, other feature representations are conceivable, which could yield higher values.

$$\text{score}(Q, \mathbf{g}) = -\sum_{w \in Q} D(P(\cdot|w)||P(\cdot|M_{\mathbf{g}})) \tag{6.16}$$

The score is inverted, because relative entropy measures the degree of dissimilarity.

Finally, scores for retrieval units U are calculated by summing the scores that the contained word images received for the query Q:

$$\text{score}(Q, U) = \sum_{\mathbf{g} \in U} \text{score}(Q, \mathbf{g}) \tag{6.17}$$

In the next section, we evaluate the performance of these three cross-modal retrieval models and compare it to the retrieval results based on recognition.

6.3 Experimental Results

Our first set of experiments was conducted on 100 pages of test data, with training sets of 20 and 100 pages. All three models were evaluated and compared to the retrieval based on HMM recognition output. In a second experiment, the probabilistic annotation model with continuous features was used to test the retrieval performance on a large test collection of 1000 pages.

6.3.1 100 Pages of Test Data

The test data (dataset C) in the following experiments consists of 21324 word images from 100 page images. Both manual and automatic segmentation output were used. Two datasets were used for training:

Dataset A: 20 pages, manually segmented into 4860 word images with annotations.

Dataset B: 100 pages, manually segmented into 24696 word images with annotations.

The three data sets coincide with the datasets A, B and C used in the evaluation of the HMM recognizer in chapter 5. Depending on the model, each word image was

represented using either discrete or continuous features. The same 400 queries of length 1 to 4 (100 of each length) that were used in the evaluation of the recognize-then-retrieve approach were used to retrieve lines and pages as described in sections 6.2.1 and 6.2.2. Each model has two tuning parameters that were determined empirically on the training set by splitting it into a training and a validation portion of equal size. Separate parameter settings were determined for data sets A and B.

Tables 6.1 and 6.2 show mean average precision scores obtained from retrieval with 20 pages of training data. The results were calculated from the actual ranked lists and lists that have been padded to include all retrieval units in the test set (see the alternate retrieval evaluation in section 5.2.2). Tables 6.3 and 6.4 show the same results for 100 pages of training data. Our discussion here is restricted to the evaluation scores obtained with the padded lists, because they do not depend on the length of the returned list (which has an effect on mean average precision calculation; see section 5.2.2).

The test data was structured into pages and lines using the manual segmentation output. In order to test the impact of the segmentation errors due to automatic segmentation on retrieval performance, we repeated the page retrieval experiments on the automatically segmented test set.

The best model appears to be the probabilistic annotation model with continuous-space features (CPA). In most cases, it outperformed not only the other cross-modal retrieval models, but also the retrieval approach based on HMM recognition output. On data set A, the HMM only surpasses the other models for page retrieval using queries with 3 and 4 words. The DPA model performs best for multi-word queries on automatic segmentation output. We believe this somewhat mixed picture of performance can be attributed to the tuning parameters, which are not close enough to their optimal settings. This is due to the small size of the training set A, which was used to determine the parameters. The larger training set B, which consists of

Experiment	Query length	DPA	CPA	DCM	A/HMM
Line Retrieval w/ Manual Segmentation	1 word	.1052∗	**.1385**	.0898∗	.0933∗
	2 words	.2046∗	**.2685**	.1164∗	.1655∗
	3 words	.3142	**.3357**	.1353∗	.2630∗
	4 words	.3217∗	**.3495**	.1481∗	.2903∗
Page Retrieval w/ Manual Segmentation	1 word	.2318∗	**.2960**	.1946∗	.1818∗
	2 words	.2327∗	**.2668**	.1766∗	.2451∗
	3 words	.2175∗	.2769	.2042∗	**.2777**
	4 words	.2908∗	.3161∗	.2584∗	**.3874**
Page Retrieval w/ Automatic Segmentation	1 word	.1841	**.2129**	.1628∗	n/a
	2 words	**.1769**	.1660	.1633	n/a
	3 words	**.2549**	.1724∗	.1763∗	n/a
	4 words	**.2737**	.1560∗	.1550∗	n/a

Table 6.1. Mean average precision scores for retrieval experiments on 100 pages of test data, using 20 pages of training data (data set A). The scores are calculated for the ranked lists as they are returned by the retrieval process. Results that are significantly different from the best result in each row are marked with an asterisk (∗).

Experiment	Query length	DPA	CPA	DCM	A/HMM
Line Retrieval w/ Manual Segmentation	1 word	.1070∗	**.1392**	.0940∗	.0979∗
	2 words	.2048∗	**.2685**	.1168∗	.1662∗
	3 words	.3142	**.3357**	.1355∗	.2631∗
	4 words	.3217∗	**.3495**	.1482∗	.2903∗
Page Retrieval w/ Manual Segmentation	1 word	.2774	**.3141**	.2526∗	.2740∗
	2 words	.2358∗	**.2672**	.1846∗	.2574
	3 words	.2176∗	.2769	.2067∗	**.2811**
	4 words	.2908∗	.3161∗	.2589∗	**.3880**
Page Retrieval w/ Automatic Segmentation	1 word	.2331	**.2371**	.2292	n/a
	2 words	**.1811**	.1667	.1720	n/a
	3 words	**.2554**	.1724∗	.1801∗	n/a
	4 words	**.2737**	.1560∗	.1556∗	n/a

Table 6.2. Mean average precision scores for retrieval experiments on 100 pages of test data, using 20 pages of training data (data set A). The ranked lists were padded to full length before the score calculation. Results that are significantly different from the best result in each row are marked with an asterisk (∗).

Experiment	Query length	DPA	CPA	DCM	B/HMM
Line Retrieval w/ Manual Segmentation	1 word	.1001∗	**.1602**	.0995∗	.0826∗
	2 words	.1716∗	**.2843**	.0753∗	.1175∗
	3 words	.2111∗	**.2695**	.0832∗	.1312∗
	4 words	.2592∗	**.3827**	.1313∗	.1394∗
Page Retrieval w/ Manual Segmentation	1 word	.2322∗	**.2993**	.2129∗	.1623∗
	2 words	.2147∗	**.3272**	.1785∗	.1984∗
	3 words	.2132∗	**.2860**	.1732∗	.2097∗
	4 words	.2289∗	**.3406**	.2232∗	.2200∗
Page Retrieval w/ Automatic Segmentation	1 word	.2073∗	**.2416**	.1653∗	n/a
	2 words	.1939∗	**.2276**	.1676∗	n/a
	3 words	.2081	**.2438**	.1682∗	n/a
	4 words	.2292∗	**.3089**	.2271	n/a

Table 6.3. Mean average precision scores for retrieval experiments on 100 pages of test data, using 100 pages of training data (data set B). The scores are calculated for the ranked lists as they are returned by the retrieval process. Results that are significantly different from the best result in each row are marked with an asterisk (∗).

Experiment	Query length	DPA	CPA	DCM	B/HMM
Line Retrieval w/ Manual Segmentation	1 word	.1011∗	**.1614**	.1043∗	.0878∗
	2 words	.1717∗	**.2843**	.0758∗	.1186∗
	3 words	.2111∗	**.2695**	.0833∗	.1314∗
	4 words	.2592∗	**.3827**	.1314∗	.1395∗
Page Retrieval w/ Manual Segmentation	1 word	.2580∗	**.3283**	.2701∗	.2629∗
	2 words	.2148∗	**.3281**	.1868∗	.2208∗
	3 words	.2132∗	**.2861**	.1760∗	.2163∗
	4 words	.2289∗	**.3406**	.2236∗	.2228∗
Page Retrieval w/ Automatic Segmentation	1 word	.2350∗	**.2678**	.2284∗	n/a
	2 words	.1942∗	**.2279**	.1754∗	n/a
	3 words	.2081	**.2438**	.1717∗	n/a
	4 words	.2292∗	**.3089**	.2279	n/a

Table 6.4. Mean average precision scores for retrieval experiments on 100 pages of test data, using 100 pages of training data (data set B). The ranked lists were padded to full length before the score calculation. Results that are significantly different from the best result in each row are marked with an asterisk (∗).

100 page images, yielded better tuning parameter settings and shows the superior performance of the CPA model more clearly. It consistently outperforms the other models in all experiments.

On the large training set (B), the performance of both the discrete models (DPA and DCM) and the HMM generally tends to be lower. One reason for this is the increased vocabulary of the training collection. Another is the inability of the discrete models to make fine distinctions between features. The feature discretization technique lumps together feature values with small differences. However, such fine-grained information may be useful for distinguishing word classes. The continuous-space annotation model, which uses kernels for feature comparisons, can make such distinctions. Another disadvantage of the discrete models is the smoothing of feature distributions, which does not take into account how the feature tokens were generated. In particular, an improved smoothing should take into account that the location of bins carries some information about the contained feature values. This could be exploited to implement a coarse notion of feature distance, similar to the kernel density estimate for continuous-space features.

In the majority of the cases, CPA performs substantially better with more training data than with less. This is particularly true of the document retrieval results on automatic segmentation output. It appears that the fine-grained modeling of feature distributions is also of significant benefit in this case. While the performance on automatic segmentation output is generally lower than on manual segments, it is still satisfying.

Tables 6.5 and 6.6 show precision scores at the top 5 retrieved items for all experiments. Similarly to the mean average precision scores in Tables 6.1 through 6.4, CPA only clearly shows its superior performance with 100 pages of training data. The precision scores decrease with longer queries and tend to be low. This may be explained by Table 5.3, which shows that the number of relevant items per query de-

Experiment	Query length	DPA	CPA	DCM	A/HMM
Line Retrieval w/ Manual Segmentation	1 word	0.1680	**0.2100**	0.1960	0.1680
	2 words	**0.1080**	0.1000	0.0380∗	0.0660∗
	3 words	**0.1120**	**0.1120**	0.0520∗	0.0840
	4 words	0.0900	**0.1040**	0.0600∗	0.0800∗
Page Retrieval w/ Manual Segmentation	1 word	0.2940	**0.3160**	0.2560∗	0.3060
	2 words	0.2000	**0.2320**	0.1420∗	0.2120
	3 words	0.1340∗	0.1760	0.1260∗	**0.1900**
	4 words	0.1320∗	0.1260∗	0.1040∗	**0.1620**
Page Retrieval w/ Automatic Segmentation	1 word	**0.2360**	0.2260	0.2280	n/a
	2 words	**0.1540**	0.1160	0.1200	n/a
	3 words	**0.1360**	0.1040∗	0.1320	n/a
	4 words	**0.1120**	0.0620∗	0.0840∗	n/a

Table 6.5. Precision scores at the top 5 retrieved items using 20 pages of training data. The ranked lists were padded to full length before the score calculation. Results that are significantly different from the best result in each row are marked with an asterisk (∗).

Experiment	Query length	DPA	CPA	DCM	B/HMM
Line Retrieval w/ Manual Segmentation	1 word	0.1480∗	**0.2360**	0.2040	0.1740∗
	2 words	0.0700∗	**0.1180**	0.0360∗	0.0540∗
	3 words	0.0720∗	**0.0980**	0.0460∗	0.0560∗
	4 words	0.0740∗	**0.1160**	0.0380∗	0.0500∗
Page Retrieval w/ Manual Segmentation	1 word	0.2500∗	**0.3420**	0.2580∗	0.2940∗
	2 words	0.1720∗	**0.2640**	0.1520∗	0.1940∗
	3 words	0.1720∗	**0.1900**	0.1300∗	0.1640
	4 words	0.1120∗	**0.1380**	0.0900∗	0.1140
Page Retrieval w/ Automatic Segmentation	1 word	**0.2620**	0.2600	0.2360	n/a
	2 words	0.1540	**0.1900**	0.1620	n/a
	3 words	0.1380	**0.1660**	0.1240∗	n/a
	4 words	0.1080	**0.1120**	0.0940	n/a

Table 6.6. Precision scores at the top 5 retrieved items using 100 pages of training data. The ranked lists were padded to full length before the score calculation. Results that are significantly different from the best result in each row are marked with an asterisk (∗).

creases with the length of the query. For queries consisting of 4 words, the expected number of relevant items that fall into the top 5 ranks is 2.03 for page retrieval and 1.18 for line retrieval assuming perfect ranking (all relevant items at the top). This translates into expected precision scores of .406 for page retrieval and .236 for line retrieval, again assuming perfect retrieval. Seen from this perspective, the precision scores of the CPA model are quite good.

6.3.2 1100 Pages of Test Data

The test collection we used in the previous experiments is large in terms of word images (21324) and space (609MB), but there are only 100 pages. Compared to collection sizes that are typically used in the information retrieval of text, this is very small. In order to get an idea of the scalability of our cross-modal retrieval approach, an evaluation of its performance on larger collection is desirable. Unfortunately, relevance judgments are hard to obtain, even for the limited definition of relevance judgments that is used here. The relevance judgments are generated from transcriptions, which need to be mapped to the retrieval units 1-to-1.

Almost 16,000 transcriptions for the roughly 152,000 papers of George Washington are available at the Library of Congress' website [110]. On the site, each image of a page may be linked to 0 or more transcriptions. Many pages contain one or more letters, which are all transcribed in separate text files. This technique is desirable for the organization of the collection into letters which may extend beyond page boundaries, but unfortunately not for our purposes. We do not perform any document layout analysis and do not know the beginning and end of documents, hence we perform page retrieval. When trying to obtain the transcription of an entire page, several problems may occur. An image may contain multiple letters, but not all of them may be transcribed, resulting in an incomplete transcription of the page. Another problem is caused by letters that span multiple pages. This makes it

necessary to align portions of the available transcription with each of the pages that the transcription is linked with, a non-trivial problem in itself [111, 49].

We avoid problems that fall into the latter category by generating a collection that only consists of page images which link to one transcription. Furthermore, we do not use images if they are linked to by more than one transcription. Even though this guarantees a 1-to-1 mapping of transcriptions to page images, there may still be some smaller problems: For example, the page may still consist of multiple letters, of which only one is transcribed (yielding an incomplete transcription), and hyphenated words in the image are typically transcribed as one word (causing tainted relevance judgments). Given the cost of human annotation, we will use the collection as it is for automatic relevance judgment generation, and manually inspect some retrieval results to assess how often relevance has been misjudged. The resulting test set consists of 1100 page images.

The training collection is the same set of 100 pages as used before, and retrieval is performed on the output of the probabilistic annotation approach with continuous-space features (CPA), because it resulted in the best performance. We used 39 features: 6 scalar features and 33 DFT coefficients (the optimal number that has been determined in section 3.2.2). The queries are the same as above, but queries with no relevant items in the test set are removed. There are now 96, 80, 61, and 27 queries with lengths of 1 to 4 words respectively (previously there were 100 queries per category).

Table 6.7 shows the MAP results obtained on this dataset. The performance has decreased compared to the results on 100 test pages. Several factors have contributed to this (see Figure 6.4 for illustrations):

Dataset selection: The dataset has been selected entirely based on whether ground truth data is available for the pages. As a result, pages were selected from all portions of the collection, causing a greater variability in writing style and

Query length:	1 word	2 words	3 words	4 words
MAP (short ranked lists):	.0765	.0391	.0553	.0841
MAP (padded ranked lists):	.0994	.0413	.0558	.0842

Table 6.7. Mean average precision scores for retrieval experiments on 1100 pages of test data, using 100 pages of training data (data set B). The first row shows the scores that were calculated from the (short) ranked lists that were returned by the ranking algorithm. The second row shows the scores that were obtained when the ranked lists were padded to full length.

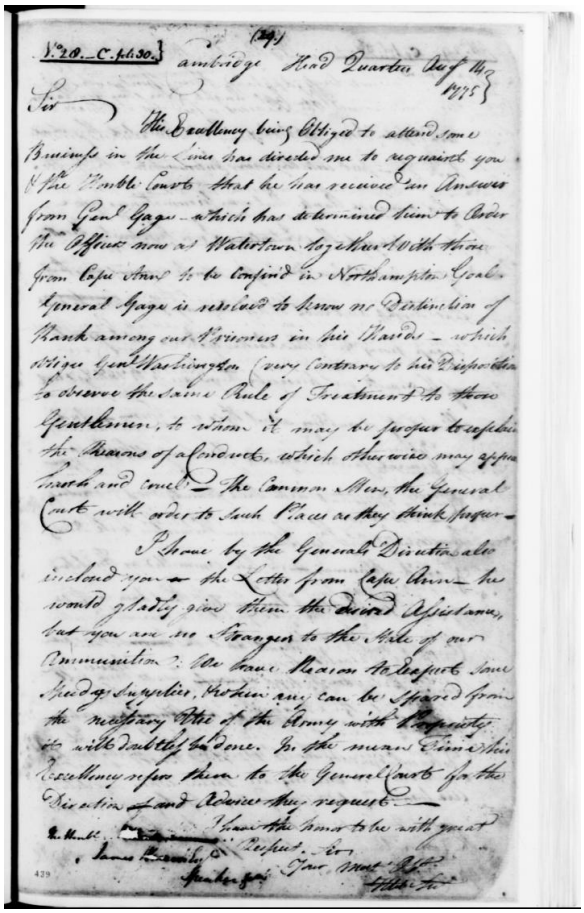

(a) Severe image degradation.

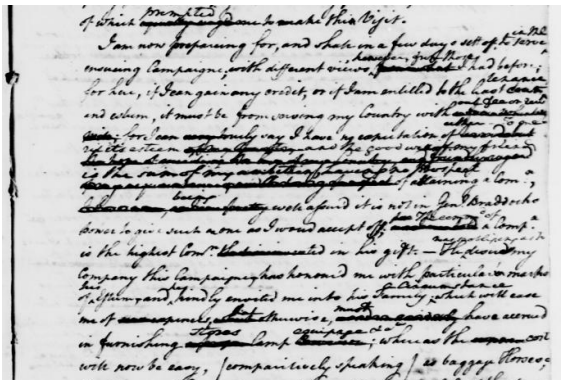

(b) Crossing out of words, writing in between lines.

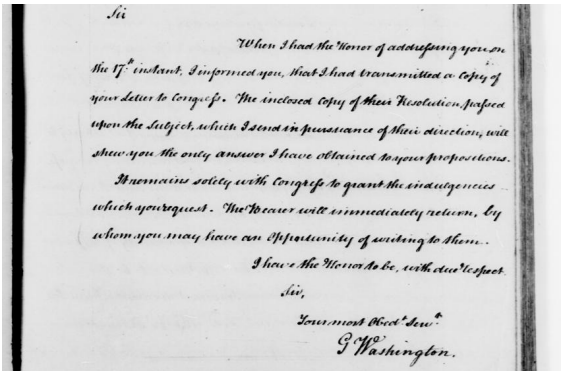

(c) Narrow writing style with no available training data, difficult to segment.

Figure 6.4. Example images from the 1100 pages test set, showing the difficulty of this data set.

possibly more writers. Our training data was selected from a mostly coherent portion of the collection, so it may not be adequate to cover all the observed writing styles.

Image quality: A substantial number of the images are of such poor quality that they are hard to read. The page images in previous test sets are generally readable.

Segmentation quality: Due to the decreased image quality, and the fact that the segmentation algorithm was evaluated on our training sets, a visual inspection of the segmentation output indicated that the segmentation quality is worse than on the datasets it has been evaluated on. This affects the retrieval quality.

Partial transcriptions: A visual inspection of the alignment between the available transcriptions and the word image content in 100 of the 1100 page images showed that on average about 85% of the word content in a page image is transcribed (the standard deviation is 20%). Since the relevance judgments are based on whether the query terms appear in the transcription, it is likely that some relevant pages have been judged non-relevant, because one or more of the query terms occurred in the non-transcribed portion of the page. For this reason we expect the true MAP scores to be slightly higher than the ones in Table 6.7.

We believe it is possible to improve the results in Table 6.7, using linguistic post-processing and enhanced image processing and document analysis techniques.

6.3.3 10k Pages

We have set up a system that is based on 10,000 test images and 200 pages of training data. The size of this data set makes it very difficult to obtain page-aligned ground truth data, which would be necessary for an evaluation of page retrieval performance. Non-aligned, and potentially partial ground truth data is available for

all test pages. However, the ground truth transcriptions are organized into letters and not pages. When the problem of transcript alignment (for example, see [49] or [111]) is solved to a satisfactory degree, an evaluation would be possible.

6.4 Learning Behavior

In this section we look at the learning behavior of the cross-modal retrieval approach, specifically the probabilistic annotation approach with continuous-space features (CPA). We conducted experiments with 100 pages of test data and subsets of varying size from 100 pages of training data to test the influence of more training data on retrieval performance. Starting with two pages, the training set size is increased in steps of two pages up to the full size of 100 pages. The test data was structured into lines and documents for retrieval with the same set of 1 to 4 word queries used before.

Figure 6.5(a) shows the relation of retrieval performance (measured using mean average precision) to the number of training pages used. As more training pages become available the performance improves, because an increasing number of query words is encountered in the training set. The performance increases sharply for queries of all lengths at around 35 training pages, indicating that a substantial portion of the queries has relevant training instances in that portion of the training data. At around 70% of the training set, the performance levels off. Using more training data does not further increase mean average precision.

To further investigate what causes the performance increase with larger training sets, we plotted the training instances for query terms. Figure 6.5(b) shows the fraction of training instances for query words included in the training set (including repetitions), Figure 6.5(c) shows the fraction of query terms for which at least one training instance is available. The latter shows a clear correlation with Figure 6.5(a): the "hump" in the beginning, the sharp increase around 35 training pages, and the

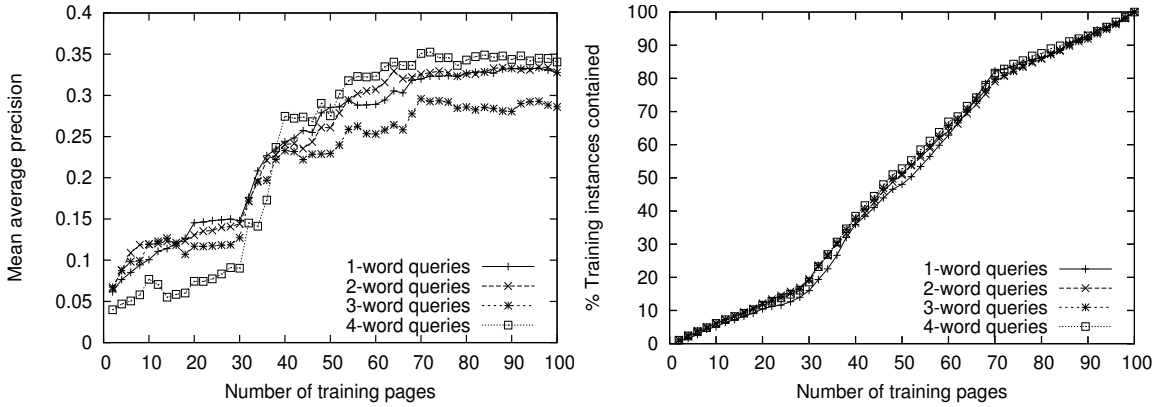

(a) Mean average precision.

(b) Training instances used.

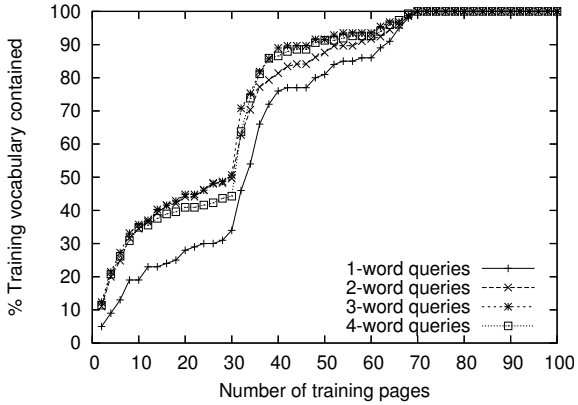

(c) Query vocabulary coverage.

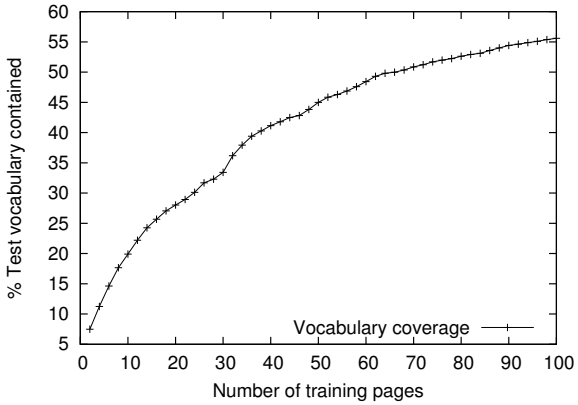

(d) Test vocabulary coverage.

Figure 6.5. Plots showing the learning behavior of the CPA cross-modal retrieval model. Coverage of the vocabulary used in queries and the percentage of the training data used as a function of the number of training pages.

leveling off around 70 pages. While the plots in Figures 6.5(a) and 6.5(b) correlate, the relationship is not as distinctive. After a certain number of training instances has been reached, more training data does not seem to improve retrieval performance any more. An indication for this is that the mean average precision does not increase beyond 70 training pages, although this portion of the training set contains almost 20% of the total training instances.

Figure 6.5(d) shows the coverage of the test vocabulary, which shows the characteristics of Heaps' law (see section 4.4.1). The maximum vocabulary coverage is 55%, meaning no queries can be constructed for 45% of the words in the test set. Furthermore, the rate of increase shows that a substantially larger test set vocabulary coverage can only be achieved with much larger training collections. This would mean increasing the size of the training set beyond that of the test collection, which is not practical. A practical approach is to use synthetic training data to increase the vocabulary coverage. In section 6.7 we take a first look at this idea.

6.5 Linguistic Post-Processing of Annotation Results

So far, our annotation models have ignored a word image's context, that is, the adjacent word images in the sequence defined by the reading order. That means our calculation of classification probabilities only uses features that are associated with the image we would like to annotate.

However, the occurrence of a particular word in a text is typically not independent of previous words. It has been shown that the quality of handwriting recognizers can be improved significantly, when the context of a word image in a text is taken into account [77, 58, 117]. A common way of modeling sequence data where neighboring samples are constrained with respect to one another is the Hidden Markov Model, which we have used in chapter 5 to recognize word image sequences.

6.5.1 Constraint Model

Here we use an HMM to model the dependencies between adjacent words in the image sequence that we annotate probabilistically. The dependencies take the form of a word bigram model, which constrains the annotations that are chosen for adjacent word images. This model is a post-processing step, in the sense that the HMM is

placed on top of the probabilistic annotation output. The approach described here only applies to the probabilistic annotation models (CPA and DPA).

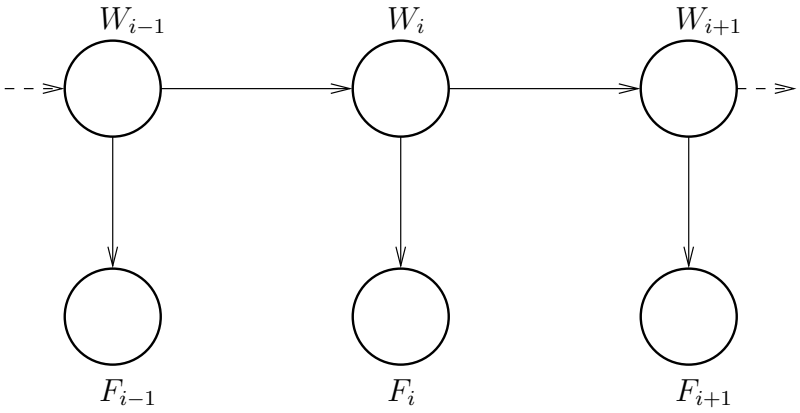

Figure 6.6. Graphical representation of a Hidden Markov Model. The W_i are hidden state variables, the F_i are observations.

As we have seen in section 5.1.3, HMM-based recognizers typically use the Viterbi algorithm [25] to determine the most likely state sequence $\hat{w}_1, \ldots, \hat{w}_N$ that generated the observed feature vectors $f_1, \ldots, f_N$. This is particularly useful when the states correspond to words in a vocabulary and the resulting state sequence is to be interpreted as text (a sentence, paragraph, ...). However, we would like to argue here that another optimality criterion is better suited to retrieval, which is our target application. Here the goal is not to create readable text, but to correctly annotate as many states as possible. Therefore, we would like to maximize the expected number of correct states. That is, at each point i in a sequence of length N, we are looking for

$$\begin{aligned}
\hat{w}_i &= \operatorname*{argmax}_w \; P(W_i = w | F_1 = f_1, \ldots, F_N = f_N) \qquad (6.18)\\
&= \operatorname*{argmax}_w \; P(W_i = w, F_1 = f_1, \ldots, F_N = f_N) \\
&= \operatorname*{argmax}_w \; P(W_i = w, f_1, \ldots, f_i) P(f_{i+1}, \ldots, f_N | W_i = w, f_1, \ldots, f_i) \\
&= \operatorname*{argmax}_w \; P(W_i = w, f_1, \ldots, f_i) P(f_{i+1}, \ldots, f_N | W_i = w) \\
&= \operatorname*{argmax}_w \; \alpha_i(w) \; \beta_i(w),
\end{aligned}$$

where $\alpha_i(w)$ and $\beta_i(w)$ can be computed using the forward and backward algorithms [86], which are dynamic programming techniques similar to the Viterbi algorithm. For our retrieval application we are not interested in recognition, i.e. determining the element $\hat{w}_i$ which yielded the maximum probability in equation (6.18). Instead we will calculate

$$P(W_i = w | F_1 = f_1, \ldots, F_N = f_N)$$

for all $w \in \mathcal{V}$. The result is an annotation distribution for the i-th word image in the sequence, which now takes into account *all* observations $f_1, \ldots, f_N$, whereas the probabilistic annotation based on the original cross-modal model only uses the observation f_i.

What remains is the calculation of the forward and backward probabilities $\alpha_i(w)$ and $\beta_i(w)$. We show the recursive calculation of the forward probability, the backward algorithm is similar:

$$\begin{aligned}
\alpha_i(w) &= P(W_i = w, f_1, \ldots, f_i) \\
&= P(f_i | W_i = w, f_1, \ldots, f_{i-1}) P(W_i = w, f_1, \ldots, f_{i-1}) \\
&= P(f_i | W_i = w) \sum_{w' \in \mathcal{V}} P(W_i = w, W_{i-1} = w', f_1, \ldots, f_{i-1}) \qquad (*) \\
&= P(f_i | W_i = w) \sum_{w' \in \mathcal{V}} P(W_i = w | W_{i-1} = w', f_1, \ldots, f_{i-1}) P(W_{i-1} = w', f_1, \ldots, f_{i-1}) \\
&= P(f_i | W_i = w) \sum_{w' \in \mathcal{V}} P(W_i = w | W_{i-1} = w') \alpha_{i-1}(w') \qquad (*) \\
\alpha_1(w) &= P(f_1 | W_1 = w) P(W_1 = w),
\end{aligned}$$

where $(*)$ indicates that we have used the fact that a random variable is independent of the ancestors of its parent, given its parent (factoring according to the HMM graph in Figure 6.6).

Both the forward and backward algorithm require prior probabilities $P(W_1 = w)$, a transition probability table with entries $P(W_i = w | W_{i-1} = w')$ and emission

probabilities $P(f_i|W_i = w)$. The word priors and transition probabilities may be estimated from the annotations of the training collection $\mathcal{T}$ and other text sources $\mathcal{O}$ as described in section 5.1.2:

$$\begin{aligned} P(W_1 = w) &= \frac{1}{3}\frac{c(w,\mathcal{T})}{|\mathcal{T}|} + \frac{1}{3}\frac{c(w,\mathcal{O})}{|\mathcal{O}|} + \frac{1}{3}\frac{1}{|\mathcal{V}|}, \\ P(W_i = w|W_{i-1} = w') &= \frac{1}{3}\frac{c(w'w,\mathcal{T})}{\sum_{v\in\mathcal{V}} c(w'v,\mathcal{T})} + \frac{1}{3}\frac{c(w'w,\mathcal{O})}{\sum_{v\in\mathcal{V}} c(w'v,\mathcal{O})} + \frac{1}{3}P(W_1 = w). \end{aligned}$$

The emission model may be partly determined from the cross-modal annotation probabilities and equation (6.19):

$$P(f_i|W_i = w) = \frac{P(W_i = w|f_i)P(f_i)}{P(W_i = w)} \tag{6.19}$$

$P(W_i = w|f_i)$ is the output of the probabilistic annotation model, and $P(W_1 = w)$ may be used in place of $P(W_i = w)$.[6] Since we are only interested in the relative probabilities that are determined by the forward and backward algorithms, and not the actual values, $P(f_i)$ may be regarded as a constant that is factored out.

6.5.2 Experimental Results

Our experiments with the linguistic post-processing technique were conducted on 100 pages of test data, using 100 pages of training data ($\mathcal{T}$), all manually segmented. The probabilistic annotation model is CPA. The test data was annotated probabilistically and we performed retrieval of documents and lines, using the same queries as in previous experiments. Then the annotation output was post-processed page-by-page with a bigram language model determined from $\mathcal{T}$ and the Jefferson collection ($\mathcal{O}$, 200,000 words) that was used previously with our HMM recognizer.

[6] $P(W_1 = w)$ is really a prior that is valid for all positions i in the sequence.

MRR before	MRR after	Improvement	# pages improved / worse
.5020	.5378	.0358	99/1

Table 6.8. Mean Reciprocal Rank (MRR) performance scores for 100 test pages, shown before and after linguistic post-processing.

The first evaluation looks at the improvement of the per-word-image annotation distributions with the post-processing. Table 6.8 shows mean reciprocal rank (MRR) scores before and after the post-processing step. To calculate this score, the annotation distribution of each word image is ordered by decreasing annotation probability. Then the MRR for a page is the reciprocal rank of the correct annotation term, averaged for all word images of that page. If the correct annotation term is always assigned the highest probability, the MRR would be 1. When the correct annotation term tends to occur at lower ranks, MRR approaches zero. If the correct annotation term is not contained in the annotation distribution, which can happen if the term is not contained in the annotation vocabulary or if the annotation list is truncated, we set the reciprocal rank to 0. The results clearly show that the post-processing is beneficial. Although the improvement in MRR is modest, it is very consistent. The MRR score improved for 99 out of the 100 test pages. The MRR scores also show that the probabilistic annotation technique performs well. On average, the correct annotation term appears at rank two in the annotation distribution. This is quite good, especially when considering that OOV terms have been included in the evaluation.

We now take a look at the impact of linguistic post-processing on retrieval performance. Table 6.9 shows the mean average precision scores that were obtained with the probabilistic annotation output using continuous-space features, before and after the post-processing step. The retrieval performance has clearly benefitted from applying word bigram constraints. After post-processing, the precision scores are substantially higher than before. The difference in mean average precision is even greater than the

Experiment	Query length	Before post-proc.	After post-proc.
Page Retrieval w/ Manual Segmentation	1 word	.3277	**.3706**
	2 words	.3279	**.3757**
	3 words	.2861	**.3247**
	4 words	.3406	**.4234**
Line Retrieval w/ Manual Segmentation	1 word	.1627	**.2207**
	2 words	.2843	**.3650**
	3 words	.2695	**.3441**
	4 words	.3827	**.4569**

Table 6.9. Mean average precision scores shown for retrieval on probabilistic annotation output, shown before and after linguistic post-processing. The annotation was performed using continuous-space features.

modest improvement in MRR would lead to think. Since the current text source for the estimation of word bigram probabilities is quite small, it is possible that with a larger text source further performance improvements could be made.

6.6 Related Cross-Modal Work

Cross-modal models can be applied for any combination of media, given suitable content representations. Here we discuss cross-modal models that have been proposed for other domains and compare our model to them. Initially, cross-media models were proposed by Jeon et al. [41] and Lavrenko et al. [57] for automatic annotation and retrieval of individual color photographs. Our work extends them to the retrieval of images of handwriting, which are organized in arbitrary text units (e.g. lines or documents). Furthermore, this work shows how a bigram language model may be used to constrain the annotations of adjacent word images, which substantially improves retrieval performance.

Feng et al. [24] and Lavrenko et al. [56] proposed cross-media models that extends Jeon et al.'s work to perform annotation and retrieval of video keyframes and color photographs. Their models use a multiple-Bernoulli distribution to describe the gen-

eration of annotation terms (Jeon et al. used a multinomial), which is better suited for the annotation of photographs. In a multinomial model, the annotations *house* and *car* would compete for probability mass, causing the available probability mass to be split if both objects occur together. If only one of them is present, all the probability mass will be concentrated in the corresponding term. This would rank a photograph with one object in it higher than one with multiple objects (even if the target object is present). The multiple-Bernoulli model assigns annotation probabilities that do not suffer from this problem.

Both Feng et al. and Jeon et al. used color and texture features. In the handwriting domain, such features are not available, only shape can be used. Furthermore, where discrete image representations are required, we are using a feature discretization that allows more fine-grained decisions than previously used techniques. Earlier work represents entire feature vectors with a single discrete token by clustering feature representations before the annotation process. We believe this corresponds to making a classification decision in feature space, that removes details which could aid in the annotation process. We are adopting a more fine-grained discretization strategy (see section 3.3) that clusters feature vector entries dimension-by-dimension, leaving classification decisions up to the cross-modal model.

The annotation vocabulary that was used in previous work is much smaller (e.g. 371 words in [41]) than in our case (up to 4226). In addition, since photograph and video annotations are inherently ambiguous, the problem of OOV terms is not a major concern, as long as the annotation vocabulary provides a reasonable coverage of the content. If no annotation word is available for a particular photograph, one can always resort to using a more general or generic description of the content. For example, *person* could be used instead of *swimmer* or *water* in place of *pool*. In the handwriting domain, this is not possible. Each word image has exactly one correct annotation that cannot be replaced.

In the remainder of this chapter we investigate the use of synthetic word images for replacing or complementing natural training data. Such training data could also be used in a word spotting or recognition-based approach. However, since the cross-modal models have shown very good retrieval performance and practicability, we have chosen to evaluate the synthetic data with this approach.

6.7 Synthetic Training Data

Words as the atomic units of recognition and retrieval are convenient, but there are also some drawbacks associated with this approach. The two main criticisms are that it is virtually impossible to obtain training data for all words in the test vocabulary (cf. Figure 6.5(d)) and even if there is training data, it may not be sufficient to allow the accurate estimation of the conditional feature distributions. In this section we investigate to what degree these shortcomings can be addressed by generating synthetic training data that complements existing *natural* samples of writing.

There has been very little work in this area for handwriting data. Until recently, there has been no work on synthetic data for cursive Roman script [12]. In that presentation, Bunke proposed the generation of artificial training data from templates and by distorting existing handwritten text. He demonstrated how increasingly realistic renderings of word images can be generated by obtaining character N-grams of increasing length N from existing data and using them to render synthetic words. At the same conference, Varga and Bunke [114] presented a system for generating synthetic training data using random perturbations of existing natural samples. All of these experiments were conducted on modern handwriting samples of high scanning quality. Recently, Howe et al. [35] showed how distortions of historical writing can be used to improve the recognition accuracy of a holistic recognizer.

Ishidera and Nishiwaki [37] described a top-down word image synthesis approach which they used for handwriting recognition. Their word generation process uses a

probabilistic model which places character templates on a canvas. The style of each character, as well as position and size of the character are sampled at random, to imitate the typical handwriting variations.

We pursue two strategies for creating artificial data using a template-based approach. The first is to use a TrueType font, which is similar in appearance to the target writing, to generate training instances. The second strategy uses a bitmap font, which has been obtained from the target writing, to create training data by *pasting* together images of individual characters. The following sections describe the training data generation and the retrieval experiments that were used to assess the effectiveness of using synthetic data in lieu of natural data.

6.7.1 TrueType Font

The general handwriting style that is typically found in the George Washington collection is called *Copperplate* or *round hand*. This writing, which was used in British commerce in the 18th century, is typical for the founding fathers [81]. Despite its age, this style has not dropped out of fashion, and a number of *TrueType* computer fonts that mimic it can be found.

TrueType [2] is a format for scalable computer fonts developed by *Apple Computer, Inc.*. The shapes of characters are defined by curves, which can be easily scaled to any desired size without distorting the appearance of the characters. For our experiments, we chose the fonts *CounselorScript*, *CommScriptTT*, and *CACChampagne*. Figure 6.7 shows some sample renderings with these fonts.

The renderings from TrueType fonts are designed to be clean and uniform, and thus do not exhibit features that are typical of historical handwriting, such as noise, loss of contrast and variations of slant and skew as well as the writing speed. In order to generate training data that is closer in appearance to actual historical handwriting samples, the black-and-white renderings were randomly distorted in a number of ways.

(a) *CounselorScript* font.

(b) *CommScriptTT* font.

(c) *CACChampagne* font.

Figure 6.7. Sample renderings with the 3 TrueType fonts that were used in the generation of synthetic training data.

(a) Synthetic. (b) Synthetic. (c) Synthetic. (d) Natural.

(e) Synthetic. (f) Synthetic. (g) Synthetic. (h) Natural.

Figure 6.8. Sample renderings of the words *same* and *Regiment* using TrueType fonts, after adding noise and distortions to simulate historical data. The rightmost images are natural examples provided for comparison.

First, variations in writing speed are simulated by duplicating, preserving or removing image columns according to statistics that have been gathered from actual dynamic time warps of matching word images (cf. section 4.2.1). The statistics, which consist of the relative frequencies of the three moves (duplication, preservation, removal), were collected from dynamic time warps performed in [91]. Then the image

is smoothed and binarized using a randomized threshold to create the thinning effect in historical documents, which frequently breaks up thin strokes. We use a technique similar to the *Threshold* defect model described in [4]. In the next step, random *salt and pepper* noise is added to a rendered image, which is then smoothed. This simulates the effect of dirt on a page together with the smoothing effect that is created by ink slowly being soaked up by the paper. Then the image is slanted with a small angle that is selected at random. This is to simulate the mistakes introduced by the deslanting algorithm. Finally, the word image is cleaned (see section 2.3.2) to remove variations in the background (paper) intensity, and passed through the deskewing algorithm. The resulting images are then passed to the feature extraction routine. Some typical examples of the simulated historical writing samples can be seen in Figure 6.8.

6.7.2 Bitmap Font

A bitmap font contains an image of each allowed character. This finished representation makes it difficult to scale the font without loss of quality, which usually occurs due to aliasing and other problems. The advantage of such a font is that renderings can be done very efficiently at the native character size of the font.

The *Copperplate* fonts in the previous section provide a reasonable approximation to the writing style used in the George Washington collection. However, with a bitmap font that was obtained from the collection itself, an even better match is possible. We collected exemplars of all 52 upper- and lower-case characters (A-Z & a-z) as well as all ten digits, and combined them in a bitmap font. The character and digit images were manually cleaned using an image manipulation program, in order to remove dirt and parts from other characters. Figure 6.9 shows all 62 characters of the resulting bitmap font. Before synthetic word images can be rendered, the slant

of each character, as well as the upper and lower baselines were determined and the slant angle was normalized to 90 degrees.

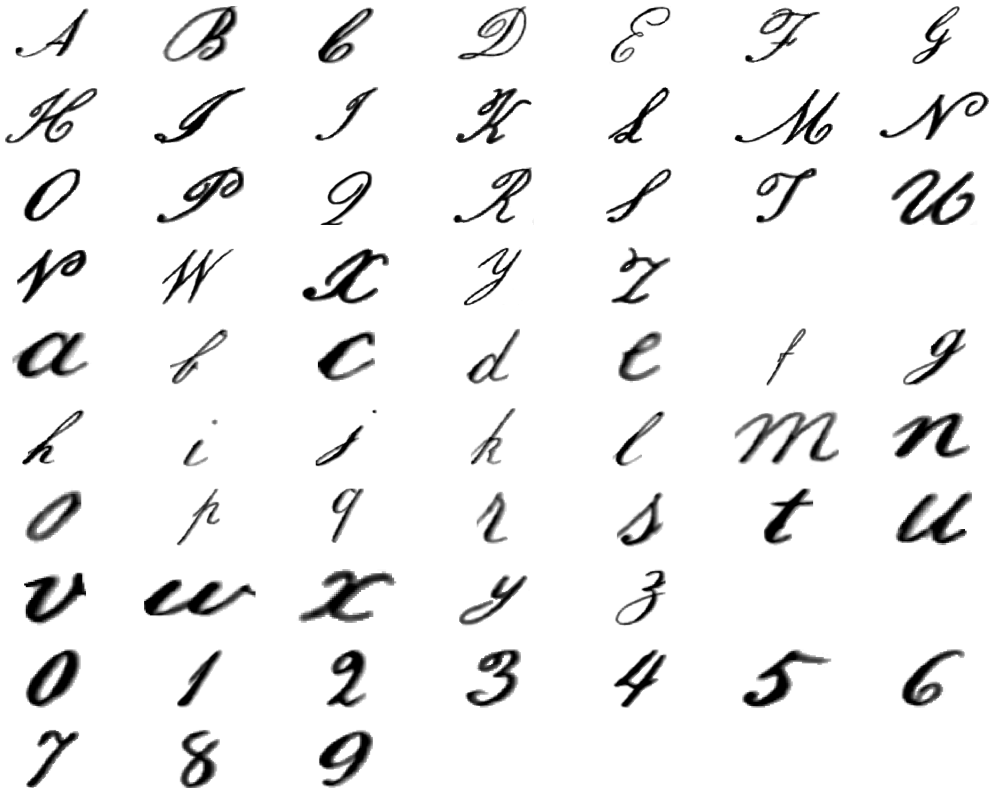

Figure 6.9. All 62 character and digit images that make up the bitmap font of the writing used in the George Washington collection.

(a) Synthetic. (b) Synthetic. (c) Synthetic. (d) Natural.

(e) Synthetic. (f) Synthetic. (g) Synthetic. (h) Natural.

Figure 6.10. Sample renderings of the words *same* and *Regiment* with the Bitmap Font extracted from the George Washington collection. The rightmost images are natural examples provided for comparison.

Term	Freq.	Term	Freq.	Term	Freq.	Term	Freq.
1st	16/3	28th	15/1	Colonel	20/55	Commissary	16/4
Court	15/44	further	15/11	give	24/22	Given	17/17
great	27/12	hope	17/10	last	29/18	little	19/12
make	27/30	money	28/14	October	19/1	Officers	15/11
orders	15/45	part	15/18	proceed	18/22	proper	16/12
receive	25/20	regard	20/5	Regiment	28/17	same	23/13
take	23/23	terms	17/3	want	15/16	way	16/9
Winchester	33/62	wish	15/6				

Table 6.10. List of queries that were used for evaluating the retrieval effectiveness when using synthetic training data. Next to each query term are the corresponding absolute frequencies of occurrence in the training and test sets.

Synthetic word images are rendered by scaling the three word zones[7] of each character image to predetermined sizes. The size-normalized character templates are then aligned vertically by padding them and combining them into a word image. Just like the TrueType renderings, the synthetic word images are then randomly distorted by simulating varying writing speeds with inverse time warps. Figure 6.10 shows typical writing samples obtained with this procedure. Preprocessing is limited to a cleaning and a deskewing step, before the rendered images are handed to the feature extraction process.

6.7.3 Experiments and Results

We conducted retrieval experiments on the same data set as used earlier (100 training pages and 100 test pages). The annotation was performed using the probabilistic annotation model with probabilistic features. We randomly chose 30 1-word queries, which frequently occur in the training set, but also occur in the test set, to evaluate the retrieval effectiveness that can be achieved with synthetic data. Table 6.10 shows a list of the queries used in our experiments.

[7]The three zones are the ascender-, center- and descender-zone (see Figure 2.3).

Our experiments include line and word image retrieval. The latter is of particular interest in this case, because it allows us to to directly assess how well our training data can mimic actual writing samples. A retrieved word image was only judged relevant if it had the exact same surface form as the query. That is, the retrieved word and the query term had to be identical letter-by-letter (in previous experiments we considered a word relevant if it has the same stem as the query term). The reason for this is that training data does not have to be generated for every potential surface form of a term. With this setup, the following experiments were conducted:

Only natural training data: this test run forms the baseline for the subsequent experiments. Only actual writing samples from the George Washington collection are used for training.

Only synthetic TrueType data: here we remove all natural training instances for the query terms in Table 6.10, and replace them with simulated writing samples that are rendered using the TrueType method. 50 training instances are rendered per query term. The remaining training instances for words that are not in the query list are kept. This experiment allows us to assess whether retrieval can be done for queries for which no training data is available. That is, the goal is to test the suitability of synthetic data for the retrieval of out-of-vocabulary words.

Only synthetic bitmap font data: the same as above, only that the synthetic images are rendered using the bitmap font.

Natural and TrueType data: here we add the synthetic TrueType training data to the natural training instances. This is useful to judge whether a small training sample for a particular word can be successfully augmented by synthetic TrueType data. The idea behind this is to increase the robustness of an anno-

tation (or recognition) process by providing a larger sample for estimating word models.

Original and bitmap font data: the same as above, only here the synthetic data is generated from a bitmap font.

The results of these experiments are shown in Figure 6.11 using recall-precision plots.

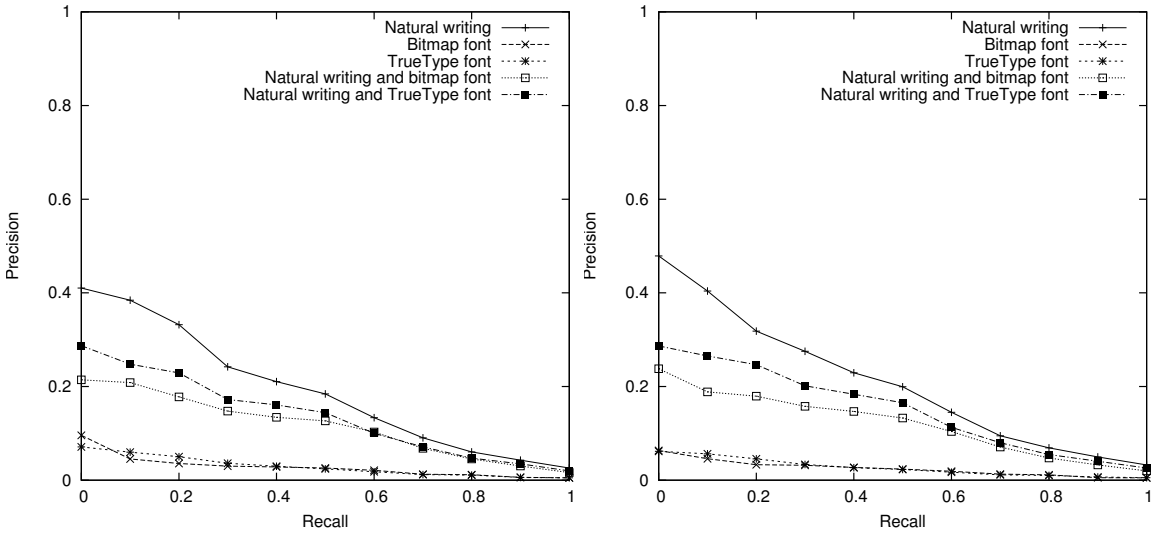

(a) Line retrieval.

(b) Word image retrieval.

Figure 6.11. Recall-precision curves for line and word image retrieval experiments with synthetic training data. The curves show the performance when using only natural handwriting samples for training, when using only synthetic data (both TrueType and Bitmap renderings), as well as when using both synthetic and natural training data together.

Clearly, the retrieval runs with synthetic training data do not perform well. In the cases where only synthetic training data is used, the performance is the worst, with the bitmap and TrueType data performing very similarly. When synthetic and natural data are mixed, the retrieval performance is better, but still substantially worse than the run which uses only natural training data. The synthetic training data seems to "pollute" the natural data rather than result in synergetic effects, causing retrieval performance to decrease.

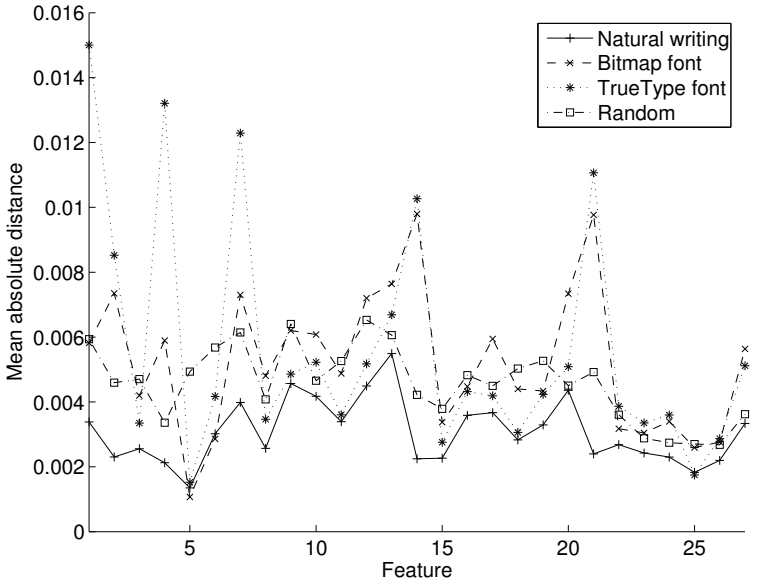

Figure 6.12. Feature-by-feature evaluation of the modeling capabilities of synthetic data. For each feature, the mean absolute distance of the test feature values to the mean of the features values in the model is shown. The shown models are derived from natural handwriting examples ("natural writing" and "random") and synthetic writing samples based on the bitmap and TrueType font.

In order to gain some insight into why our synthetic word images could not be used in place of natural writing samples, we conducted a feature-by-feature evaluation. For each query word, we extracted all relevant feature vectors from the training set and the test set. For each feature dimension, we plot the mean absolute distance of the values in the test set to the mean of the values in the training set, averaged over all queries. We used the natural writing and the two synthetic data sets as training. As a baseline, we also plotted a *random* model. The random model consists of the natural training instances of a word we selected at random. The random model is varied every time a different query is evaluated.

The results in Figure 6.12 show clearly that the natural writing yields the smallest average distance for most feature dimensions. The ranking between the two synthetic models is not as clear. The bitmap font-rendered samples perform as good or better than the TrueType-rendered samples for scalar features (features 1 through 6), but

the synthetic TrueType samples result in a slightly better model for profile features (features 7 and up).

It is plausible that the bitmap-rendered samples provide a better match in the scalar features. These features measure global word similarity, such as the width and aspect ratio of the bounding box, which can be simulated more effectively with actual writing samples taken from the dataset that should be modeled. It appears, however, that the spacing between the character bitmap images is off, causing the TrueType-rendered samples to be a better model for the profile features. The distance values that were achieved with the random model show clearly that the modeling of the synthetic training data needs significant refinement, before the synthetic data can replace natural writing.

In summary, it must be concluded that natural training data cannot be replaced with the presented synthetic rendering techniques. No synergetic effects can be expected when natural writing samples are mixed with synthetic data and the modeling of out-of-vocabulary terms needs significant improvement in order to be useful. Of course, this does not mean that creating synthetic training data cannot be done. Our investigation here should be considered as the first step. Successful simulation of training data still holds great promise for overcoming the out-of-vocabulary problem.

CHAPTER 7

CONCLUSIONS AND FUTURE WORK

In this work, we have presented the first retrieval system for handwritten historical document images which allows text queries. In building our prototype retrieval system, we have tackled numerous challenges in a number of areas, including image processing techniques, feature representations, content annotation techniques and the design of a user interface (see appendix A). Here we summarize our findings and describe how the system can be improved to reach the maturity of a commercial grade system.

7.1 Summary

The development of image processing techniques was based on the observation of typical properties of historical manuscripts, namely large amounts of noise and handwriting variations. By adopting a holistic approach to the analysis of word images we avoid the word segmentation problem, which is one of the most difficult problems even when analyzing modern manuscripts with little noise. Using various image cleaning and normalization techniques, we remove much of the noise and handwriting variations that complicate the recognition of word images.

Various features were presented for representing word images in historical manuscripts. For pair-wise matching of word images with Dynamic Time Warping, we use profile features, which capture a word's shape in great detail. For classification approaches that require vectors of the same dimensionality, we use discrete Fourier transform descriptors corresponding to low frequencies obtained from the profile fea-

tures. Finally, we have shown how to describe multi-dimensional continuous-space feature vectors in terms of a discrete vocabulary, by discretizing the range of observed feature values along each feature dimension.

The extracted features were used in the evaluation of three models for the creation of collection indexes. These are word spotting, recognition followed by retrieval, and cross-modal retrieval models. In word spotting, word matching is used to create a partial index for a collection in a semi-automatic way, which requires no training data. Previous work was only concerned with designing word image matching approaches. We showed how to carry out the entire word spotting process by investigating clustering algorithms and by demonstrating how cluster candidates for an index can be selected automatically.

Document recognition is the principal application of handwriting analysis. We built a Hidden Markov Model recognizer that treats words holistically. The recognition output was used for text retrieval based on the language modeling approach. This system was used as a baseline for comparison with other retrieval techniques.

The cross-modal retrieval approach uses a model of the joint distribution of word image features and annotations. These models allow the retrieval in the feature domain, by mapping query terms to features, and in the annotation domain, by creating probabilistic annotation vectors for word images. We compared cross-modal models that use both discrete and continuous-space feature representations with the retrieval based on HMM recognition output. The best performing model was the probabilistic annotation model with continuous-space features. We also demonstrated that performance can be increased even further by applying word bigram constraints to the probabilistic annotation output.

Using the cross-modal retrieval model approach, we have built a prototype system for the retrieval of historical manuscript images from the George Washington

collection (`http://ciir.cs.umass.edu/demos/`). The system allows text queries and provides a retrieval interface similar to web search engines.

7.2 Future Work

Our prototype system is a proof-of-concept for the feasibility of historical manuscript image retrieval. Because of the size of this system, which did not allow us to work out all components to the smallest detail, and the numerous challenges the problem poses, various limitations remain that need improvement. Here we propose directions for future work, paying special attention to making our system practicable.

7.2.1 System Improvements

Building an entire retrieval system is a big effort that requires making numerous decisions. Due to time constraints, some of our choices in this work are not based on an in-depth investigation of what the optimal alternative would be, but are rather informed "guesses". Examples are our particular choice of features and the number of bins we used to discretize continuous-space features. Since the system performance depends on such choices, it would be useful to perform a sensitivity analysis to test the influence of various system parameters on the retrieval performance.

Many of the current system's shortcomings lie in the document processing step. The manuscript segmentation algorithm assumes a very simple letter-like layout. In order to handle a greater variety of layouts, the segmentation must take into account the possibility of multiple text columns and the presence of images or drawings. Another shortcoming is that various document image distortions are not taken into account. This includes simple distortions, such as slightly rotated pages, and the more complicated distortions that occur when pages are scanned with the binding still in place.

We have experimented with a number of features, but the set we used here should not be considered ideal. Many features are reported in the literature and we believe that significant performance increases can be achieved with better features. Our investigation has focused on holistic word features, but it may be necessary to use features that take into account local characteristics when making classification decisions.

It is also possible to improve the retrieval models: the cross-modal model in particular suffers from a problem that is related to the out-of-vocabulary problem. Some images do not have any word content (e.g. stamps), or contain words that are illegible (e.g. because they have been crossed out), or they just contain OOV terms. In those cases the cross-modal model is forced to associate some "random" annotation words with these images. This could be prevented by allowing the models to reject images if their features do no resemble any training instance.

Our work here has focused on the papers of George Washington. Many other collections exist and the techniques presented in this work need to be validated and refined to allow successful retrieval of a variety of document images. Preliminary experiments with scanned field notes by Joseph Grinnell[1] are promising.

7.2.2 Making the System Practicable

One of the main factors that hamper the quick deployment of this system as a commercial product is its dependency on author-specific training data. The size of the George Washington collection, paired with the single-author assumption, has allowed us to spend a substantial amount of time to acquire training data. Since training data preparation requires considerably more time per page than human transcription, automatic document analysis approaches based on author-specific training data are

[1] Joseph Grinnell (1877-1939) was a professor of zoology at the University of California Berkeley and the first director of the university's Museum of Vertebrate Zoology.

only feasible for large test collections.[2] Currently, it may be more economical to manually transcribe a smaller collection (up to a few hundred pages) to allow retrieval using keywords.

So far, our assumption has been that the analyzed document collection has a single writer (or very few writers). Although we have not investigated the performance of our system on a collection with many writers, we expect the retrieval performance to decrease with the current training set, because of the differences in writing style. This problem could be solved with training data for the relevant writing styles, or by using representations of word shape that are invariant to changes in writing style. Because of the large variety of handwriting styles, we expect that the former approach will provide better performance. A small number of datasets have been used in the literature, both online (e.g. the UNIPEN database [29]) and offline (e.g. the IAM data set [75]). They could provide a starting point for more training data, but unfortunately no historical datasets are available with high-quality ground truth (except for a set of 20 pages we have made available).

The current approach to training data acquisition is slow. It requires an annotator to transcribe entire pages and then to map the transcriptions to automatic segmentation output, which itself has to be corrected manually. One way to speed up this process is to use a transcription mapping approach that automatically determines correspondences between a transcription and the automatic segmentation of a document image. Kornfield et al. [49] presented a solution based on a dynamic programming algorithm, which can map transcriptions and segmentation output page-by-page. Rothfeder [97] described another solution for the same problem based on a Hidden Markov Model. More complicated scenarios still need to be addressed, for example when transcriptions span multiple physical pages as is the case in the George

[2]Training data preparation does not only involve the transcription of a document, but also the segmentation of the document image and the alignment with the transcription (see section 1.5.2).

Washington collection. Another idea is to use word spotting to reduce the amount of human transcription work. Word spotting could be used to cluster a small collection of unlabeled training images. Once the word images have been grouped, the training set could be annotated by labeling either some or all clusters. This approach would greatly reduce the labeling work when compared to a full transcription of the entire training collection.

Even when training data is available for a collection, it is unlikely that it covers the entire vocabulary of the test data. Many words such as proper names will be out-of-vocabulary. We have conducted some preliminary experiments with TrueType and bitmap font word images in order to create synthetic training data for OOV terms. The current synthesis models were not able to replace or complement natural writing samples. More complex models are needed to mimic the variability in human writing. With a working synthesis model artificial writing samples could be generated at query time, when the query contains OOV terms.

To a large extent, the problem of OOV terms is due to our holistic approach to word image analysis. It is unrealistic to expect training collections of a manageable size to contain all words in the test set. One way around this limitation could be to analyze word images analytically (bottom-up). Such approaches usually suffer from very large search spaces, with high computational demands. In order to prune the search space, a combined analytic and holistic approach could be used.

In the past, retrieval techniques have been mostly concerned with electronic documents in a symbolic encoding, such as those encountered on the web. Digital libraries are a relatively recent phenomenon and require new approaches to retrieval. This work contributes to this field retrieval techniques for handwritten historical documents, which form a substantial portion of library collections around the world. While the present retrieval system can still be improved, we hope to have convinced

the reader that this work represents a significant step towards extending retrieval capabilities to historical manuscripts.

APPENDIX A

RETRIEVAL INTERFACE

Most of the popular web search engines follow the same idea when it comes to the user interface. A text field is used to collect query terms from the user and a ranked list of documents is returned. In order to help the user decide quickly which documents are of interest, the title of each document is displayed, together with snippets of text around occurrences of the query terms in the document. Our demonstration retrieval system may be accessed at `http://ciir.cs.umass.edu/demos/`.

The current retrieval interface was developed based on the assumption that the above interface is widely accepted by users and hence desirable for handwritten document retrieval as well. Unfortunately, it is not straightforward to convert web search engine interfaces to this new domain. The main reason is that there is no ASCII text representation of a document. The probabilistic nature of the retrieval approach leaves some uncertainty about word image identities, so it is not entirely clear which portions of a document are relevant to the query. Additionally, since there is currently no layout analysis being performed, the annotation information is unstructured. This makes it impossible to display information such as the title of a document.

Figure A.1 shows the preliminary user interface of the retrieval system with the top ranks for the query *Fort Cumberland*. The shown retrieval system performs page retrieval, so the system returns a ranked list of page images on the left. Since the images are very big, they are shown at thumbnail size. The thumbnails are intended to take on the role of the document titles in web search engines, because they allow the user to get a rough idea of the document content. For example, the user can

Figure A.1. Screenshot of the user interface for the retrieval system with results for the query *Fort Cumberland*.

decide whether a ranked document contains tabular information or whether it is a letter.

To the right of the thumbnails, portions of the document that are likely to match the query terms are displayed. One such "snippet" is created for each query term the user supplied. Each snippet consists of the word image with the highest annotation probability for the corresponding query term, plus some additional words (two in the figure) to the left and right to provide context. Because the snippet selection uses a probabilistic approach, it is possible that the snippets do not contain the query terms, but they do appear in the returned page. In such cases it is up to the user to decide whether to read the page or whether to move on to the next result.

At the top of the ranked list, query confidence scores are displayed to provide feedback about the choice of query terms. Words that occur infrequently in the training set yield low query confidence scores and tend to give worse results. With the confidence scores, users can adapt their choice of query terms based on the feedback they receive. By clicking on a document thumbnail or any of the snippet words, a full-size version of the page is displayed, with the selected snippet word highlighted. The ranked list is shown 8 documents at a time, with some *page forward/backward* controls at the bottom of the web page (not shown in Figure A.1).

At the moment, the retrieval interface is functional, but there are no browsing controls for reading through the collection page-by-page. With such functionality and more advanced browsing capabilities, such as cross-reference following, the current user interface could be extended to satisfy commercial needs.

APPENDIX B

DYNAMIC TIME WARPING LOWER-BOUNDING

In the following we provide some additional information about our proposed lower bound LB_MV for DTW dissimilarity calculations of multivariate time series (see section 4.3.1).

B.1 Fast kNN Sequential Scanning

In section 4.3.1 we described the `seq_scan` algorithm, which makes use of a lower bound lb to speed up the search for the nearest neighbor to a query in a data set. Table B.1 shows the algorithm `seq_scan_knn`, which extends `seq_scan` to search for the set of k nearest neighbors to a given query Q.

B.2 Proof of the Lower-Bound Property

In section 4.3.1.2 we proposed the lower bound LB_MV for the DTW dissimilarity measure for multivariate time series. Here we provide a proof of its lower-bounding property, which follows the line of thought in Keogh's work [45].

Proposition: For any two sequences $\mathbf{Q}$ and $\mathbf{C}$ of the same length n, for any global constraint on the warping path of the form $j - r \leq i \leq j + r$ (i.e. Sakoe-Chiba band of width r), the following inequality holds: $LB\_MV(\mathbf{Q}, \mathbf{C}) \leq DTW(\mathbf{Q}, \mathbf{C})$.

```
seq_scan_knn(Q, k):
N=∅;
% initialize set of k nearest neighbors N
for i = 1 to k
   d = f (Q, db_entry(i));
   add (i,d) to N;
end
% keep track of maximum distance within N
m = max_(i′, d′)∈N (d′);

% scan rest of data base sequentially
for i = k+1 to num_db_entries
   l = lb (Q, db_entry(i));
   if l ≥ m
      continue;                    % discarded using lower bound (1)
   d = f (Q, db_entry(i));
   if d ≥ m
      continue;                                % discarded using f (2)

   % db_entry(i) is new nearest neighbor, remove maximum (3)
   % entry in N and add db_entry(i)
   remove (argmax_(i′, d′)∈N(d′)) from N;
   add (i, d) to N;
   m = max_(i′, d′)∈N (d′);
end

% return k nearest neighbors to the query
return N;
```

Table B.1. Fast sequential scanning algorithm for k nearest neighbors search using the lower bound lb for f.

Proof: We need to prove

$$\sqrt{\sum_{i=1}^{n}\sum_{p=1}^{d}\begin{cases}(c_{i,p}-u_{i,p})^2 & \text{if } c_{i,p}>u_{i,p}\\ (c_{i,p}-l_{i,p})^2 & \text{if } c_{i,p}<l_{i,p}\\ 0 & \text{otherwise}\end{cases}} \leq \sqrt{\sum_{k=1}^{K}\sum_{p=1}^{d}(q_{i_k,p}-c_{j_k,p})^2},$$

The square root is a monotonic function, so we can remove it:

$$\sum_{i=1}^{n}\sum_{p=1}^{d}\begin{cases}(c_{i,p}-u_{i,p})^2 & \text{if } c_{i,p}>u_{i,p}\\ (c_{i,p}-l_{i,p})^2 & \text{if } c_{i,p}<l_{i,p}\\ 0 & \text{otherwise}\end{cases} \leq \sum_{k=1}^{K}\sum_{p=1}^{d}(q_{i_k,p}-c_{j_k,p})^2.$$

We can prove this inequality by showing that for every summation term on the left-hand side there exists an equal or greater term on the right-hand side. Since the length K of the warping path is greater than or equal to n, every term of the summation $\sum_{i=1}^{n}\ldots$ on the left-hand side of the above equation can be matched with a greater or equal term of the summation $\sum_{k=1}^{K}\ldots$ on the right-hand side. Specifically, for a given index i on the left-hand side, we select (i_k, j_k) on the right-hand side, such that $i = i_k$ for some j_k. A summation term with $i_k = i$ is guaranteed to exist because of the local continuity constraint. Summation terms on the right-hand side are not matched more than once, since i is different for every matched term on the left-hand side.

We have left to show

$$\sum_{p=1}^{d}\begin{cases}(c_{i,p}-u_{i,p})^2 & \text{if } c_{i,p}>u_{i,p}\\ (c_{i,p}-l_{i,p})^2 & \text{if } c_{i,p}<l_{i,p}\\ 0 & \text{otherwise}\end{cases} \leq \sum_{p=1}^{d}(c_{i,p}-q_{j_k,p})^2,$$

which we can prove by showing that every summation term on the left is less than or equal to the corresponding term on the right. We have three cases:

Case $c_{i,p} > u_{i,p}$:

$$(c_{i,p}-u_{i,p})^2 \leq (c_{i,p}-q_{j_k,p})^2 \tag{B.1}$$

We can take the square root of both sides, because the terms in parentheses are positive: the left-hand side follows from the case $(c_{i,p} > u_{i,p})$ we are treating.

By definition, our global path constraint guarantees $j_k - r \leq i \leq j_k + r$, from which we can deduce $i - r \leq j_k \leq i + r$. Using the definition of $u_{i,p} = max(q_{i-r,p} : q_{i+r,p})$, we get $q_{j_k,p} \leq u_{i,p}$. Since $u_{i,p} < c_{i,p}$ (definition of case), $c_{i,p} - q_{j_k,p}$ is positive.

Hence, we get

$$\begin{aligned} c_{i,p} - u_{i,p} &\leq c_{i,p} - q_{j_k,p} && \text{(B.2)} \\ -u_{i,p} &\leq -q_{j_k,p} && \text{(B.3)} \\ q_{j_k,p} &\leq u_{i,p} && \text{(B.4)} \end{aligned}$$

which is true.

Case $c_{i,p} < l_{i,p}$:

This proof is straightforward with an argument similar to the above.

Case $l_{i,p} \leq c_{i,p} \leq u_{i,p}$:

Trivially we have

$$0 \leq (c_{i,p} - q_{j_k,p})^2,$$

where the right-hand side is non-negative. □

BIBLIOGRAPHY

[1] Antonacopoulos, A., Gatos, B., and Karatzas, D. ICDAR 2003 page segmentation competition. In *Proc. of the 7th Int'l Conf. on Document Analysis and Recognition* (Edinburgh, Scotland, August 3-6 2003), vol. 2, pp. 688–692.

[2] Apple Computer, Inc. TrueType Reference Manual. Electronically published on the Internet at http://developer.apple.com/fonts/TTRefMan/, October 1996.

[3] Baeza-Yates, R., and Ribeiro-Neto, B. *Modern Information Retrieval*. Addison-Wesley, Reading, MA, 1999.

[4] Baird, H. S. Document image defect models. In *Structured Document Image Analysis*, H. S. Baird, H. Bunke, and K. Yamamoto, Eds. Springer-Verlag, Berlin, 1992, pp. 546–556.

[5] Barnard, K., Duygulu, P., de Freitas, N., Forsyth, D., Blei, D., and Jordan, M. I. Matching words and pictures. *Journal of Machine Learning Research 3*, 6 (2003), 1107–1135.

[6] Barnard, K., and Forsyth, D. Learning the semantics of words and pictures. In *Proc. of the Int'l Conf. on Computer Vision* (Vancouver, Canada, July 9-12 2001), vol. 2, pp. 408–415.

[7] Belongie, S., Malik, J., and Puzicha, J. Shape matching and object recognition using shape contexts. *IEEE Trans. on Pattern Analysis and Machine Intelligence 24*, 4 (2002), 509–522.

[8] Blei, D. M., and Jordan, M. I. Modeling annotated data. In *Proc. of the 26th Annual Int'l ACM SIGIR Conf.* (Toronto, Canada, July 28-August 1 2003), pp. 127–134.

[9] Blei, D. M., Ng, A. Y., and Jordan, M. I. Latent dirichlet allocation. *Journal of Machine Learning Research 3* (2003), 993–1022.

[10] Bozinovic, R. M., and Srihari, S. N. Off-line cursive script word recognition. *IEEE Trans. on Pattern Analysis and Machine Intelligence 11*, 1 (1989), 68–83.

[11] Breuel, T. M. An algorithm for finding maximal whitespace rectangles at arbitrary orientations for document layout analysis. In *Proc. of the 7th Int'l Conf. on Document Analysis and Recognition* (Edinburgh, Scotland, August 3-6 2003), vol. 1, pp. 66–70.

[12] Bunke, H. Recognition of cursive Roman handwriting - past, present and future. Keynote address at the 7th Int'l Conf. on Document Analysis and Recognition, August 3-6 2003.

[13] Cai, D., He, X., Wen, J.-R., and Ma, W.-Y. Block-level link analysis. In *Proc. of the 27th Annual Int'l ACM SIGIR Conf.* (Sheffield, UK, July 25-29 2004), pp. 440–447.

[14] Cao, H., Ding, X., and Liu, C. Rectifying the bound document image captured by the camera: A model based approach. In *Proc. of the 7th Int'l Conf. on Document Analysis and Recognition* (Edinburgh, Scotland, August 3-6 2003), vol. 1, pp. 71–75.

[15] Cattell, J. M. The time taken up by cerebral operations. *Mind 11* (1886), 220–242.

[16] Chakrabarti, K., and Mehrotra, S. The hybrid tree: An index structure for high-dimensional feature spaces. In *Proc. of the Int'l Conf. on Data Engineering* (Sydney, Australia, March 23-26 1999), pp. 440–447.

[17] Chen, F. R., and Bloomberg, D. S. Summarization of imaged documents without OCR. *Computer Vision and Image Understanding 70*, 3 (1997), 307–320.

[18] Danielsson, P.-E. Euclidean distance mapping. *Computer Graphics and Image Processing 14* (1980), 227–248.

[19] Duda, R. O., Hart, P. E., and Stork, D. G. *Pattern Classification*, 2nd ed. Wiley-Interscience, New York, NY, 2000.

[20] Duygulu, P., Barnard, K., de Freitas, N., and Forsyth, D. Object recognition as machine translation: Learning a lexicon for a fixed image vocabulary. In *Proc. of the 7th European Conf. on Computer Vision* (Copenhagen, Denmark, May 27-June 2 2002), vol. 4, pp. 97–112.

[21] Edwards, J., Teh, Y. W., Forsyth, D., Bock, R., Maire, M., and Vesom, G. Making latin manuscripts searchable using gHMM's. In *Proc. of the 18th Annual Conf. on Neural Information Processing Systems* (Vancouver, Canada, December 14-16 2004), p. (to appear).

[22] Faloutsos, C. Multimedia IR: Indexing and searching. In *Modern Information Retrieval*, R. Baeza-Yates and B. Ribeiro-Neto, Eds. Addison-Wesley, Reading, MA, 1999, pp. 743–747.

[23] Feldbach, M., and Tönnies, K. D. Line detection and segmentation in historical church registers. In *Proc. of the 6th Int'l Conf. on Document Analysis and Recognition* (Seattle, WA, September 10-13 2001).

[24] Feng, S. L., Manmatha, R., and Lavrenko, V. Multiple Bernoulli relevance models for image and video annotation. In *Proc. of the Conf. on Computer Vision and Pattern Recognition* (Washington, DC, June 27-July 2 2004), vol. 2, pp. 1002–1009.

[25] Forney, G. D. The Viterbi algorithm. *Proc. of the IEEE 61* (March 1973), 268–278.

[26] Freund, J. E. *Mathematical Statistics*, 5 ed. Prentice Hall, Upper Saddle River, NJ, 1992.

[27] Gorski, N., Anisimov, V., Augustin, E., Baret, O., Price, D., and Simon, J. A2iA check reader: A family of bank check recognition systems. In *Proc. of the 5th Int'l Conf. on Document Analysis and Recognition* (Bangalore, India, September 20-22 1999), vol. 1, pp. 523–526.

[28] Guttman, A. R-trees: A dynamic index structure for spatial searching. In *Proc. of the ACM SIGMOD Conf.* (Boston, MA, June 18-21 1984), pp. 47–57.

[29] Guyon, I., Schomaker, L., Plamondon, R., Liberman, M., and Janet, S. UNIPEN project of on-line data exchange and recognizer benchmarks. In *Proc. of the Int'l Conf. on Pattern Recognition* (Jerusalem, Israel, October 9-13 1994), pp. 29–33.

[30] Haralick, R. M. Document image understanding: Geometric and logical layout. In *Proc. of the Conf. on Computer Vision and Pattern Recognition* (Seattle, WA, June 21-23 1994), pp. 385–390.

[31] Hastie, T., Tibshirani, R., and Friedman, J. *The Elements of Statistical Learning: Data Mining, Inference and Prediction*. Springer-Verlag, New York, 2001.

[32] Heaps, H. S. *Information Retrieval: Computational and Theoretical Aspects*. Academic Press, Orlando, FL, 1978.

[33] Herman, S. G. *The Naturalist's Field Journal: A Manual of Instruction Based on a System Established by Joseph Grinnell*. Buteo Books, 1986.

[34] Hofmann, T. Learning and representing topic. a hierarchical mixture model for word occurrences in document databases. In *Proc. of the Conf. on Automated Learning and Discovery* (Pittsburgh, PA, June 11-13 1998).

[35] Howe, N. R., Rath, T. M., and Manmatha, R. Boosted decision trees for word recognition in handwritten document retrieval. In *Proc. of the 28th Annual Int'l ACM SIGIR Conf.* (Salvador, Brazil, August 15-19 2005). (to appear).

[36] Hutchison, L. A. D., and Barrett, W. A. Fast registration of tabular document images using the fourier-mellin transform. In *Proc. of the Int'l Workshop on Document Image Analysis for Libraries* (Palo Alto, CA, January 23-24 2004), pp. 253–267.

[37] Ishidera, E., and Nishiwaki, D. A study on top-down word image generation for handwritten word recognition. In *Proc. of the 7th Int'l Conf. on Document Analysis and Recognition* (Edinburgh, Scotland, August 3-6 2003), vol. 2, pp. 1173–1177.

[38] Itakura, F. Minimum prediction residual principle applied to speech recognition. *IEEE Trans. on Acoustics, Speech, and Signal Processing 23*, 1 (1975), 67–72.

[39] Jain, A. K., and Namboodiri, A. Indexing and retrieval of on-line handwritten documents. In *Proc. of the 7th Int'l Conf. on Document Analysis and Recognition* (Edinburgh, Scotland, August 3-6 2003), vol. 2, pp. 655–659.

[40] Jelinek, F., Bahl, L. R., and Mercer, R. L. Design of a linguistic statistical decoder for the recognition of continuous speech. *IEEE Trans. on Information Theory 21* (1975), 250–256.

[41] Jeon, J., Lavrenko, V., and Manmatha, R. Automatic image annotation and retrieval using cross-media relevance models. In *Proc. of the 26th Annual Int'l ACM SIGIR Conf.* (Toronto, Canada, July 28-August 1 2003), pp. 119–126.

[42] Jones, G. J. F., Foote, J. T., Jones, K. Sparck, and Young, S. J. Video mail retrieval: The effect of word spotting accuracy on precision. In *Proc. of the Int'l Conf. on Acoustics, Speech and Signal Processing* (Detroit, MI, May 8-12 1995), vol. 1, pp. 309–312.

[43] Kane, S., Lehman, A., and Partridge, E. Indexing george washington's handwritten manuscripts. Tech. rep., Center for Intelligent Information Retrieval, Univ. of Massachusetts Amherst, 2001.

[44] Kavallieratou, E., Fakotakis, N., and Kokkinakis, G. A slant removal algorithm. *Pattern Recognition 33*, 7 (2000), 1261–1262.

[45] Keogh, E. Exact indexing of dynamic time warping. In *Proc. of the 28th Very Large Databases Conf.* (Hong Kong, China, August 20-23 2002), pp. 406–417.

[46] Kim, G., Govindaraju, V., and Srihari, S. N. An architecture for handwritten text recognition systems. *Int'l Journal on Document Analysis and Recognition 2*, 1 (1999), 37–44.

[47] Kim, S. H., Jeong, C. B., Kwag, H. K., and Suen, C. Y. Word segmentation of printed text lines based on gap clustering and special symbol detection. In *Proc. of the Int'l Conf. on Pattern Recognition* (Québec City, Canada, August 11-15 2002), vol. 2, pp. 320–323.

[48] Kołcz, A., Alspector, J., Augusteijn, M., Carlson, R., and Popescu, G. V. A line-oriented approach to word spotting in handwritten documents. *Pattern Analysis & Applications 3*, 2 (2000), 153–168.

[49] Kornfield, E. M., Manmatha, R., and Allan, J. Text alignment with handwritten documents. In *Proc. of the Int'l Workshop on Document Image Analysis for Libraries* (Palo Alto, CA, January 23-24 2004), pp. 195–209.

[50] Krovetz, R. Viewing morphology as an inference process. In *Proc. of the 16th Annual Int'l SIGIR Conf.* (Pittsburgh, PA, June 27-July 1 1993), pp. 191–202.

[51] Kwok, T., Perrone, M. P., and Russell, G. F. Ink retrieval from handwritten documents. In *Proc. of the Conf. on Intelligent Data Engineering and Automated Learning* (Hong Kong, China, December 13-15 2000), pp. 461–466.

[52] Lagarias, J. C., Reeds, J. A., Wright, M. H., and Wright, P. E. Convergence properties of the nelder-mead simplex method in low dimensions. *SIAM Journal of Optimization 9*, 1 (1998), 112–147.

[53] Lavrenko, V., Choquette, M., and Croft, W. B. Cross-lingual relevance models. In *Proc. of the 25th Annual Int'l SIGIR Conf.* (Tampere, Finland, August 11-15 2002), pp. 175–182.

[54] Lavrenko, V., and Croft, W. B. Relevance-based language models. In *Proc. of the 24th Annual Int'l SIGIR Conf.* (New Orleans, LA, September 9-13 2001), pp. 120–127.

[55] Lavrenko, V., and Croft, W. B. Relevance models in information retrieval. In *Language Modeling for Information Retrieval*, W. B. Croft and J. Lafferty, Eds. Kluwer Academic Publishers, Dordrecht, The Netherlands, 2003.

[56] Lavrenko, V., Feng, S. L., and Manmatha, R. Statistical models for automatic video annotation and retrieval. In *Proc. of the Int'l Conf. on Acoustics, Speech and Signal Processing* (Montréal, QC, May 17-21 2004).

[57] Lavrenko, V., Manmatha, R., and Jeon, J. A model for learning the semantics of pictures. In *Proc. of the 16th Annual Conf. on Neural Information Processing Systems* (Vancouver, Canada, December 9-11 2003). (to appear).

[58] Lavrenko, V., Rath, T. M., and Manmatha, R. Holistic word recognition for handwritten historical documents. In *Proc. of the Int'l Workshop on Document Image Analysis for Libraries* (Palo Alto, CA, January 23-24 2004), pp. 278–287.

[59] Leedham, G., Varma, S., Patankar, A., and Govindaraju, V. Separating text and background in degraded documents images — a comparison of global thresholding techniques for multi-stage thresholding. In *Proc. of the 8th Int'l Workshop on Frontiers in Handwriting Recognition* (Niagara-on-the-Lake, Canada, August 6-8 2002), pp. 244–249.

[60] Lindeberg, T. *Scale-Space Theory in Computer Vision.* Kluwer Academic Publishers, Dordrecht, Netherlands, 1994.

[61] Lopresti, D., and Tomkins, A. On the searchability of electronic ink. In *Proc. of the 4th Int'l Workshop on Frontiers in Handwriting Recognition* (Taipei, Taiwan, December 7-9 1994), pp. 156–165.

[62] Lu, Y., and Shridhar, M. Character segmentation in handwritten words - an overview. *Pattern Recognition 29*, 1 (1996), 77–96.

[63] Luhn, H. P. The automatic creation of literature abstracts. *IBM Journal 2* (April 1958), 159–165.

[64] Madhvanath, S., and Govindaraju, V. Using holistic features in handwritten word recognition. In *Proc. of the U.S. Postal Service Advanced Technology Conf.* (Washington, DC, November 30 - December 2 1992), pp. 183–199.

[65] Madhvanath, S., and Govindaraju, V. The role of holistic paradigms in handwritten word recognition. *Trans. on Pattern Analysis and Machine Intelligence 23*, 2 (2001), 149–164.

[66] Mahadevan, U., and Nagabushnam, R. C. Gap metrics for word separation in handwritten lines. In *Proc. of the 3rd Int'l Conf. on Document Analysis and Recognition* (Montréal, Canada, August 14-15 1995), vol. 1, pp. 124–127.

[67] Manmatha, R., and Croft, W. B. Word spotting: Indexing handwritten manuscripts. In *Intelligent Multimedia Information Retrieval*, Mark T. Maybury, Ed. MIT Press, Cambridge, MA, 1997, pp. 43–64.

[68] Manmatha, R., Han, C., and Riseman, E. M. Word spotting: A new approach to indexing handwriting. In *Proc. of the Conf. on Computer Vision and Pattern Recognition* (San Francisco, CA, June 18-20 1996), pp. 631–637.

[69] Manmatha, R., Han, C., Riseman, E. M., and Croft, W. B. Indexing handwriting using word matching. In *Digital Libraries '96: 1st ACM Int'l Conf. on Digital Libraries* (Bethesda, MD, March 20-23 1996), pp. 151–159.

[70] Manmatha, R., and Rothfeder, J. L. A scale space approach for automatically segmenting words from historical handwritten documents. *IEEE Trans. on Pattern Analysis and Machine Intelligence* (2005). (to appear).

[71] Manmatha, R., and Srimal, N. Scale space technique for word segmentation in handwritten manuscripts. In *Proc. of the Second Int'l Conf. on Scale-Space Theories in Computer Vision* (Corfu, Greece, September 26-27 1999), pp. 22–33.

[72] Manning, C. D., and Schütze, H. *Foundations of Statistical Natural Language Processing*. MIT Press, Cambridge, MA, 2001.

[73] Marr, D. *Vision*. W. H. Freeman and Company, New York, NY, 1982.

[74] Marti, U.-V. *Offline Erkennung handgeschriebener Texte*. Inauguraldissertation, Philosophisch-naturwissenschaftliche Fakultät der Universität Bern, November 1 2000.

[75] Marti, U.-V., and Bunke, H. The iam-database: an English sentence database for off-line handwriting recognition. *Int'l Journal on Document Analysis and Recognition 5*, 1 (2000), 39–46.

[76] Marti, U.-V., and Bunke, H. Text line segmentation and word recognition in a system for general writer independent handwriting recognition. In *Proc. of the 6th Int'l Conf. on Document Analysis and Recognition* (Seattle, WA, September 10-13 2001), pp. 159–163.

[77] Marti, U.-V., and Bunke, H. Using a statistical language model to improve the performance of an HMM-based cursive handwriting recognition system. *Int'l Journal of Pattern Recognition and Artifical Intelligence 15*, 1 (2001), 65–90.

[78] Mohanty, N., Rath, T. M., Lee, A., and Manmatha, R. Learning shape for image classification and retrieval. In *Int'l Conf. on Image and Video Retrieval* (Singapore, Singapore, July 20-22 2005). (to appear).

[79] Mori, Y., Takahashi, H., and Oka, R. Image-to-word transformation based on dividing and vector quantizing images with words. In *1st Int'l Workshop on Multimedia Intelligent Storage and Retrieval Management* (Orlando, FL, October 30 1999).

[80] Mukherjee, S., Yang, G., Tan, W., and Ramakrishnan, I. V. Automatic discovery of semantic structures in HTML documents. In *Proc. of the 7th Int'l Conf. on Document Analysis and Recognition* (Edinburgh, Scotland, August 3-6 2003), vol. 1, pp. 245–249.

[81] Nash, R. Handwriting of the founding fathers. *Manuscripts 7*, 4 (1955), 208–213.

[82] National Institute of Standards and Technology (NIST), and U. S. Department of Defense. Text retrieval conference (trec), 1992.

[83] Pacquet, T., and Lecourtier, Y. Recognition of handwritten sentences using a restricted lexicon. *Pattern Recognition 26*, 3 (1993), 391–407.

[84] Plamondon, R., and Srihari, S. N. On-line and off-line handwriting recognition: A comprehensive survey. *IEEE Trans. on Pattern Analysis and Machine Intelligence 22*, 1 (2000), 63–84.

[85] Ponte, J., and Croft, W. B. A language modeling approach to information retrieval. In *Proc. of the 21st Annual Int'l ACM SIGIR Conf.* (Melbourne, Australia, August 24-28 1998), pp. 275–281.

[86] Rabiner, L. R. A tutorial on hidden Markov models and selected applications in speech recognition. *Proc. of the IEEE 77*, 2 (1989), 257–286.

[87] Ratanamahatana, C. A., and Keogh, E. Making time-series classification more accurate using learned constraints. In *Proc. of the 4th SIAM Int'l Conf. on Data Mining* (Lake Buena Vista, FL, April 22-24 2004), pp. 11–22.

[88] Rath, T. M., Kane, S., Lehman, A., Partridge, E., and Manmatha, R. Indexing for a digital library of George Washington's manuscripts: A study of word matching techniques. Tech. rep., Center for Intelligent Information Retrieval, Univ. of Massachusetts Amherst, 2000.

[89] Rath, T. M., and Manmatha, R. Features for word spotting in historical manuscripts. In *Proc. of the 7th Int'l Conf. on Document Analysis and Recognition* (Edinburgh, Scotland, August 3-6 2003), vol. 1, pp. 218–222.

[90] Rath, T. M., and Manmatha, R. Lower-bounding of dynamic time warping distances for multivariate time series. Tech. rep., Center for Intelligent Information Retrieval, Univ. of Massachusetts Amherst, 2003.

[91] Rath, T. M., and Manmatha, R. Word image matching using dynamic time warping. In *Proc. of the Conf. on Computer Vision and Pattern Recognition* (Madison, WI, June 18-20 2003), vol. 2, pp. 521–527.

[92] Rath, T. M., Manmatha, R., and Lavrenko, V. A search engine for historical manuscript images. In *Proc. of the 27th Annual Int'l ACM SIGIR Conf.* (Sheffield, UK, July 25-29 2004), pp. 369–376.

[93] Rath, T. M., Rothfeder, J. L., and Lvin, V. B. The BoxModify tool, 2004. (computer program).

[94] Ratzlaff, E. H. Inter-line distance estimation and text line extraction for unconstrained online handwriting. In *Proc. of the 7th Int'l Workshop on Frontiers in Handwriting Recognition* (Amsterdam, The Netherlands, September 11-13 2000), pp. 33–42.

[95] Ravela, S., and Manmatha, R. Retrieving images by appearance. In *Proc. of the Int'l Conf. on Computer Vision* (Bombay, India, January 4-7 1998), pp. 608–613.

[96] Reicher, G. M. Perceptual recognition as a function of meaningfulness of stimulus material. *Journal of Experimental Psychology 81* (1969), 275–280.

[97] Rothfeder, J. L. Aligning transcripts to automatically segmented historical documents. M.S. project report, University of Massachusetts Amherst, 2005.

[98] Rothfeder, J. L., Feng, S., and Rath, T. M. Using corner feature correspondences to rank word images by similarity. In *Proc. of the Workshop on Document Image Analysis and Retrieval (electronically published)* (Madison, WI, June 20 2003).

[99] Russell, G., Perrone, M. P., Chee, Y.-M., and Ziq, A. Handwritten document retrieval. In *Proc. of the 8th Int'l Workshop on Frontiers in Handwriting Recognition* (Niagara-on-the-Lake, Canada, August 6-8 2002), pp. 233–238.

[100] Sakoe, H., and Chiba, S. Dynamic programming algorithm optimization for spoken word recognition. *IEEE Trans. on Acoustics, Speech and Signal Processing 26* (1980), 623–625.

[101] Salton, G., and Buckley, C. The trec_eval program, 1991. (contains modifications by other authors).

[102] Sankoff, D., and Kruskal, J. B. *Time Warps, String Edits, and Macromolecules: The Theory and Practice of Sequence Comparison.* Addison-Wesley, Reading, MA, 1983.

[103] Sayre, K. M. Machine recognition of handwritten words: A project report. *Pattern Recognition 5*, 3 (1973), 213–228.

[104] Scott, G. L., and Longuet-Higgins, H. C. An algorithm for associating the features of two patterns. *Proc. of the Royal Society of London B224* (1991), 21–26.

[105] Song, F., and Croft, W. B. A general language model for information retrieval. In *Proc. of Int'l Conf. on Information and Knowledge Management* (Kansas City, MO, November 2-6 1999), pp. 316–321.

[106] Srihari, S. N., Huang, C., and Srinivasan, H. A search engine for handwritten documents. In *Document Recognition and Retrieval XII, Proc. of SPIE* (San Jose, CA, January 19-20 2005), vol. 5676, pp. 66–75.

[107] Steinherz, T., Rivlin, E., and Intrator, N. Offline cursive script word recognition - a survey. *Int'l Journal on Document Analysis and Recognition 2*, 2-3 (1999), 90–110.

[108] Tan, C. L., Cao, R., and Shen, P. Restoration of archival documents using a wavelet technique. *IEEE Trans. on Pattern Analysis and Machine Intelligence 24*, 10 (2002), 1399–1404.

[109] Tan, C. L., Huang, W., Yu, Z., and Xu, Y. Imaged document text retrieval without OCR. *IEEE Trans. on Pattern Analysis and Machine Intelligence 24*, 6 (2002), 838–844.

[110] The Library of Congress. George Washington Papers. Electronically published at http://memory.loc.gov/ammem/gwhtml/gwhome.html, 2004.

[111] Tomai, C. I., Zhang, B., and Govindaraju, V. Transcript mapping for historic handwritten document images. In *Proc. of the 8th Int'l Workshop on Frontiers in Handwriting Recognition* (Niagara-on-the-Lake, Canada, August 6-8 2002), pp. 413–418.

[112] Triebel, R. Automatische Erkennung von handgeschriebenen Worten mithilfe des Level-building Algorithmus, December 1999. Student Thesis, Institut für Informatik, Albert-Ludwigs-Universität Freiburg (in German).

[113] Trier, Ø. D., Jain, A. K., and Taxt, T. Feature extraction methods for character recognition - a survey. *Pattern Recognition 29*, 4 (1996), 641–662.

[114] Varga, T., and Bunke, H. Generation of synthetic training data for an HMM-based handwriting recognition system. In *Proc. of the 7th Int'l Conf. on Document Analysis and Recognition* (Edinburgh, Scotland, August 3-6 2003), vol. 1, pp. 618–622.

[115] Vinciarelli, A. A survey on off-line cursive word recognition. *Pattern Recognition 35*, 7 (2002), 1433–1446.

[116] Vinciarelli, A. Application of information retrieval techniques to single writer documents. *Pattern Recognition Letter* (2004). (to appear).

[117] Vinciarelli, A., Bengio, S., and Bunke, H. Offline recognition of unconstrained handwritten texts using HMMs and statistical language models. *IEEE Transactions on Pattern Analysis and Machine Intelligence 26*, 6 (2004), 709–720.

[118] Vinciarelli, A., and Luettin, J. Off-line cursive script recognition based on continuous density HMM. In *Proc. of the 7th Int'l Workshop on Frontiers in Handwriting Recognition* (Amsterdam, The Netherlands, September 11-13 2000), pp. 493–498.

[119] Wolf, C., Jolion, J.-M., and Chassaing, F. Text localization, enhancement and binarization in multimedia documents. In *Proc. of the Int'l Conf. on Pattern Recognition* (Québec City, Canada, August 11-15 2002), vol. 4, pp. 1037–1040.

[120] Woodworth, R. S. *Experimental Psychology*. Holt, New York, 1938.

[121] Wu, V., Manmatha, R., and Riseman, E. M. Textfinder: An automatic system to detect and recognize text in images. *IEEE Trans. on Pattern Analysis and Machine Intelligence 21*, 11 (1999), 1224–1229.

[122] Yi, B.-K., Jagadish, H. V., and Faloutsos, C. Efficient retrieval of similar time sequences under time warping. In *Proc. of the 14th Int'l Conf. on Data Engineering* (Orlando, FL, February 23-27 1998), pp. 201–208.

[123] Yosef, I. Bar, Kedem, K., Dinstein, I., Beit-Arie, M., and Engel, E. Classification of hebrew calligraphic handwriting styles: Preliminary results. In *Proc. of the Int'l Workshop on Document Image Analysis for Libraries* (Palo Alto, CA, January 23-24 2004), pp. 299–305.

[124] Zhai, C. *Risk Minimization and Language Modeling in Text Retrieval*. PhD thesis, Carnegie Mellon University, Pittsburgh, PA, July 2002.

[125] Zheng, Y., Li, H., and Doermann, D. Text identification in noisy document images using Markov random field. In *Proc. of the 7th Int'l Conf. on Document Analysis and Recognition* (Edinburgh, Scotland, August 3-6 2003), vol. 1, pp. 599–603.

[126] Zhu, Y., and Shasha, D. Warping indexes with envelope transforms for query by humming. In *Proc. of the ACM SIGMOD Conf.* (San Diego, CA, June 9-12 2003), pp. 181–192.

[127] Zipf, G. *Human Behaviour and the Principle of Least Effort*. Addison-Wesley, Cambridge, MA, 1949.